BAYLOR GEOLOGICAL STUDIES

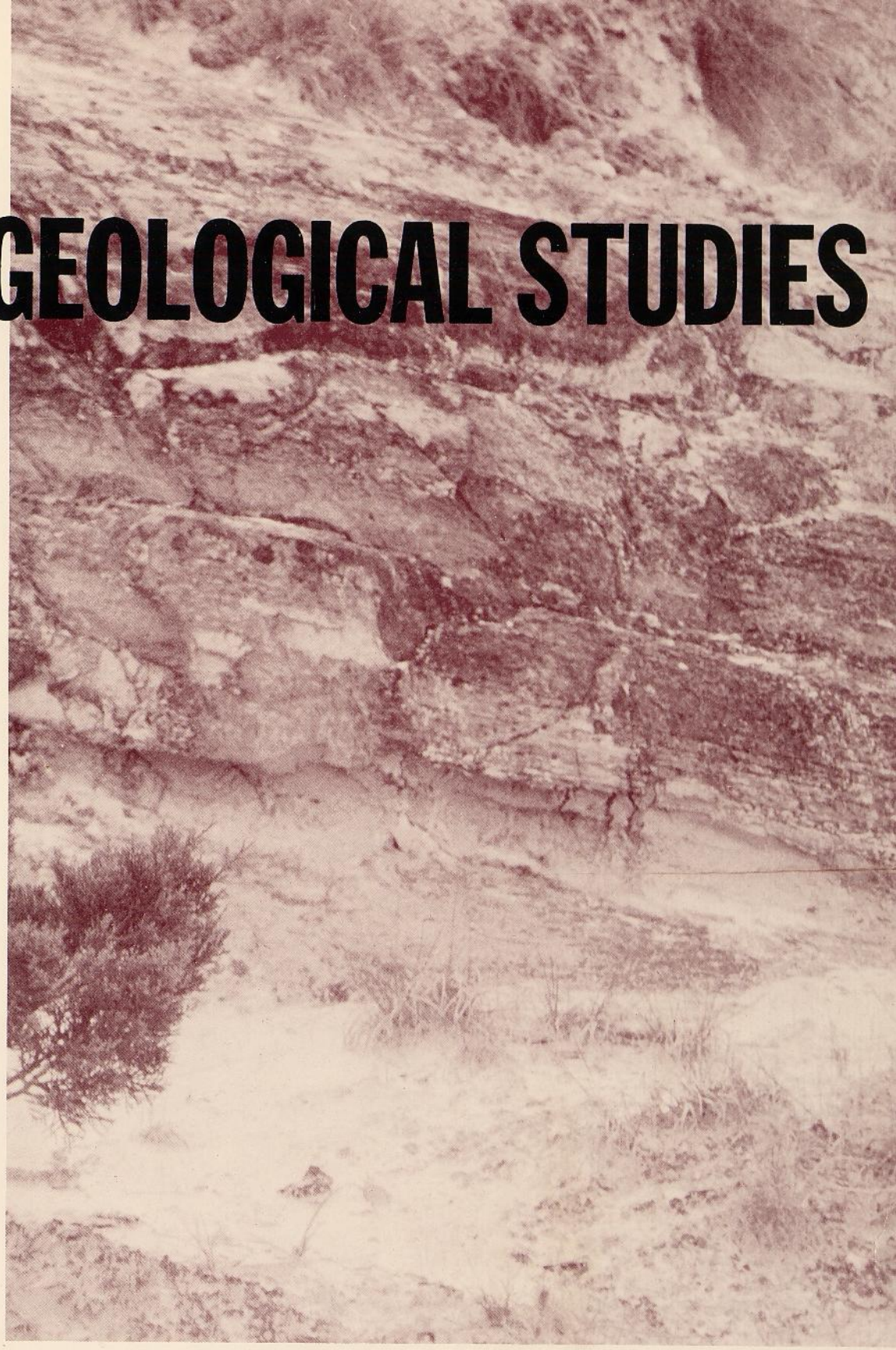

FALL 1990

Bulletin No. 50

BAYLOR UNIVERSITY - WACO, TEXAS
FOUNDED PRO ECCLESIA PRO TEXANA 1845

Thesis Abstracts

"Creative thinking is more important than elaborate equipment--"

FRANK CARNEY, PH.D.
PROFESSOR OF GEOLOGY
BAYLOR UNIVERSITY
1929-1934

Objectives of Geological Training at Baylor

The training of a geologist in a university covers but a few years; his education continues throughout his active life. The purposes of training geologists at Baylor University are to provide a sound basis of understanding and to foster a truly geological point of view, both of which are essential for continued professional growth. The staff considers geology to be unique among sciences since it is primarily a field science. All geologic research including that done in laboratories must be firmly supported by field observations. The student is encouraged to develop an inquiring objective attitude and to examine critically all geological concepts and principles. The development of a mature and professional attitude toward geology and geological research is a principal concern of the department.

Cover: Massive sandstone section in the Paluxy Sand between Walnut Springs and Iredell in Bosque County (from Crumpler).

THE BAYLOR PRINTING SERVICE
WACO, TEXAS

BAYLOR GEOLOGICAL STUDIES

BULLETIN NO. 50

THESIS ABSTRACTS

These abstracts are taken from theses written in partial fulfillment of degree requirements at Baylor University. The original, unpublished versions of the theses, complete with appendices and bibliographies, can be found in the Ferdinand Roemer Library, Department of Geology, Baylor University, Waco, Texas.

BAYLOR UNIVERSITY
Department of Geology
Waco, Texas
Fall 1990

Baylor Geological Studies

EDITORIAL STAFF

Janet L. Burton, *Editor*

O. T. Hayward, Ph.D., *Advisor, Cartographic Editor*
general and urban geology and what have you

Joe C. Yelderman, Jr., Ph.D., *Associate Editor*
hydrogeology

Peter M. Allen, Ph.D.
urban and environmental geology, hydrology

Harold H. Beaver, Ph.D.
stratigraphy, petroleum geology

Rena Bonem, Ph.D.
paleontology, paleoecology

William Brown, Ph.D.
structural tectonics

S. Norman Domenico, D.Sc.
geophysics

Thomas Goforth, Ph.D.
geophysics

Robert C. Grayson, Ph.D.
stratigraphy, conodont biostratigraphy and sedimentary petrology

Don M. Greene, Ph.D.
physical geography, climatology, earth sciences

Cleavy L. McKnight, M.S.
geological and environmental remote sensing

Don F. Parker, Ph.D.
igneous geology, volcanology, mineralogy, petrology

Laurie L. C. Tsuchiya, M.S.
climatology, earth sciences

Kenneth T. Wilkins, Ph.D.
vertebrate paleontology, biogeography, systematics

STUDENT EDITORIAL STAFF

Brad Parish, *Cartographer*
Victoria French, *Cartographer*

The Baylor Geological Studies Bulletin is published by the Department of Geology at Baylor University. The Bulletin is specifically dedicated to the dissemination of geologic knowledge for the benefit of the people of Texas. The publication is designed to present the results of both pure and applied research which will ultimately be important in the economic and cultural growth of the State.

ISSN 0005-7266

Additional copies of this bulletin can be obtained from the Department of Geology, Baylor University, Waco, Texas 76798.

CONTENTS

Biostratigraphy and Paleoecology of the Grayson Formation, McLennan County, Central Texas

Duncan B. Aepli

The clay-dominated Grayson Formation records a period of marine sedimentation on the Central Texas Platform during the Upper Comanchean, Cretaceous System. Although the Grayson Formation has been the subject of several studies, many questions remain concerning the ecology and environment that existed during deposition of Grayson strata. By subdividing the Grayson Formation within McLennan County into biostratigraphic zones, a basis for paleoecological and paleoenvironmental interpretation was established.

Within the Grayson Formation six fossil assemblages are recognized: (1) *Kingena* assemblage; (2) *Ilymatogyra* assemblage; (3) stunted assemblage; (4) *Neithea* assemblage; (5) *Plicatula* assemblage; and (6) *Texigryphaea* assemblage. Based upon these assemblages and other sedimentological evidence, Grayson deposition may be divided into three depositional stages: the progradational stage, the transitional stage, and the transgressive stage.

Following deposition of the Georgetown Formation, a general shallowing of water and reduction of current activity occurred as a result of a regressive sea movement and the Stuart City Reef Trend. During Grayson deposition, fine-grained sediments began to accumulate, slowly replacing the carbonate deposition of the Georgetown Formation. The accumulation adversely affected the environment by producing a soft substrate, increasing turbidity, and causing mildly reducing conditions beneath the sediment/water interface. The fine-grained clays and fossil associations found within the formation suggest low to moderate energy and normal marine conditions.

The change of environmental conditions during Grayson deposition exerted a significant control on the successive fossil associations present (Figs. 1, 2). As a result, only those organisms best adapted for the conditions survived.

The progradational stage reflects deposition of the lower Grayson Formation and is dominated by the *Kingena* assemblage and the *Ilymatogyra* assemblage. *Ilymatogyra* oysters flourished briefly toward the end of this stage, due in part to their soft substrate adaptation.

The transitional stage represents middle Grayson deposition. Rocks deposited during this stage contain the stunted assemblage and the *Neithea* assemblage. Abundant mud, both carbonate and terrigenous, coupled with shallowing water depths, produced an increase in water turbidity. Turbidity favored smaller-sized gill-bearing organisms and normal-sized organisms like echinoderms that respire using a water vascular system. Other adaptations to the soft substrate include the development of broad, thin shells of oysters and *Neithea*, which allowed the bivalves to distribute weight over a maximum surface area and float on top of the mud.

The transgressive stage occurred during upper Grayson deposition. Rocks deposited during this stage contain the *Plicatula* assemblage and *Texigryphaea* assemblage. A gradual increase in sea level during this stage caused a return to normal marine conditions and steadily increasing faunal diversity. *Texigryphaea* oysters and thin interbedded limestone benches mark the return to conditions similar to those of Georgetown deposition.

Pyritization of fossils in the middle Grayson appears to be the result of early diagenesis related to reducing conditions within sediments. Although mild to moderate at best, diagenesis may have altered original sedimentalogical trends during middle Grayson deposition by consuming carbonate sediments beneath the sediment/water interface (Fig. 3). Further alteration of the uppermost Grayson strata occurred during the pre-Woodbine erosional event.

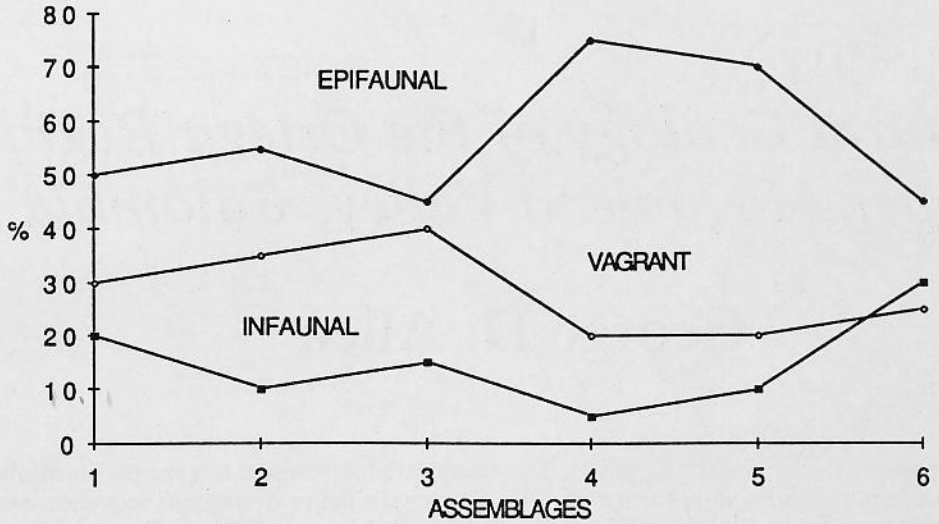

Fig. 1. Graph contrasting the substrate life habits of each fossil assemblage found within the study area. Sessile epifaunal organisms are dominant throughout Grayson deposition, averaging 57% of the fauna, while vagrant and infaunal lifestyles comprise 28% and 15%, respectively. For ease of labeling, each assemblage has been assigned a number: 1 = *Kingena* assemblage, 2 = *Ilymatogyra* assemblage, 3 = stunted assemblage, 4 = *Neithea* assemblage, 5 = Plicatula assemblage, and 6 = *Texigryphaea* assemblage. Note the sharp change occurring around the stunted assemblage.

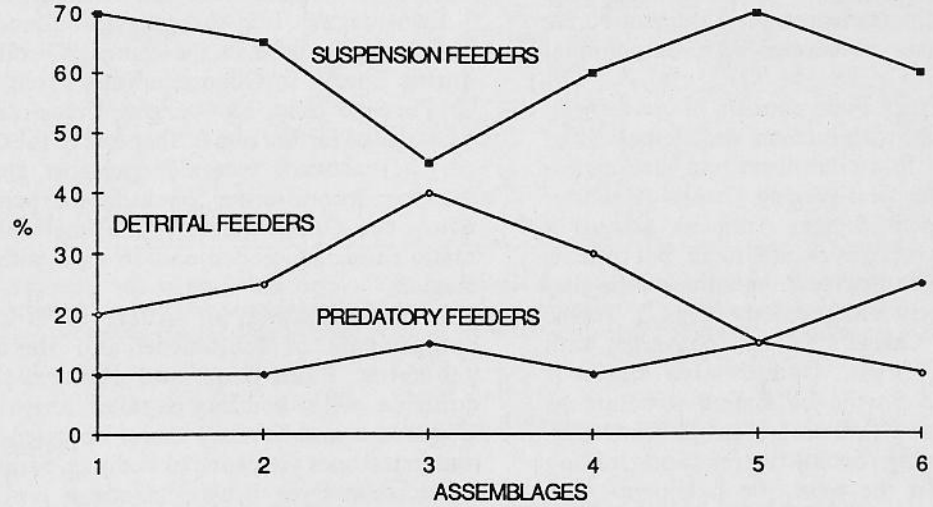

Fig. 2. Graph contrasting the feeding habits of each fossil assemblage found within the study area. Suspension-feeding organisms are dominant throughout Grayson deposition, averaging 62%, while detrital and predatory feeders comprise 23% and 15%, respectively. See Figure 1 for explanation of assemblage code numbers.

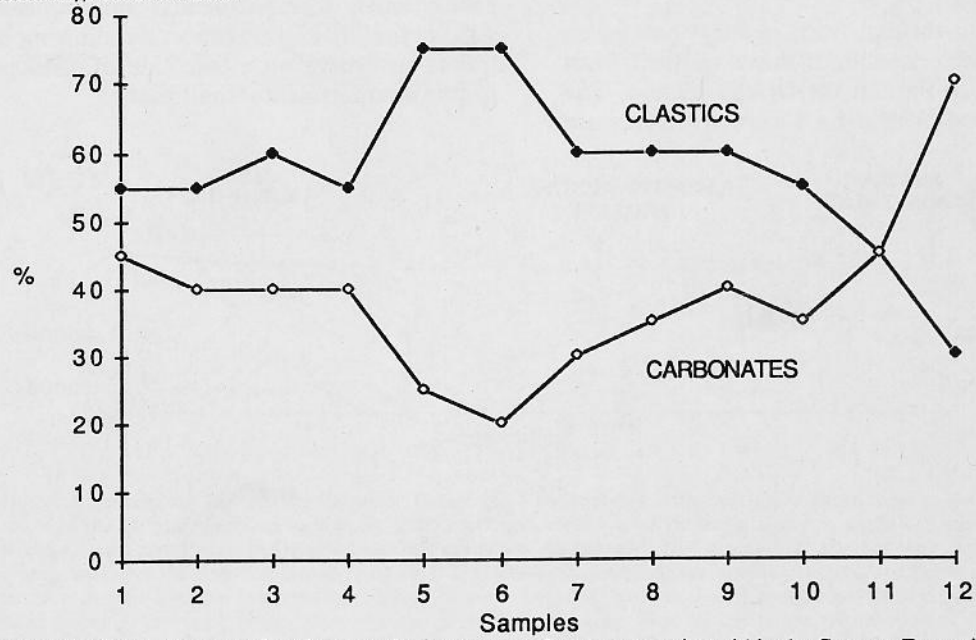

Fig. 3. Graph contrasting the percentages of terrigenous clastics versus carbonates occurring within the Grayson Formation, McLennan County. Note the sharp change in carbonate content that occurred as a result of early diagenesis during lower middle Grayson deposition. The change is roughly contemporaneous with the stunted assemblage.

Structural Geology of the Ortega Region, Upper Magdalena Valley, Colombia

George D. Allen

Convergent plate motion of the South American, Nazca, and Caribbean plates coincides with northwest-southeast compressional stress in the three Cordilleran ranges of the Colombian Andes. Foreland and overthrust style fold-thrust belts characterize the Upper Magdalena Valley and the Ortega Region within the Andes (Fig. 1). Convergent dip-slip transport on basement-cored, first-order fold-thrusts coincides with detachment folding.

Structure at the Ortega Field consists of convergent, third-order fold-thrusts, with internal decollement (Fig. 2). Tight flexural-slip folds imbricate and tectonically thicken upward on the west-verging Ortega Anticline. The buried, east-vergent Salado Anticline acts as a buttress to westward propagation at Ortega, but retreats along strike to allow the Porvenir Anticline to develop a low, broad, fault-bend fold geometry (Fig. 2). To the south, the Sortija-La Calera Fold Belt converges with the Cucuana Fold-Thrust. Compressive stress is distributed within the Sortija-La Calera structure as cross-crestal folding and thrusting (Sortija Anticline), and as opposite-verging backthrusting and folding (Tetuan Anticline). To the west, the basement-cored Vergel and Calarma fold-thrusts converge and coincide with tight, steep to overturned folding in the Chiquinima Syncline.

Five orders of fold-thrusts, from regional basement-involved to small-scale anticlines, have evolved from Oligocene to Pliocene time in the Ortega Region. The Ortega, Porvenir, and Sortija-La Calera structures are considered third-order structures. Third-order structures shorten the entire Cretaceous sequence, and may detach within the Jurassic-Triassic Payande Group. Typically preserved in the footwall of basement-cored, second-order fold-thrusts like the Cucuana Fold-Thrust, the third-order structures are significant as oil and gas traps.

East-verging fold-thrusts, accommodating crustal shortening focused in the central Cordillera, occurred during Eocene to Oligocene time. From late Oligocene to Pliocene time, east-verging first-order fold-thrusts propagated farther and farther east of the Ortega Region. As the eastward tectonic transport continued, east-dipping second-order backthrusts propagated west across the Ortega Region. The latest phase of deformation thus proceeded east to west within the Ortega Region.

In cross-section, all orders of structure exhibit components of fault-bend and flexural-slip fold geometry. Fault-bend and flexural-slip geometry coincide with bedding-parallel anisotropy. Fissile Cretaceous and Tertiary shales bounded by sandstones and limestones are prone to bedding-parallel slip. Along strike, relay-style thrusts cut across previously formed folds, and long, narrow anticlines typically form where thin brittle units are underlain by thick, detachment-prone units. Compartmental faulting accommodates differential dip-slip transport by allowing different fold trends to evolve on either side of, and perpendicular to, the compartmental fault plane.

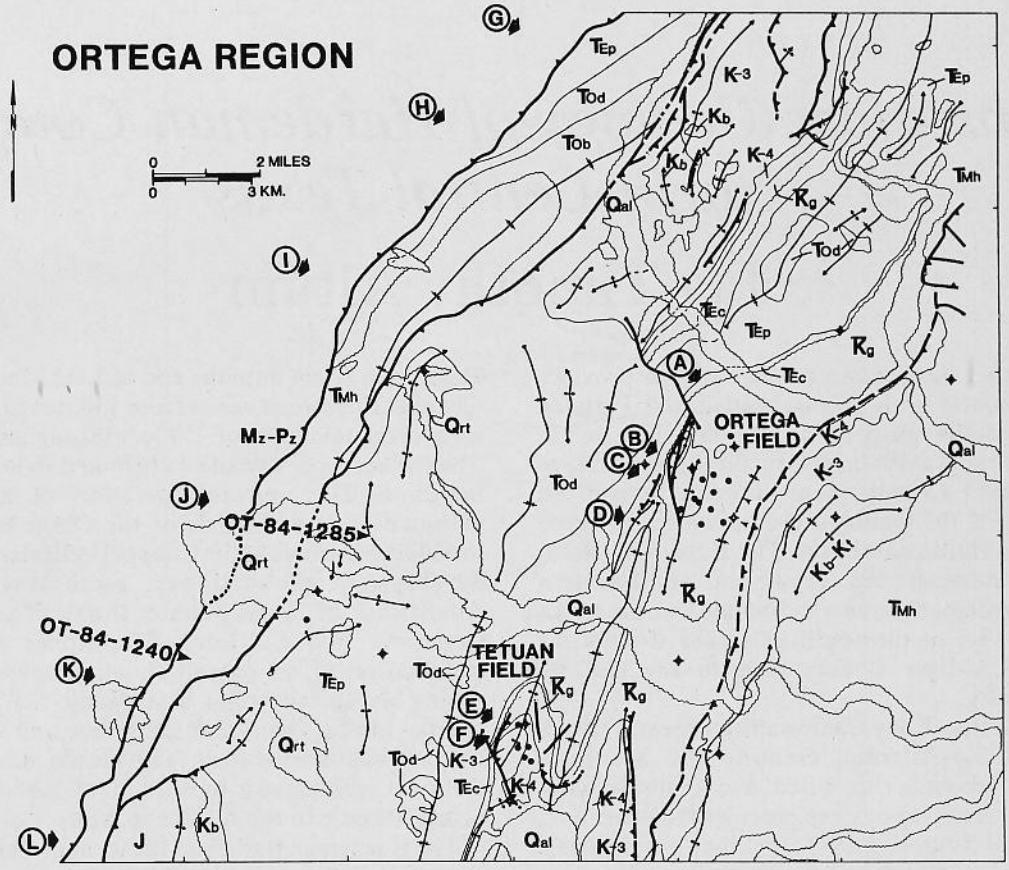

Fig. 1. Generalized geologic map of the Ortega Region. Tertiary molasse and Cretaceous marine sediments are deformed by convergent dip-slip transport on asymmetric basement-cored fold-thrusts. Multiple scales of structure evolve as volume adjustments to upward-tightening synclines. Eighty-eight percent of the surface-mapped anticlines and synclines are detached from and obscure larger structures at depth.

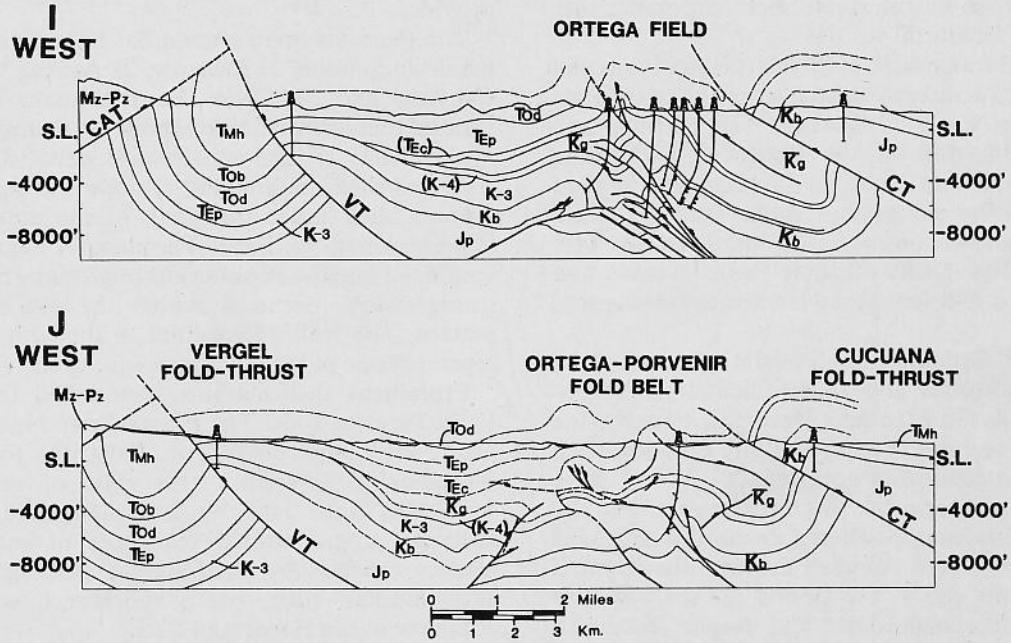

Fig. 2. Regional section. Maximum slip on the Cucuana Thrust (CT) corresponds with maximum shortening in the Cucuana Fold-Thrust footwall. Imbrication of the Ortega Anticline, as well as detachment and cross-crestal thrusting above it, cause deformation of the Guadalupe Formation (K-4) into Ortega and Porvenir Detached surface anticlines. In contrast, the structure at the Porvenir Anticline is broader, and less complex, only imbricating at the Caballos Group (Kb) level. This simpler footwall deformation corresponds to decreased slip on the Cucuana Thrust, as well as to increased distance from the converging Salado Anticline. Section J was constructed with depth-converted seismic line OT-84-1285. Dashed bedding and fault planes represent the prominent reflectors used to create the depth section. The geologic section in the wells above the Vergel Thrust (VT) appears unfaulted, constraining the Vergel Thrust to pass beneath them, and sole within the Payande Group. The Calarma Thrust (CAT) transports pre-Cretaceous crystalline basement against the Chiquinima Syncline, and is cut by the Vergel Thrust.

Subsurface Geology of Hardeman County, North-Central Texas

Jay Timothy Altum

The Hardeman Basin is an oil-rich graben province filled predominately with Pennsylvanian and Permian sediments. It is the purpose of this investigation to describe the stratigraphic and structural relationships within Hardeman County in an attempt to gain an understanding of the geologic events which occurred throughout the Hardeman Basin. The Hardeman Basin is located in north-central Texas and southwestern Oklahoma. Hardeman County is bounded to the north by the Red River, to the south by Foard County, to the west by Childress County, and to the east by Wilbarger County.

Late Precambrian-Early Cambrian continental rifting opened the proto-Atlantic, creating the Southern Oklahoma Aulacogen. This rifted and fault-bounded province is characterized by deep basement faults, which later were reactivated and form the present-day configuration of the Hardeman Basin. A reversal in plate motion, from sea floor spreading to plate convergence, occurred in early Ordovician time influencing a new stress field throughout the Texas-Oklahoma area. The rejuvenation of basement faults, due to this compressional stress, broke up the stable shelf carbonates into the present-day structural regions.

The structural framework of the Hardeman Basin and surrounding area is directly related to rifting in the Late Precambrian to Early Cambrian. This rifting, and subsequent formation of the Southern Oklahoma Aulacogen, resulted in zones of faulting proximal to the margins of the aulacogen. Major faulting within Hardeman County is confined to a dominant east-west trending fault (Fig. 1). By the Late Pennsylvanian and Early Permian, movement along reactivated fault zones had stopped.

Cambrian and Ordovician sedimentation consisted of quartz-rich sandstones and thick Ellenburger carbonates. During the Silurian and Devonian Periods, the area is thought to have been subaerially exposed, and, consequently, no deposition occurred.

Mississippian rocks lie unconformably on the Ordovician sediments. Shallow, epicontinental seas covered much of North America during Mississippian time, and near the end of this period the sea began to withdraw from the region into the deeper Anadarko Basin and the Ouachita Trough.

The Mississippian System in north-central Texas contains three series: the Osage, Meramec, and Chester. The Mississippian of Hardeman County can be divided into six formations. Lying conformably on the basal Osage Limestone are the Chappel Limestone, the St. Louis and St. Genevieve Limestones, the Barnett Shale, and the Comyn Limestone, respectively.

The Osage Limestone was deposited in an outer ramp environment. A shallowing trend continued in the Hardeman Basin until the end of Late Meramecian. The Chappel Limestone varies from 130 feet to 760 feet, with an average thickness of 350 feet throughout the county. The thicker sections can be attributed to local biohermal buildups. The upward gradation of allochthonous carbonate silts and sands of the Osage to the skeletal fossilliferous sands of the Chappel indicates a progressive development of shallower, more wave-dominated conditions of a carbonate shoal. The oolitic St. Genevieve and St. Louis Limestones represent the culmination of an overall shoaling-upwards sequence during Meramecian time. The organic-rich Barnett Shale overlies the St. Genevieve Limestone and was deposited on a normal marine shelf. This clastic influx is possibly the first sedimentary indication of the closing of the proto-Atlantic to the south and west.

The Hardeman Basin and the western Palo Duro Basin were essentially one during Pennsylvanian time. The Red River-Matador Arch system extended across north Texas during Late Pennsylvanian. This arch system acted as a buttress between the Palo Duro-Hardeman Basins and the subsiding Fort Worth Basin-Eastern Shelf province.

The Pennsylvanian section has been divided into five major rock units: 1) Morrow, 2) Atoka, 3) Strawn, 4) Canyon, and 5) Cisco. Four primary depositional systems that operated throughout the Pennsylvanian are: 1) fan-delta, 2) high-constructive delta, 3) carbonate-shelf and shelf-margin, and 4) slope and basin. A stable dipping shelf made up much of the area from Late Pennsylvanian to Early Permian. A regressive cycle continued into the Permian although many minor marine transgressions occurred within the overall regressive pattern. The Noble Limestone, a shelf-edge carbonate, repesents one of these transgressive cycles (Fig. 2).

Prominent shelf-margins surrounded the region in Early Permian time. The Precambrian highlands to the north shed large quantities of detritus to prograding fluvial-deltaic systems. This style of sedimentation continued until late Wolfcampian time, producing multiple progradational sequences of submarine fan clastics overlain by shelf-margin carbonates. By late Wolfcampian time, basin subsidence was virtually complete in the Hardeman Basin.

The Hardeman Basin is a rift-related graben that has experienced extensional and compressional tectonics. Final tectonic definition of the basin occurred during Late Mississippian and Pennsylvanian time. The stratigraphic sequences within the Hardeman Basin constitute a variety of lithologies and depositional environments ranging from Mississippian shallow-water carbonates, to Pennsylvanian fan-delta sandstones and shelf-margin carbonates, to Permian prograding shelf-margins.

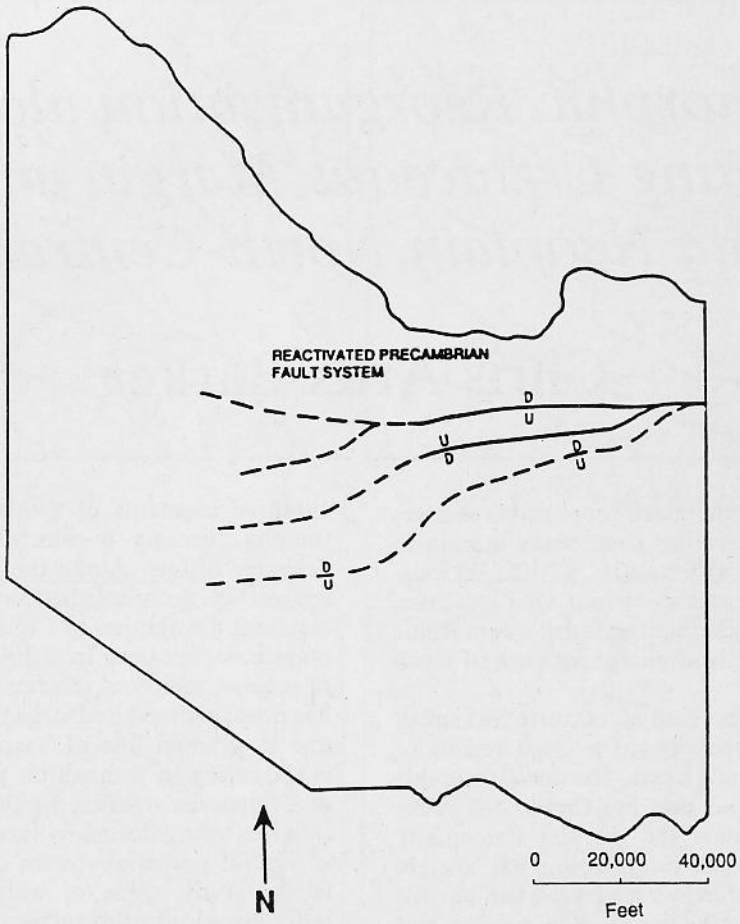

Fig. 1. Location of dominant east-west trending fault. Displacement of 500 feet across the boundary is evidenced in Ordovician formations decreasing to less than 100 feet in the Permian formations.

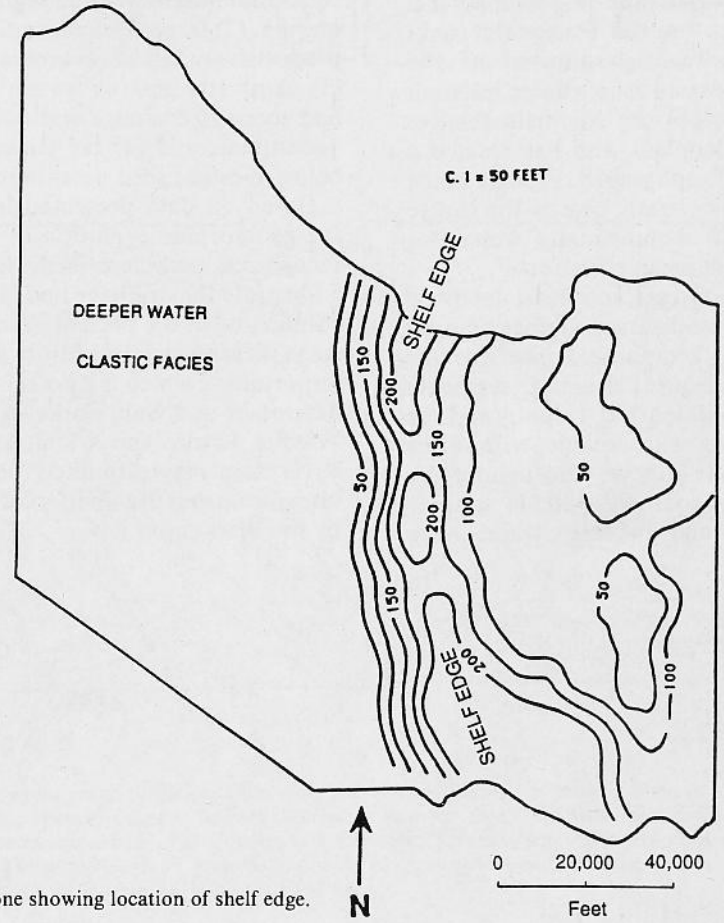

Fig. 2. Isopach of Noble Limestone showing location of shelf edge.

Geomorphic Reorganization along the Retreating Cretaceous Margin and in the Wichita Neoplain, North-Central Texas

Chris Artis Barker

This study examines pronounced geomorphic changes that occur along the retreating Cretaceous margin in a large area of north-central Texas (lat. 97-102° W, long. 31-34° N). From detailed studies at four type localities, inferences are made regarding regional geomorphic evolution as expressed in the drainage network of north Texas.

Cretaceous rocks once covered all of north Texas but have been eroded back to expose a large region of Paleozoic and early Mesozoic strata. The unconformable contact between Cretaceous and pre-Cretaceous rocks is a buried landscape called the Wichita Paleoplain. Along the retreating Cretaceous margin, that ancient landscape (which was at or below sea level when buried) is being exhumed and altered by modern erosion and is thus creating a new landscape, here named the Wichita Neoplain. The re-exposed landscape is 500-2500 feet above sea level, and relief on the Paleozoic rocks increases dramatically following removal of the Cretaceous mantle. This increased relief causes resistant units to have wider outcrops in the Neoplain relative to their subcrops in the Paleoplain, and has created a distinctive "ridge-and-valley" topography. Erosion of the uniformly dipping Paleozoic strata causes the entire Neoplain landscape to shift homoclinally westward, down-dip, while decreasing in mean elevation.

As the Cretaceous margin retreats, southeast dendritic drainage developed on Cretaceous strata is superimposed over Paleozoic rocks and is reorganized into a trellis pattern. This occurs as consequent drainage segments are defeated by resistant Paleozoic ridges, and as northeast-southwest flowing subsequent tributaries excavate the intervening shale valleys. Throughout the study area, tributaries on the southwest side of streams are extensively developed, and in many cases have captured segments of southeast consequent drainage, thereby forming a number of prominent, sinistral drainage offsets. Along the margin, drainage reorganization is accomplished by divide migration (and resultant abstraction of Cretaceous drainage) where the margin is retreating in a direction parallel to the trend of major Cretaceous streams. Past retreat of the margin has probably rendered large Cretaceous streams underfit due to gradual loss of basin area. Where the margin is retreating in a direction perpendicular to the trend of Cretaceous streams, significant drainage reorganization has been affected by large-scale stream captures.

Several potential stream capture sites are described in the study, some of which would result in major reorganizations of drainage in north Texas. Four types of streams are recognized: (1) streams on Cretaceous rocks that have never had segments west of the retreating margin; (2) large streams on Cretaceous rocks that have progressively lost basin area as the margin has retreated; (3) trunk streams (or former trunk streams) that once had access to drainage originating in the southern Rocky Mountains; and (4) far younger streams that are now being re-established on exhumed Paleozoic strata.

Based on data presented in this study, six stages in the geomorphic evolution of the Wichita Neoplain are recognized and described (Fig. 1). Stages 1 through 5 illustrate the drainage and landform changes that have culminated in the present Wichita Neoplain, and a sixth stage presents possible future drainage changes, the most important of which is a postulated capture of the Double Mountain and Salt Forks of the Brazos River by the Wichita River. The Wichita is a tributary of the Red River, and may ultimately be a product of continuing integration and domination of North American drainage by the Mississippi River.

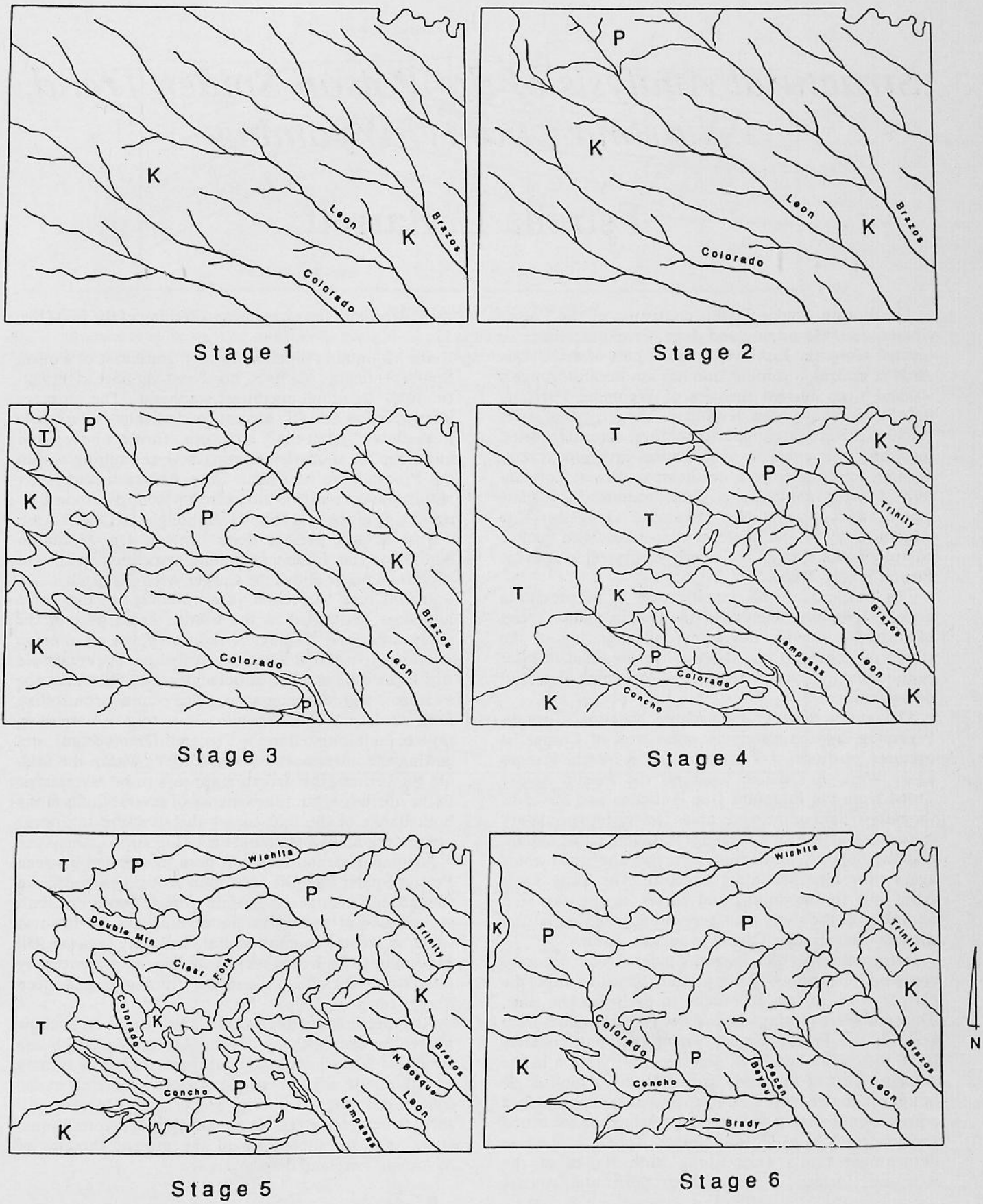

Fig. 1. Stages in the geomorphic evolution of the Wichita Neoplain and surrounding areas. Stages 1 through 6 are represented diagrammatically. The landform and drainage changes are speculative, but are based on a number of lines of evidence presented in this and in previous studies. T = Tertiary outcrop; K = Cretaceous outcrop; P = Triassic and Paleozoic outcrop. Stage 1: Cretaceous over everything; Stage 2: erosion through Cretaceous, exposure of Wichita Neoplain; Stage 3: beginning of Ogallala deposition; Stage 4: maximum eastward extent of Ogallala; Stage 5: present Wichita Neoplain; Stage 6: possible future drainage change.

Structural Analysis of the Poison Spider Trend, Natrona County, Wyoming

Estrella L. Barrett

The Poison Spider Trend, consisting of the Poison Spider, Oil Mountain, and Iron Creek anticlines, is located along the southwesternmost part of the Casper Arch in central Wyoming, and has not been thoroughly studied since current theories of Wyoming Foreland deformation have been developed. The structural styles found in this area are supportive of these current theories, including the concept of basement-involved reverse faulting resulting from a northeast-southwest horizontally directed compressive stress generated by plate convergence during the Laramide Orogeny. The structural styles and patterns associated with such a compressional system are clearly displayed within the Poison Spider Trend.

The purpose of this investigation is to present a detailed structural analysis of the Poison Spider Trend in order to provide a greater understanding of the structural geometry and styles of the area and to offer support for the present theories of Wyoming Foreland deformation.

The study area is located in Natrona County, Wyoming, approximately 16 miles west of Casper. It occupies portions of Townships 32-34 North, Ranges 82-83 West. A syncline separates the Poison Spider Trend from the Emigrant Gap Anticline and serves as the eastern limit of the study area. The western boundary terminates at the outcropping Mesaverde Formation, and the northern boundary occurs as the trend abuts against the Pine Mountain structure. The Cody Shale crops out to the south, and serves as the southern boundary of the study area, separating Iron Creek from the east-west striking Casper Mountain Fault.

Deformation of the Poison Spider Trend occurred contemporaneously with the primary thrusting along the Casper Arch in late Paleocene to early Eocene time. The southwest-verging Casper Arch Thrust exists deep beneath the Poison Spider Trend (at approximately 6,500 feet below sea level, and a seismic section in the northern part of the study area indicates a fault angle of approximately 40°. This relatively steep dip produced a prominent hanging wall arch represented by the broad asymmetric fold of Poison Spider Anticline. Reverse detachment faults exist along both flanks of the structure, formed in response to horizontal stresses associated with the ramping and arching of the fold (Fig. 1).

Oil Mountain Anticline, located southeast of Poison Spider Anticline, is a tight, northeast-verging, asymmetric fold, trending northwest-southeast. The primary interpretation for Oil Mountain Anticline is that it is a shallow "rabbit-ear" structure, thrust above, and antithetic to, southwest-verging reverse faulting within the Precambrian basement. Reverse detachment faults within the core of the structure formed in response to tightening of the fold (Fig. 2). Although the Casper Arch Thrust is still present deep beneath Oil Mountain Anticline, the basement faults associated with Oil Mountain occur above the Casper Arch Thrust.

Iron Creek Anticline, the smallest of the three anticlines, is located in the southernmost part of the study area, and displays a right stepping *en echelon* relationship with Oil Mountain Anticline. The small fold was formed by a series of detachment faults within the Paleozoic and Mesozoic strata. The primary controlling fault of Iron Creek Anticline is a southwest-verging reverse fault initiated in the Precambrian basement, and cutting the lowermost Paleozoic rocks within the fold. On the surface, the structure appears to be asymmetric to the northeast, but the existence of reverse faults along both flanks of the fold causes the structure to appear symmetric in cross sectional view (Fig. 3).

A compartmental fault has been interpreted between Poison Spider and Oil Mountain Anticlines to explain the abrupt change in surface dip between the two structures and the dissimilar asymmetries of the two folds. A second compartmental fault may separate Oil Mountain from Iron Creek Anticline, as evidenced by their structural offset, dissimilar dip angles, and steep plunge rates.

All three structures within the study area show numerous examples of detachment faults, which are thrust both northeast and southwest, and were formed as volumetric adjustments to stresses generated at the time of deformation during the Laramide Orogeny. All three structures contain many examples of deformational styles that are supportive of the present theories of Wyoming Foreland deformation.

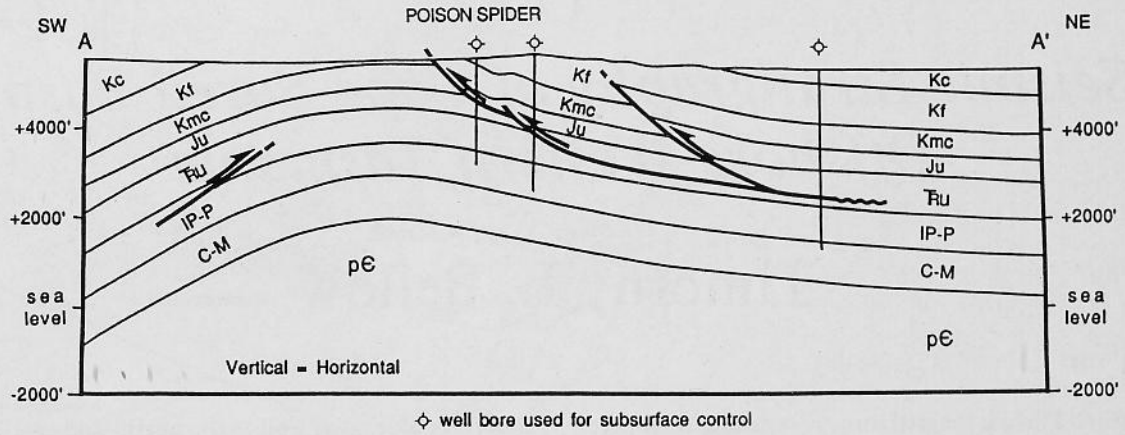

Fig. 1. Structural cross section A-A′ drawn across the southern part of Poison Spider Anticline. This broad, southwest-verging fold represents the hanging wall arch formed above the leading edge of the Casper Arch Thrust. Abbreviations: pC= Precambrian; C-M = Cambrian through Mississippian formations; IP-P =Pennsylvanian through Permian; Tru = Triassic undivided; Ju = Jurassic undivided; Kmc = Lower Cretaceous undivided; Kf = Upper Cretaceous Frontier Formation; Kc = Upper Cretaceous Cody Shale.

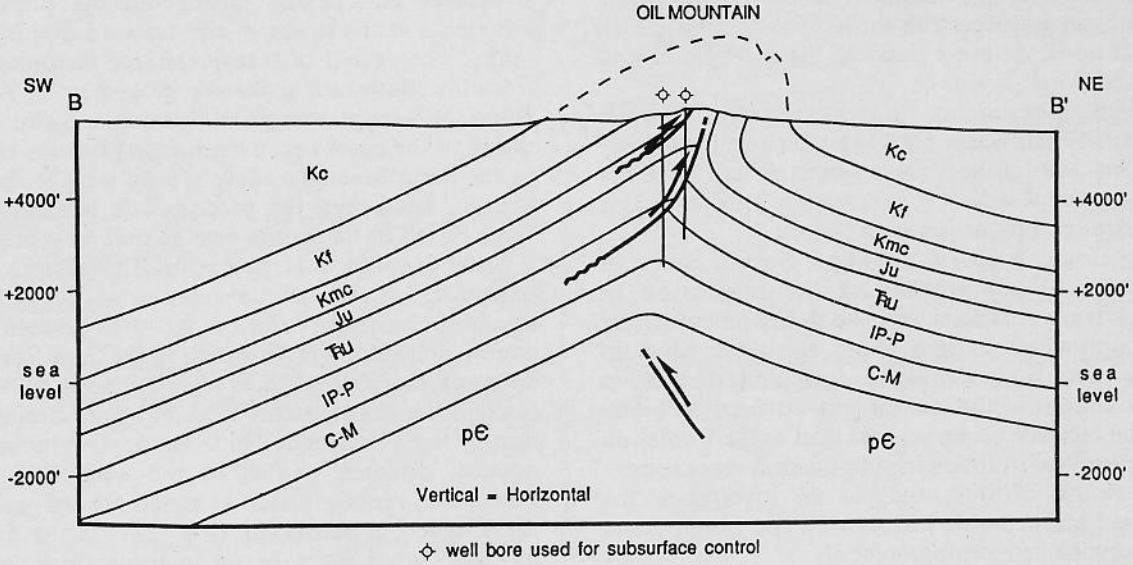

Fig. 2. Structural cross section B-B′ drawn across the central part of Oil Mountain Anticline. A small "rabbit-ear" may have existed along the northeastern flank and is shown restored above the section. Abbreviations are the same as those used in Figure 1.

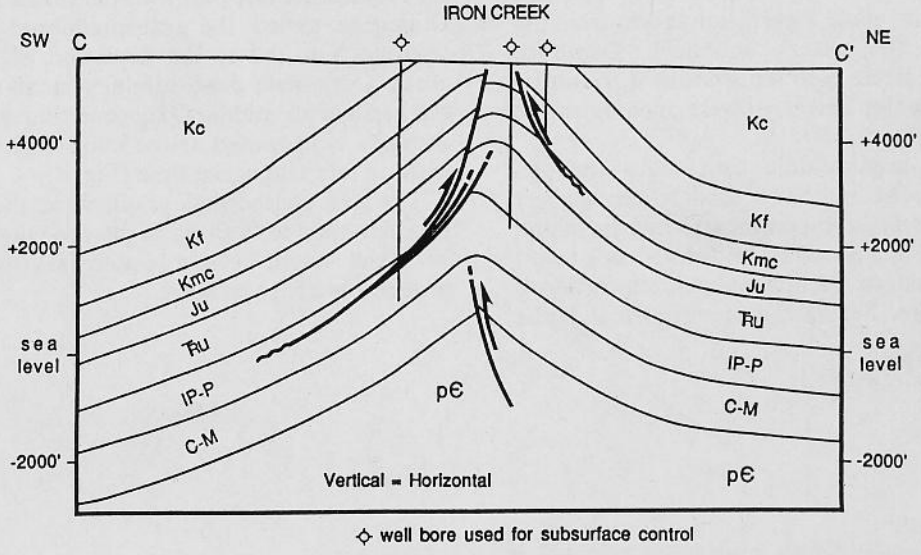

Fig. 3. Structural cross section C-C′ drawn across the northern part of Iron Creek Anticline. This tight, slightly asymmetric fold was formed by reverse detachment faulting within the Paleozoic and Mesozoic strata. Abbreviations are the same as those used in Figure 1.

Seismic Stratigraphy of Cape Sorell Basin, Offshore Western Tasmania

Timothy L. Bellow

Cape Sorell Basin is located three to ten miles offshore, midway along the western passive continental margin of Tasmania. The Cape Sorell Basin is a relatively unexplored offshore basin approximately 250 miles south of the petroleum-producing Otway Basin. This proximity and tectonic similarity to the Otway Basin, along with an unsuccessful earlier prospecting effort, warrants a more detailed study of the geologic history of the Cape Sorell Basin.

Seismic data pertaining to approximately 750 miles of the Cape Sorell Basin have been collected, but only one well has been drilled. Data from the well have not been in agreement with previous seismic interpretations of basin stratigraphy or geologic history.

The geologic history of Cape Sorell Basin is fundamental to comprehending the separation of Antarctica from Australia and the development of the passive continental margin along the west coast of Tasmania. Sediments deposited during the formation of a passive continental margin can be used to better understand tectonic processes that lead to the formation of sedimentry basins following continental separation.

The purpose of this study is to investigate the depositional and tectonic history of Cape Sorell Basin and to assess its petroleum potential.

The basin is shaped roughly like an upside-down boot and covers approximately 600 square miles, most of which lie between south latitudes 42°00′ and 42°30′. A west-northwest trending fault system forms the northern boundary of the basin, while a north-northwest trending fault system forms the eastern boundary. Depth to acoustic basement decreases to the southwest, resulting in a northern depocenter and northwest opening to the Indian Ocean.

Sediments of at least middle Cretaceous through Recent age are present and were used to reconstruct the evolution of the passive continental margin along western Tasmania. Cape Sorell Basin formed as a result of the breakup of eastern Gondwanaland, which began 160 million years ago. Seaward-dipping normal faults and fault blocks, as well as the north- and east-bounding fault systems, formed as a result of continental extension that continued into the Late Cretaceous. A period of transpressional tectonics followed continental extension, resulting in the formation of wrench zones and flower structures that persist throughout the pre-Oligocene sediments at the heads of the seaward-dipping normal faults. The period of transpressional tectonics resulted from the southward strike-slip movement of Antarctica along the western margin of Tasmania. Subsidence and tilting of the basin oceanward since the early Oligocene, as the basin became a more typical passive continental margin, have been the predominate tectonic styles of Cape Sorell Basin for the past 34 million years.

Stratigraphic interpretation of seismic profiles indicates that ten distinct depositional sequences were involved in the evolution of the western passive continental margin of Tasmania in the Cape Sorell Basin. Two non-marine sequences record deposition by alluvial fan and fan delta systems in a southward-draining basin during the Cretaceous (Fig. 1). As the Indian Ocean opened, drainage shifted to the west, and by early Paleocene, deeply incised channels flowed west across the Cretaceous sediments (Fig. 2). Marine deposition in Cape Sorell Basin began in the early Paleocene as the Indian Ocean transgressed onto the basin. Fluvial-deltaic deposition characterized the basin from the Paleocene into the Oligocene (Fig. 3). The clearance of the Antarctic Plate past the Australian Plate in the early Oligocene ended the transpressional phase of basin tectonics and led to the depletion of sediment source areas. Carbonate depositional systems have dominated the basin since middle Oligocene time and a barrier reef complex is proposed as the main depositional environment in late Oligocene time (Fig. 4).

The low geothermal gradient of the basin and the pervasiveness of faulting in the pre-Oligocene sediments give the basin a low potential for economically producible hydrocarbons.

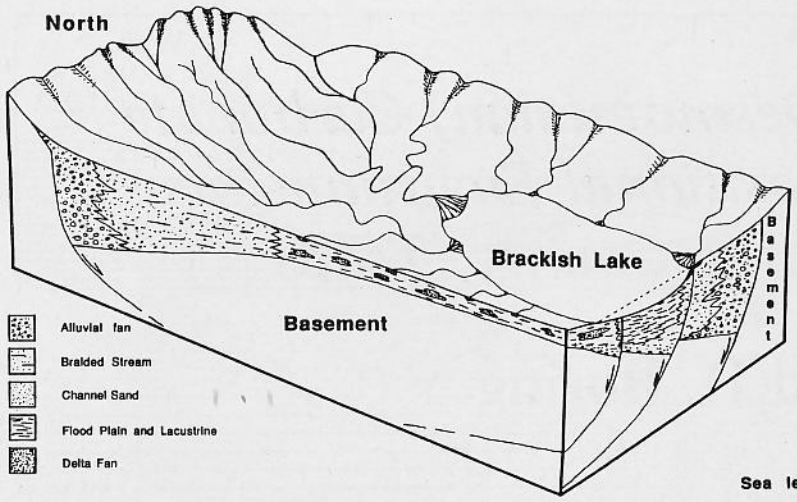

Fig. 1. Block diagram illustrating non-marine, alluvial fan and fan delta deposition during the Cretaceous.

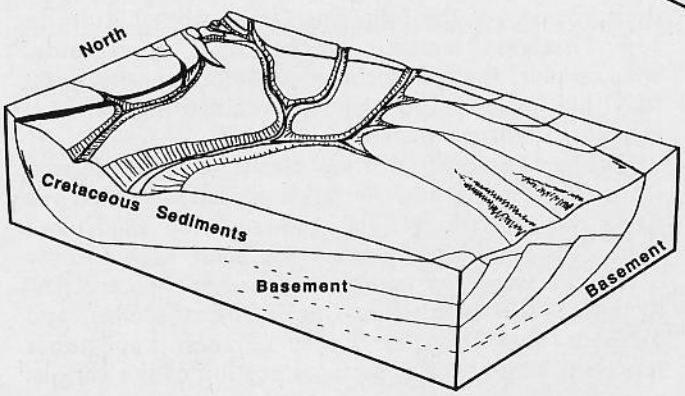

Fig. 2. Block diagram illustrating westward drainage and deeply incised canyons in the early Paleocene.

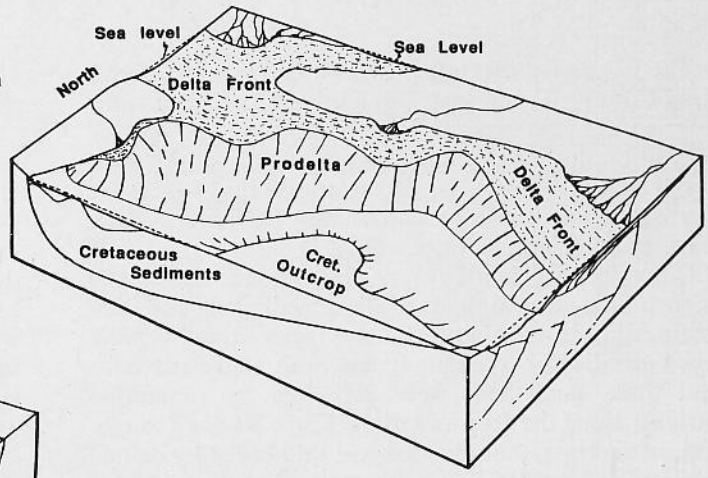

Fig. 3. Block diagram illustrating fluvial-deltaic deposition of the earliest Eocene sequence, which is characteristic of the basin depositional style from the Paleocene into the Oligocene.

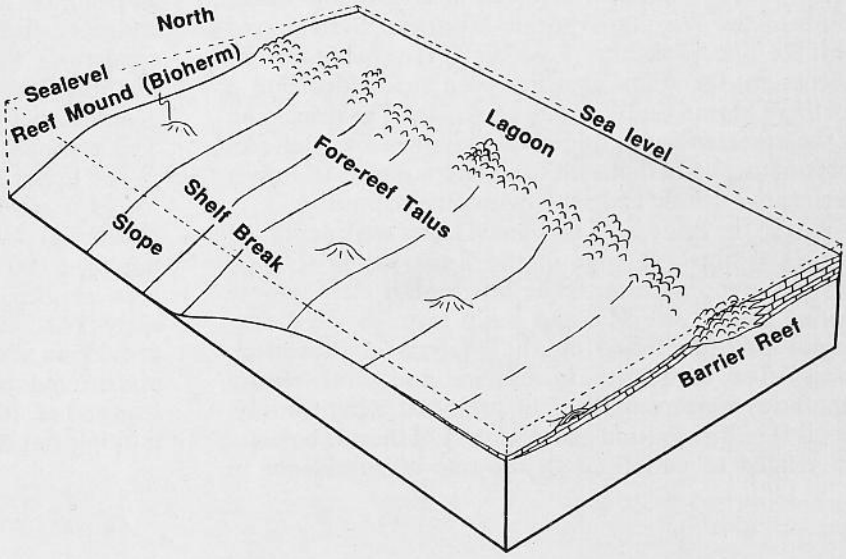

Fig. 4. Block diagram illustrating deposition of the late Oligocene sequence. A barrier reef complex is proposed as the main depositional system.

Upper Strawn (Desmoinesian) Carbonate and Clastic Depositional Environments, Southeast King County, Texas

Todd H. Boring

The Pennsylvanian upper Strawn Group of southeast King County, Texas, provides a unique setting to study interactions between coeval carbonate and clastic deposition during Desmoinesian time. One of the most perplexing problems is the relationship of massive Pennsylvanian platform carbonates to shallow-water marine and deltaic sediments (Fig. 1).

Considerable controversy has arisen about the depositional environments of clastic sediments and their relationship to massive carbonate facies in and around the Knox-Baylor Trough. It has been suggested both that these sandstones were deposited by submarine currents along the deep axis of the Knox-Baylor Trough, and, in contrast, that the area was influenced by deltaic processes. Therefore, the principal objectives of this investigation were to 1) resolve the conflicts by clearly defining the upper Strawn Group carbonate and clastic depositional environments within southeast King County, Texas, and 2) understand and interpret the facies relationships between the carbonates and clastics.

The area of investigation (approximately 270 square miles) is located in the southeast portion of King County, north-central Texas, between the cities of Lubbock and Wichita Falls. This area is on the northwestern edge of the Concho Platform, northeast of the Midland Basin, south of the Wichita-Arbuckle Mountain System, and west of the Ouachita Fold Belt. To facilitate the discussion, the study area has been subdivided into a northern region and a southern region. The discussion of the northern region addresses shallow-water platform carbonates, while that for the southern region addresses terrigenous deltaic and shallow-marine sediments.

Within the study area, carbonate facies were deposited along the northern edge of the Knox-Baylor Trough on the Spur Platform, while terrigenous clastics were carried toward the Midland Basin through the Knox-Baylor Trough. Based on the analysis of subsurface cores, five carbonate lithofacies and four clastic lithofacies were recognized in southeast King County, Texas. The distribution and geometry of these lithofacies are related to variations in the rate of subsidence in the Knox-Baylor Trough, Pennsylvanian tectonics, deltaic progradation, avulsion, and compaction.

The platform carbonates within the northern region of southeast King County record environments within the carbonate platform complex, including mid-platform, outer-platform, algal mound, and platform margin environments (Fig. 2). The typical carbonate cycle consists of the following facies, from bottom to top: 1) algal bioclastic wackestones; 2) crinoidal wackestones; 3) algal bioclastic packstones-grainstones/ fusulinid crinoidal packstones-grainstones; and 4) crinoidal bryozoan wackestones/shales.

During Desmoinesian time, clastic sediment derived from the Wichita and Arbuckle mountains filled the Knox-Baylor Trough. The quartzarenitic sandstones within the southern region of southeast King County occur in a variety of complex depositional geometries, including distributary bar fingers, lobate deltas, and offshore bars (Fig. 2). Cores of these sandstones represent mainly the uppermost portion of the various sand bodies. A typical core consists of the following facies, from bottom to top: 1) cross-bedded sandstones; 2) intercalated sandstones and shales; and 3) mudstones/ shales. The depositional model for the upper Strawn (Desmoinesian) of southeast King County has been conceptualized primarily from the tectonic setting, sandstone body geometry, sedimentary structures, textures, lateral and vertical facies relationships, and general lithologic sequence of the carbonates and clastics. This model is illustrated in Figure 2.

The upper Strawn Group provides an attractive area for exploration geology. Both carbonates and clastics provide excellent reservoirs from a depth of approximately 5,000 to 6,000 feet. Total production within the area has been over 100,000,000 barrels of oil since the early 1940s. Multiple pay zones within a 600-foot interval provide an added incentive for exploration. Areas within and around the Knox-Baylor Trough deserve additional study due to these relatively shallow, unexplored, multiple pay zones.

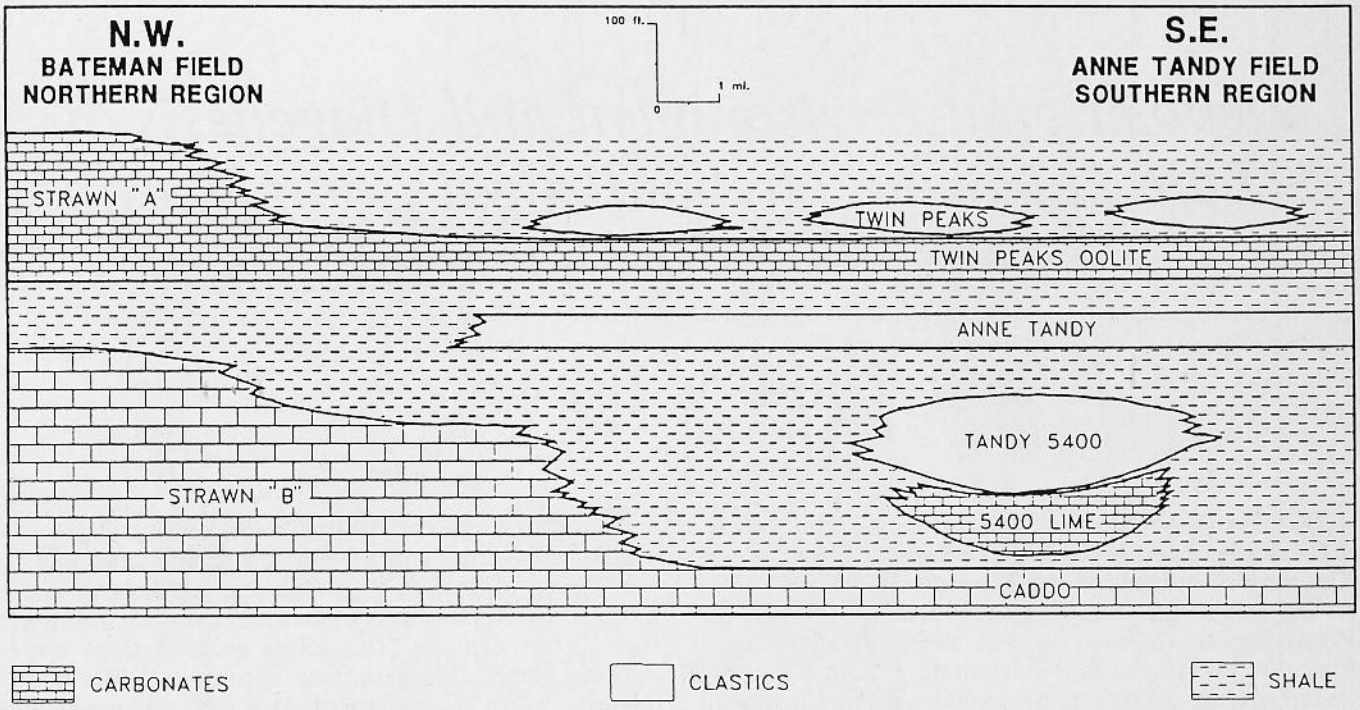

Fig. 1. Generalized cross section through southeast King County, Texas.

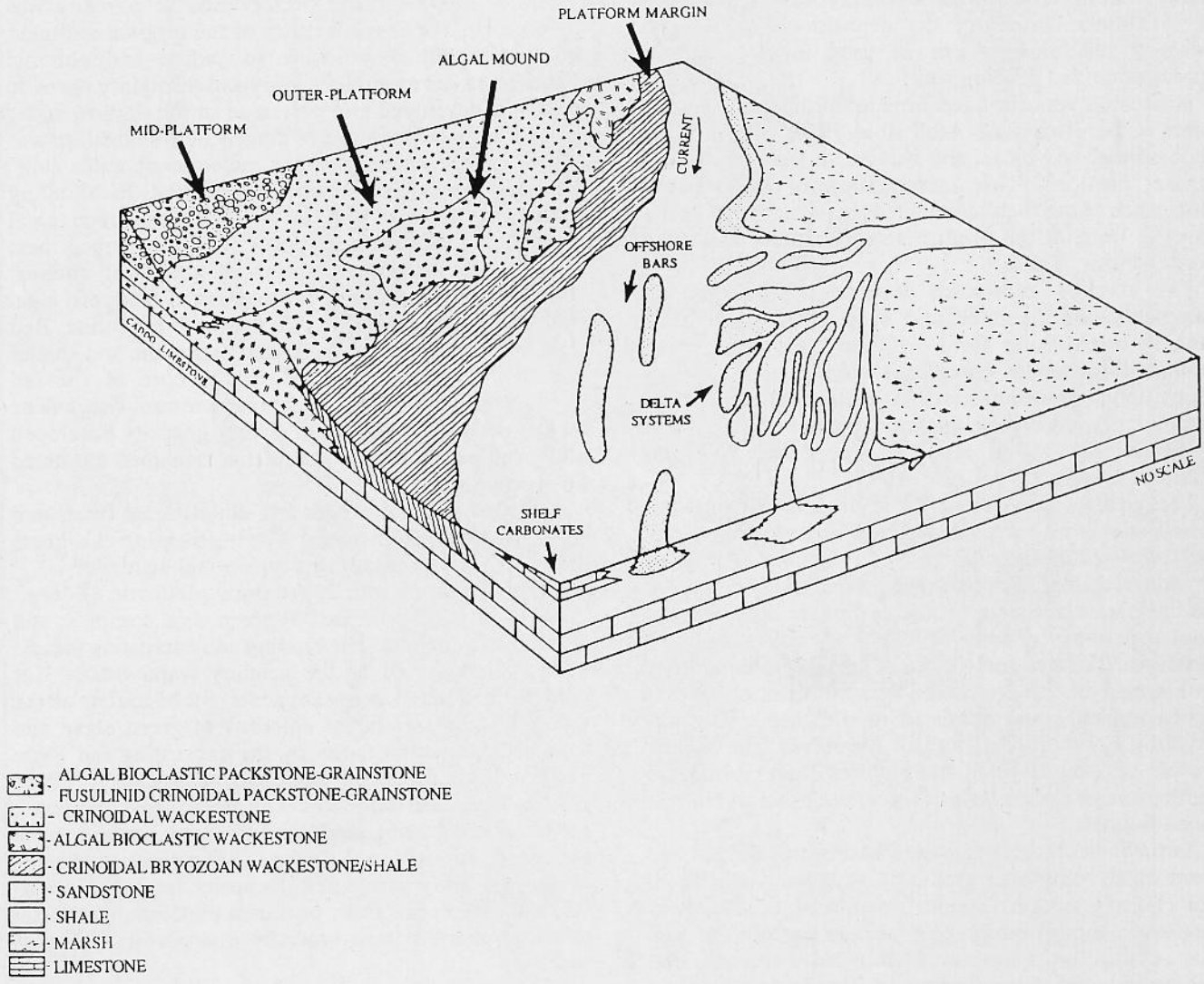

Fig. 2. Generalized depositional model and lateral facies relationships for southeast King County during upper Strawn (Desmoinesian) time.

Depositional Environment and Diagenesis of Late Paleozoic Phylloid Algal Complexes: Western Horseshoe Atoll

Todd A. Brown

The Horseshoe Atoll occupies an eight-county area in the northern part of the Midland Basin of West Texas. The western portion of the Horseshoe Atoll contains several in a series of oil fields that produce from Late Pennsylvanian (Missourian and Virgilian) and Early Permian (Wolfcampian) carbonate sediments. An understanding of the depositional setting of these carbonate accumulations can be used in predicting where similar mounded carbonate facies may occur. Knowledge of the lateral extent of the depositional facies and porosity relationships can be used in hydrocarbon exploitation and development.

Numerous reports have been published on various parts of the Horseshoe Atoll since 1950, with detailed depositional and diagenetic studies on the eastern and central portions. This investigation of the western Horseshoe Atoll was conducted by examining seven cores in three of the productive carbonate buildups in Terry County, Texas.

The stacked carbonate sequences developed as complex bioaccumulated and bioconstructed features ranging in thickness from 1,100 to 2,800 feet. These mounded carbonate complexes consist of six major depositional environments that include: 1) green algal complex; 2) red algal complex; 3) shoal and channel; 4) debris flow; 5) proximal platform; and 6) distal platform margin.

The red algal complexes contain *Archaeolithophyllum lamellosum* as an encrusting form of ancestral red algae, and *Archaeolithophyllum* cf. *A. missouriensis* as a phylloid red algae. The red algae preferentially colonized the basinward perimeter of the carbonate buildups and was a primary frame-builder and volumetrically significant skeletal contributor. Green algal complexes proliferated in the protected, leeward areas of the red algal complexes and consisted of the genera *Eugonophyllum, Epimastopora,* and cf. *Ivannovia.* The prolific growth of green dasyclad and phylloid algae constituted another major skeletal contributor, but not a significant frame-builder.

As the facies tracts prograded basinward, the red and green algal complexes gradually gave way to a shoal and channel system. Storm, wave, and tidal activity resulted in the formation of coated grainstones as well as the deposition of significant amounts of cross-bedded and graded tidal channel deposits. Also during the more emergent stages of the algal buildups, carbonate debris generated by storm and wave action accumulated along the flanks of the algal complexes. Lithoclasts and bioclasts from almost every facies are represented within these debris deposits. The debris accumulations may have developed into carbonate aprons or debris flow deposits, which became interbedded with proximal and distal platform margin deposits (Fig. 1).

The development and preservation of porosity was governed by the characteristics of the original sediment and the length of exposure to vadose and phreatic diagnetic environments. Primary and secondary porosity were best developed and preserved in the shallow water facies where the last stage of diagenetic stabilization was in the vadose zone or upper meteoric phreatic zone. The best reservoir porosities occurred in shoaling grainstone deposits and in the red and green algal complexes. Interparticle porosity is developed best between the carbonate grains of the tidal channel deposits. Moldic porosity is prevalent in the green algal complexes due to the unstable nature of aragonite. Red algal complexes are characterized by moldic and shelter porosity. Leaching occurred in the core of the red phylloid grains where unstable magnesium-rich calcite readily dissolved. Abundant shelter porosity developed under red phylloid algal grains that remained unaltered by dissolution.

The succession of prograding depositional facies and diagnetic fabrics indicates a slowly emerging carbonate platform. The prograding depositional sequence is: 1) distal platform margin; 2) proximal platform; 3) debris flow; 4) red algal complex; 5) green algal complex; and 6) shoal and channel. The binding and encrusting forams of red algae served as the primary frame-builder for these "reefal" carbonate sediments. Stabilization of the volumetrically significant amounts of green algae and shoaling grainstone facies by the encrusting red algae allowed these mounded carbonate sediments to attain very thick vertical sequences. The green algal complexes, red algal complexes, and tidal channel deposits were the only depositional facies containing consistent reservoir-quality porosities. Deposits from the grainstone shoals, debris flow, proximal platform, and distal platform margin were typically non-porous reservoir rocks.

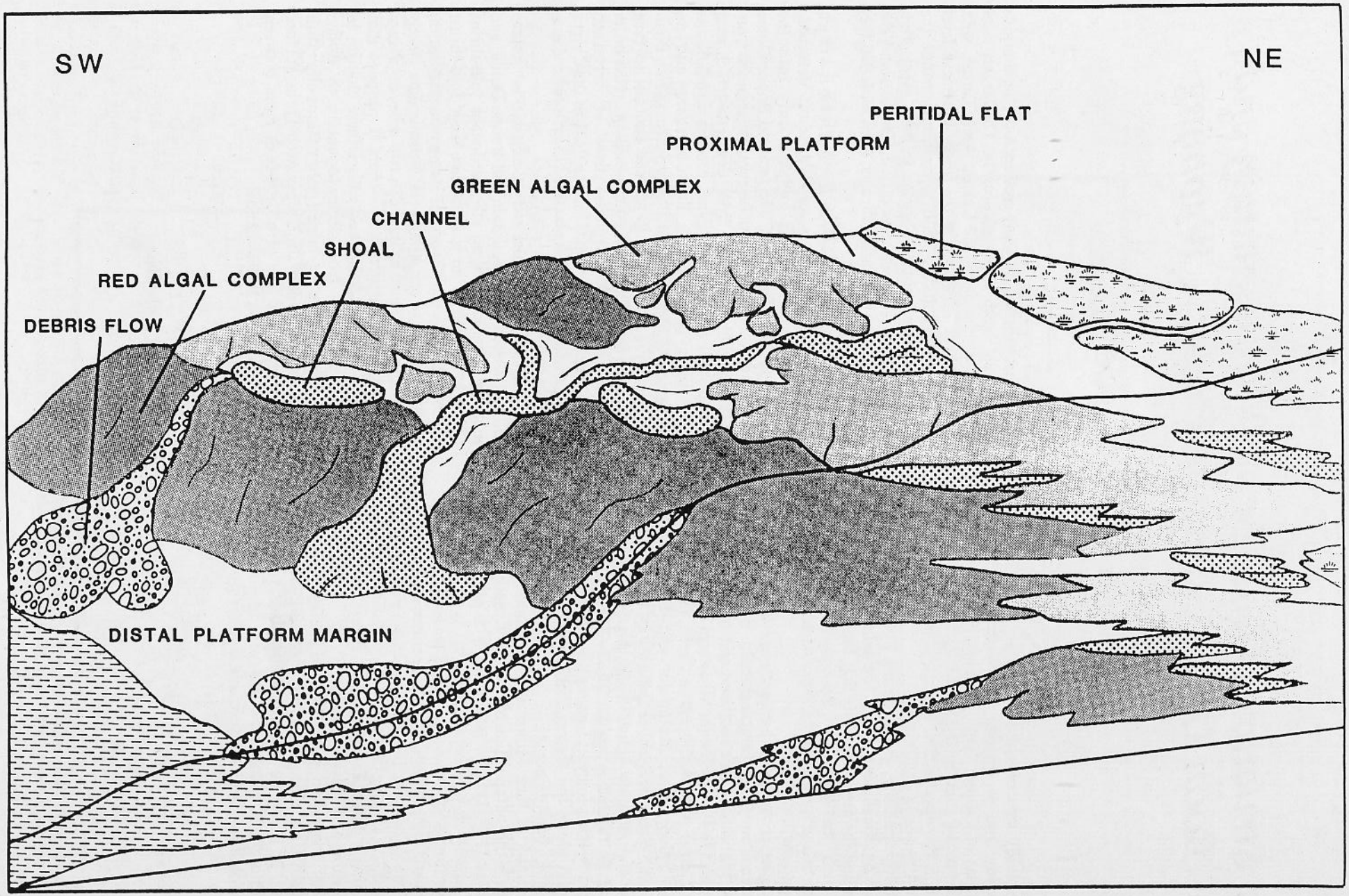

Fig. 1. Depositional model depicting the prograding environmental facies.

Structural Geology of Pine Mountain and Boon Dome, Natrona County, Wyoming

David P. Cercone

The study area occupies 110 square miles in central Wyoming and is located approximately 35 miles northwest of Casper, Wyoming on U.S. Highways 20, 26. The study area is part of the deformed Wyoming Foreland Province which, in turn, is part of the larger North American Cordillera.

Physiographically, the Wyoming Foreland is characterized by areally-extensive, low-relief intermontane basins and the majestic uplifts that border them. In the study area, the Wind River Basin forms the low-relief western boundary, while the Casper Arch forms the high-relief eastern boundary.

The Casper Arch is a Laramide-age tectonic feature that trends northwest-southeast and is terminated at Casper Mountain to the southeast and at the Owl Creek Mountains to the northwest. Structures along the trend of the Casper Arch include: Iron Creek, Oil Mountain, Poison Spider, Pine Mountain, and Boone Dome anticlines; Waltman Syncline; plus the minor structures of Lox and Arminto anticlines. Stratigraphic relationships at Hell's Half Acre (sec. 36, T. 36 N., R. 86 W.) and spore-pollen analyses from well bores document that the uplift along the Casper Arch occurred from late Paleocene to early Eocene.

The uplift of Pine Mountain and Boone Dome has resulted in the juxtaposition of two significantly different structures (Fig. 1). Pine Mountain is a near circular, open, southwest-vergent anticline that is exposed well into the Jurassic Sundance stratigraphic level. Deep well control and high-quality, multifold seismic data indicate that Pine Mountain is an advanced-stage, basement-involved, Wyoming Foreland fold-thrust structure containing a large, fault-bounded, overturned section of Paleozoic and Mesozoic rocks.

If well control from the Moncrief 1-35 West Pine Mountain Unit is projected into the line of section A-A′ (Fig. 2) it can be determined that the 21,200 feet of uplift of the Precambrian basement is accommodated by the folding of the basement, and is offset along large-displacement thrusts. In cross section A-A′, separations or individual faults vary significantly. The largest fault separation occurs along the Casper Arch Thrust, with a separation of 7,300 feet at the upper basement level cutoff. Other significant fault separations include the CAT-1 Thrust (a frontal imbricate to the Casper Arch Thrust), with a fault separation of 5,500 feet, and the Burgess and Pine Mountain thrusts, each with 300 feet of fault separation.

In contrast to Pine Mountain, Boone Dome is a much smaller surface feature. It is an asymmetric, detached, anticlinal structure and is exposed only into the Cretaceous Cody Formation. The fact that Boone Dome is a detached and rootless structure was determined from well and seismic data and from depth-to-detachment calculations. Furthermore, seismic profiles across Boone Dome imply that there is little overhang and no overturning of Mesozoic and Paleozoic rocks in a dual-fault zone (Fig. 3). This is in marked contrast to Pine Mountain, which has a basement overhang on the order of 22,000 feet and an enormous "sliver" of overturned rocks in a dual-fault system. Thus the flank of the Casper Arch under Boone Dome is classified as an intermediate-stage fold-thrust.

In order to explain the radical change in surface geology between Pine Mountain and Boone Dome, and the abrupt change from an advanced-stage fold-thrust at Pine Mountain to an intermediate-stage fold-thrust at Boone Dome, the theory of compartmentalization has been applied to the study area. Seismic data clearly show that in a distance of less than two miles an abrupt change in structural geometry occurs. I propose that a buried, left oblique-slip fault causes these changes in structural geometry from Pine Mountain to Boone Dome. Furthermore, a buried left oblique-slip fault explains the left offset of the Casper Arch Thrust surface projection and the loss of a dual-fault zone between Pine Mountain and Boone Dome.

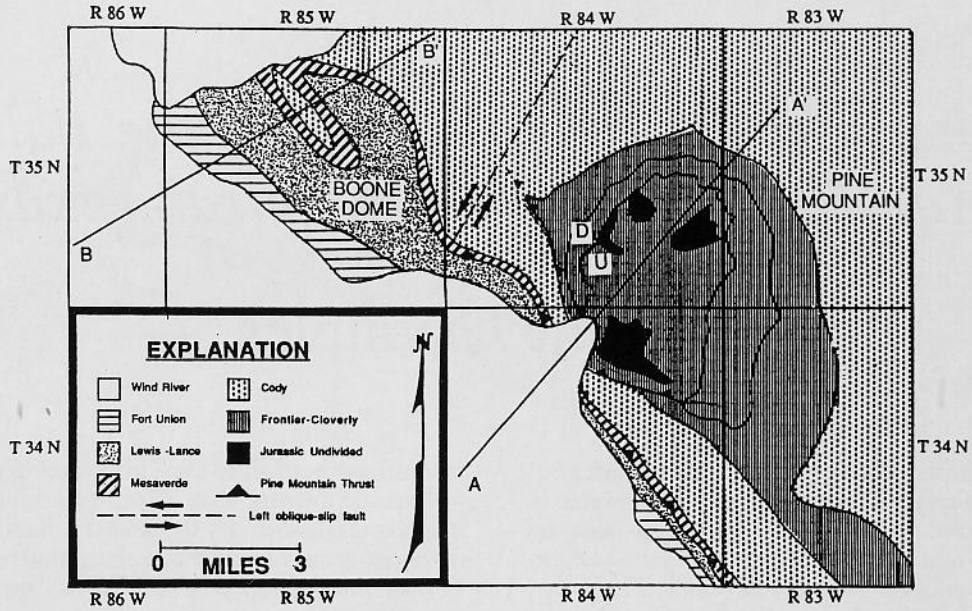

Fig. 1. Generalized geologic map of the study area. The drastic difference in the surface geology between Pine Mountain and Boone Dome may be caused by a buried, left oblique-slip fault.

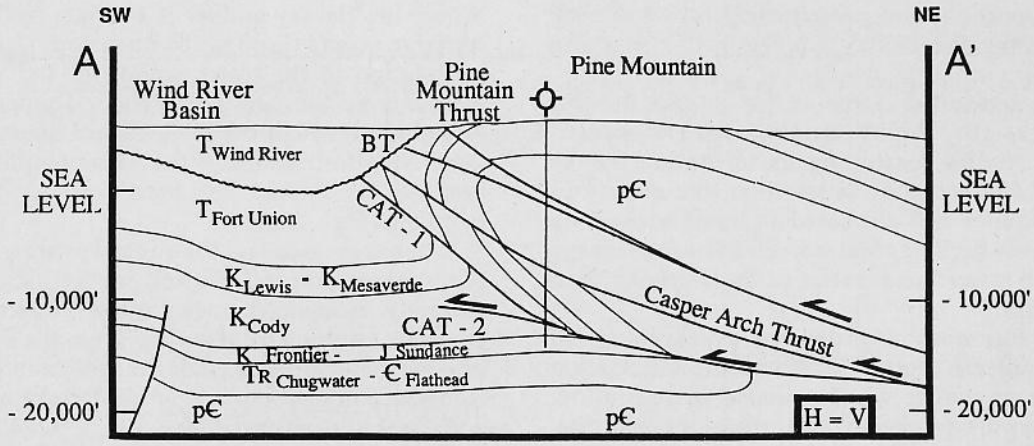

Fig. 2. Cross section A-A′ across Pine Mountain. The tremendous overturned section of Paleozoic and Mesozoic rocks in a dual-fault zone indicates that Pine Mountain is an advanced-stage, fold-thrust structure.

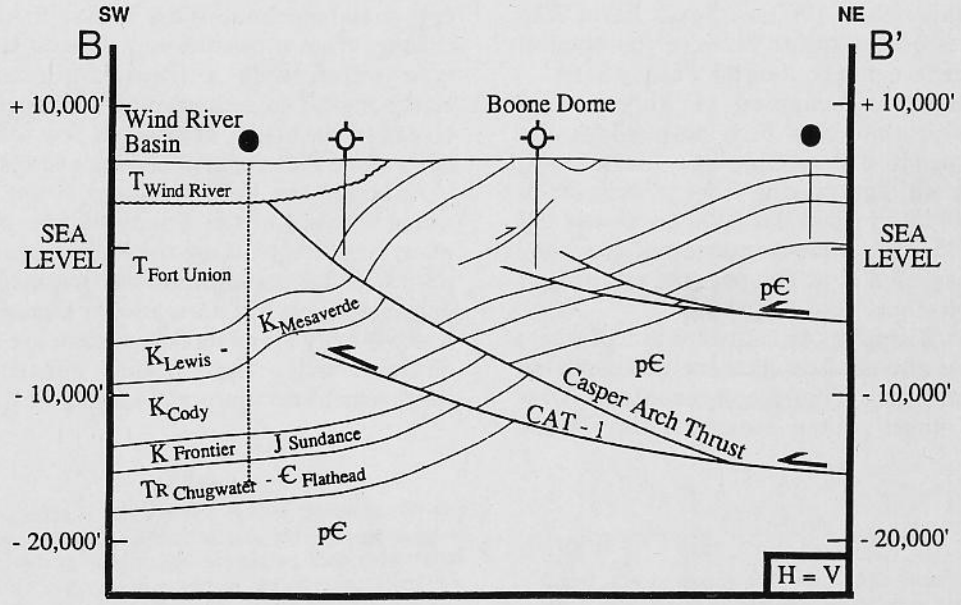

Fig. 3. Cross section B-B′ across Boone Dome. Well data and seismic data clearly show that the current petroleum production is from a detached, rootless structure in the Cody Shale. Because Boone Dome lacks a dual-fault zone it is interpreted to be an intermediate-stage, fold-thrust structure.

Recharge and Water Quality of the Paluxy Aquifer Flow System, Central Texas

Dwayne Crumpler

The Paluxy aquifer is considered a minor aquifer but serves as a significant municipal resource for water in north-central Texas. The Paluxy aquifer is also an important water resource for Bosque, Coryell, McLennan, Somervell, and Hill Counties in central Texas, but is utilized principally for domestic and stock purposes. Because the Paluxy aquifer system of central Texas is not a major municipal source, it is less studied than the northern portion, and consequently little has been written regarding the Paluxy aquifer in this southern region.

Increasing demands on the major aquifer in this southern area, the Trinity aquifer, have prompted groundwater studies concerning its utilization by the Texas Water Commission. In addition, the quality of the Trinity aquifer has decreased in some areas as a result of severely declining water levels inducing leakage from the more mineralized waters of the overlying Glen Rose Limestone.

Therefore, this study describes the hydrogeology of the Paluxy aquifer in central Texas with the anticipation that the Paluxy aquifer will be needed in the future, and these data will be an aid to future decisions regarding water management.

The study area is largely on the Central Texas Platform and extends eastward beyond the Balcones Fault Zone onto the western margin of the East Texas Basin. The study concentrates on the region between the outcrop belt and the subsurface pinchout of the Paluxy Sand.

The Paluxy Sand is composed of white to red quartzarenite, with thin clay beds throughout the formation. The sands are medium- to fine-grained, grading to coarse silt, and ranging from subangular to subrounded. The Paluxy Sand has an approximate dip of 15 feet per mile in the western portion of the study area, increasing eastward to 80 feet per mile as it crosses the Balcones Fault Zone.

Regionally, flow directions are eastward except where modified by major streams and the cone of depression near pumping centers. Topography controls flow directions more directly than structural dip in the unconfined portion of the Paluxy aquifer (Fig. 1).

Climatic factors that affect potential recharge also increase eastward. In the Paluxy Sand outcrop belt, recharge occurs primarily during short-term precipitation events (largely confined to the spring and winter months).

Recharge occurs through infiltration on the Paluxy outcrop belt and by leakage from overlying formations. Where the Paluxy aquifer is overlain by Walnut Clay, recharge occurs through the numerous flaggy limestone beds found in the lower section of the Walnut Clay. Recharge to the confined Paluxy aquifer also occurs as leakage through the Glen Rose Limestone from the underlying formations of the Trinity aquifer where the head in the Paluxy has been reduced due to heavy pumping (Figs. 2 and 3).

Discharge occurs through springs, seeps, and evapotranspiration, as well as artificially through pumping. A minipiezometer study shows an increase in baseflow resulting from leakage from the Paluxy aquifer into the major streams during the fall months. Discharge from the confined portion of the Paluxy aquifer occurs both laterally and vertically.

Total dissolved solids within the Paluxy aquifer increase eastward from 300 mg/l to 4000 mg/l. The aquifer is slightly saline from the central portion of the study area to the pinchout of the Paluxy Sand. Water quality changes from a calcium-bicarbonate to sodium-sulfate type water, with a transition phase of sodium-bicarbonate.The sodium-bicarbonate phase is a result of cation exchange of calcium for sodium within the clays of the Paluxy Sand and the overlying Walnut Clay.

Although the Paluxy aquifer is not as significant a water resource as the Trinity aquifer in central Texas, many rural residents use the Paluxy aquifer for domestic purposes. Its contribution to streams as baseflow, its dependency on interformational leakage, and changing water quality along its flow system are hydrogeological characteristics that should benefit future water management decisions and initiate further studies.

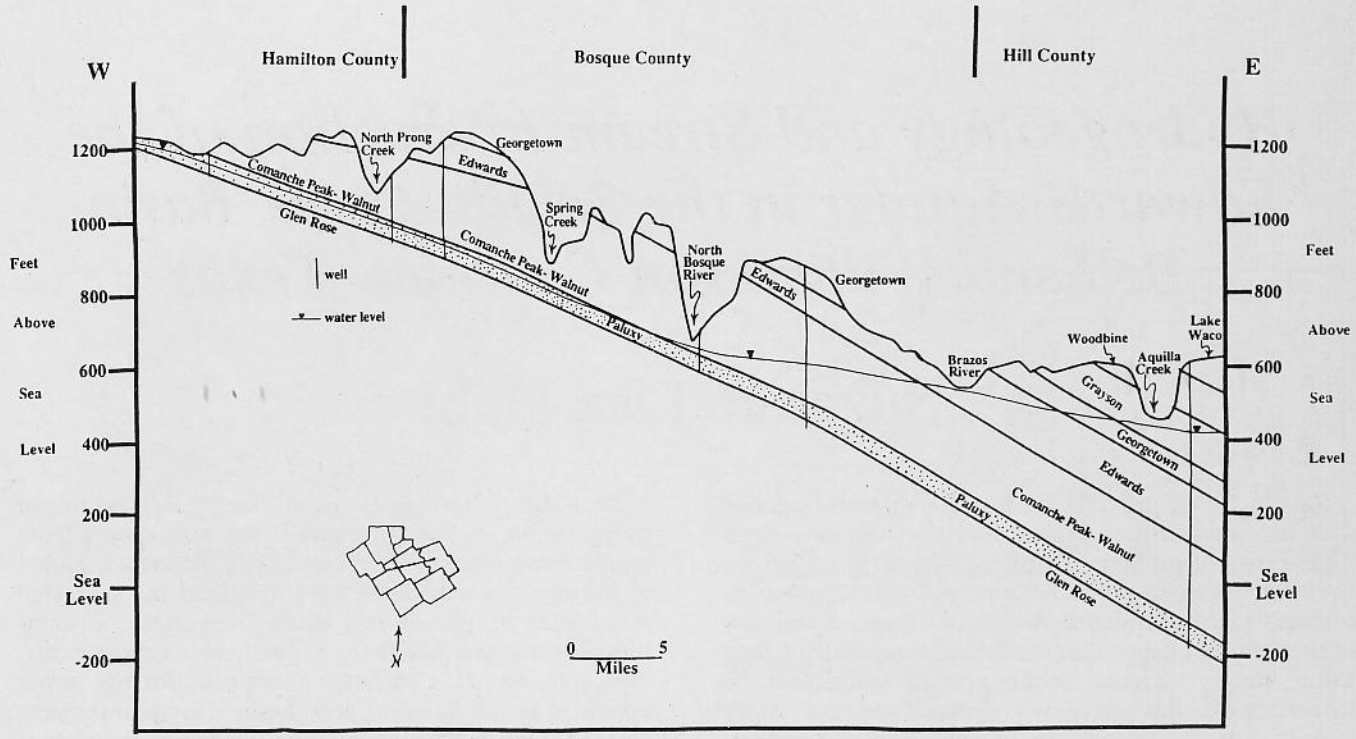

Fig. 1. Regional cross section showing topography, geology and groundwater levels. The Paluxy aquifer changes from an unconfined system to a confined system west of the North Bosque River. The water table is approximately 1200 feet above mean sea level in Hamilton County, and the potentiometric surface is about 410 feet above mean sea level in Hill County, east of Aquilla Creek.

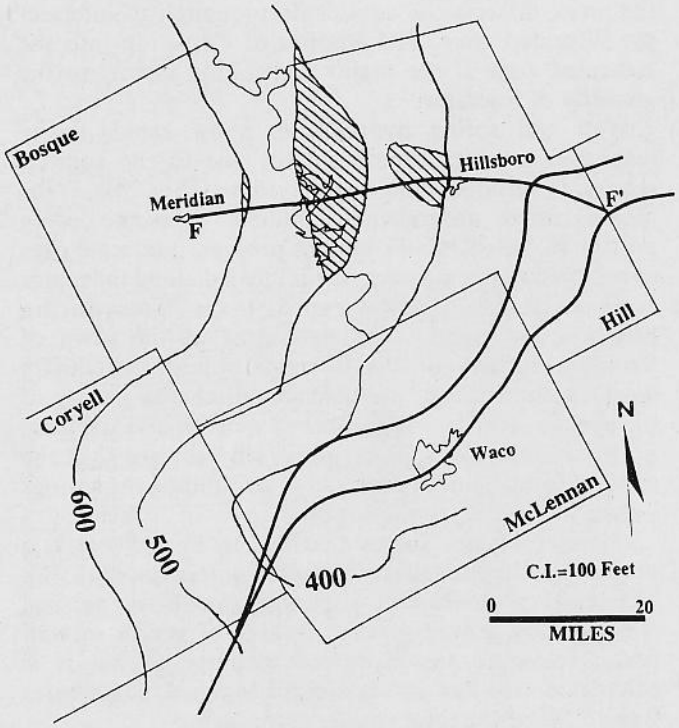

Fig. 2. Water level maps in the Hensell aquifer within the Trinity aquifer system during 1967. The shaded area indicates portions of the Hensell aquifer where head values are higher than head values in the Paluxy aquifer system and gradients are upward. Therefore, water may be migrating from the Hensell aquifer through the overlying Glen Rose Limestone into the Paluxy. This may result in a deterioration of water quality within the Paluxy aquifer in these areas, since the Glen Rose Limestone contains highly mineralized water.

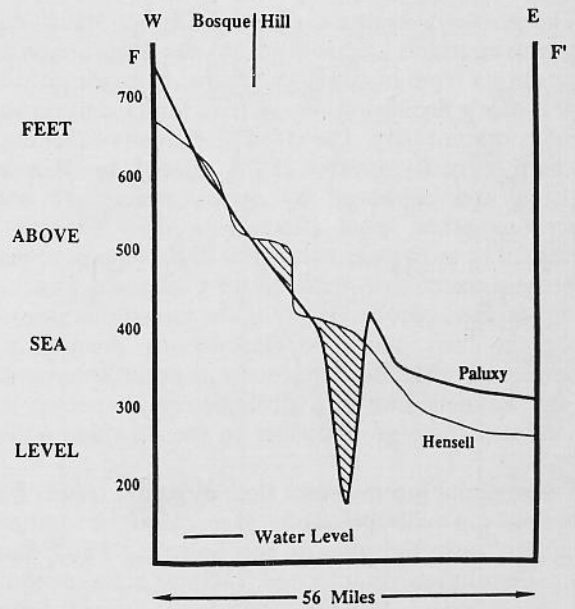

Fig. 3. Cross section F-F′ shows the head level relationship of the Paluxy and Hensell aquifers in the cross section from Meridian to the pinchout line of the Paluxy aquifer system in 1967. East of the cone of depression near Hillsboro, the Paluxy aquifer head is higher than the Hensell.

Hydrogeology and Stream Interaction of the Edwards Aquifer in the Salado Creek Basin, Bell and Williamson Counties, Texas

Suzanne Lisa Dahl

Salado Creek provides both recharge and discharge sites for the northern segment of the Balcones Fault Zone Edwards aquifer. Springs and baseflow in Salado Creek serve as a major aesthetic attraction for the tourist-oriented town of Salado. Within the basin, a majority of the residents depend on the Edwards aquifer for their water supply. Recent urban growth influenced by Interstate 35 has increased demand on the water resources of the Balcones Fault Zone Edwards aquifer, and also increased the potential for pollution. Therefore, understanding the nature of the aquifer and the interaction with Salado Creek is important to future water management decisions.

The study area includes portions of northern Williamson and southern Bell Counties. Since groundwater divides and surface water divides do not always coincide, the study area includes the Salado Creek basin and surrounding area.

The northern segment of the Balcones Fault Zone Edwards aquifer is karstic in nature, but the groundwater flow ranges from conduit to diffuse. A majority of the flow is along bedding planes, joints, faults, and through honeycomb porosity. The effective porosity is primarily fracture porosity (0.41-4.25%), related to Balcones faulting and enhanced by dissolutioning. In some cavernous areas, local effective porosity exceeds 10 percent. The most productive zone of the aquifer appears to be near the contact between the Comanche Peak and Edwards Formations. Most of the cavernous porosity occurs in this zone. The Georgetown Formation is perched above the more porous and permeable portion of the aquifer, but is hydrologically connected and contributes some groundwater to the Edwards aquifer system.

The regional groundwater flow direction results from structural dip and topographic gradient to the southeast. However, near the axis of the Balcones Fault Zone, where dissolutioned faults and fractures act as conduits, the groundwater flow is northward toward Salado Springs (Fig. 1). The aquifer is heterogeneous, due to variations in lithology, diagenesis, and degree of structural deformation. Lineament and fracture density, as well as porosity, increase in proximity to faulting (Fig. 2). Subsequently, there is a positive relationship between high transmissivity values and high lineament density (Fig. 3). Hence, lineation studies are an effective prospecting method for locating high-capacity wells in the Salado Creek basin.

Recharge is primarily from direct infiltration of precipitation on karstic uplands, but also occurs from inputs along fractures in stream beds. Along a segment of the creek, where faults have displaced the saturated zone of the aquifer 60 feet below the surface, a point-source recharge area for the groundwater system exists. This area acts as a recharge catchment for the upper one-third of the Salado Creek basin. This point-source recharge area is environmentally important, because it provides an opportunity for direct, rapid input of possible pollutants carried in storm runoffs from upstream land use practices.

In the lower two-thirds of the basin area, the groundwater is discharged into Salado Creek, because the creek dissects the aquifer deep enough to intersect the saturated zone. The amount of dissection into the saturated zone is the major controlling factor on the quantity of baseflow.

Well and spring hydrographs show rapid, flashy responses to precipitation events, due to the conduit nature of groundwater flow systems (Fig. 4). Wells located down groundwater gradient from the losing portion of Salado Creek exhibit prompt, moderate rises to infiltrating storm water. Wells located along the major zone of faulting show rapid, large rises during precipitation events. Although most of the town of Salado is located on the Edwards outcrop, chemistry data for the springs, the constant discharge nature of the springs, the fluid responses of well 10, and the local northern anisotropic flow paths, all indicate that the recharge area is not immediately surrounding the springs but some distance to the south.

A water budget shows that on an annual basis, a majority of the rainfall is evaporated or transpired (88%). The total groundwater discharge (baseflow, vertical leakage, and downdip flow) is 11% of yearly rainfall and is close to the estimated recharge (12%). It is calculated that the losing stream segment contributes 9 to 10.5% of the total aquifer recharge.

In conclusion, the Salado Creek Edwards aquifer, a representation of the northern portion of the Balcones Fault Zone Edwards aquifer, is a transitional zone between the more prolific Edwards aquifer of the Austin region and the shallow, minor Edwards aquifer of the Washita Prairie region. Water management decisions in the Salado Creek basin should reflect the unique hydrogeology and stream interaction of this portion of the Edwards aquifer.

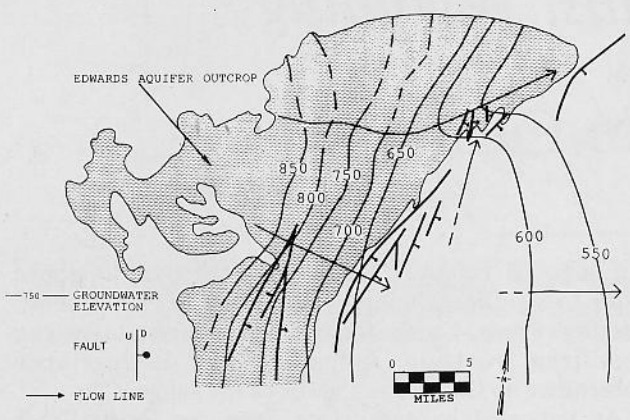

Fig. 1. Water table map showing the regional flow to the southeast and the anisotropic flow to the north.

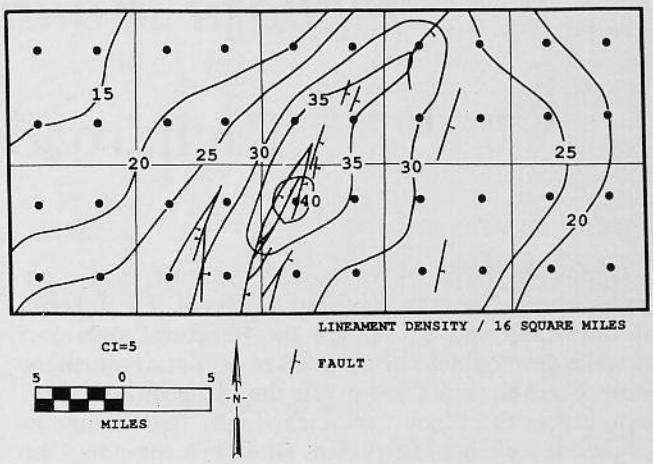

Fig. 2. Lineament density map exhibiting a higher density near Balcones faulting.

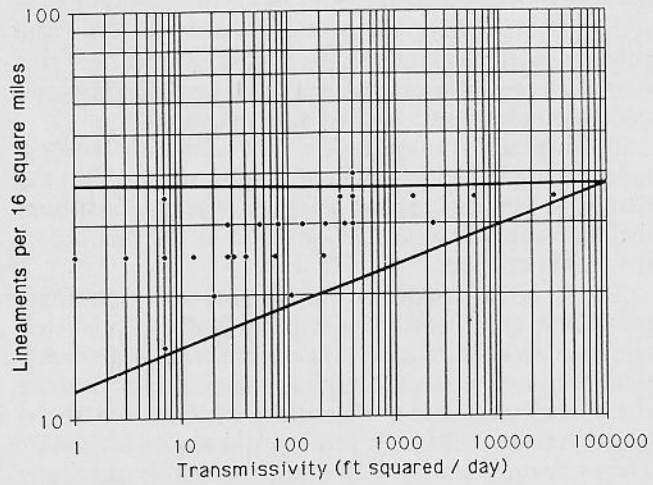

Fig. 3. Lineament density versus transmissivity. A high lineament density does not guarantee a high transmissivity value, but it is a necessary prerequisite, since high transmissivity values are not found in areas with low lineament density.

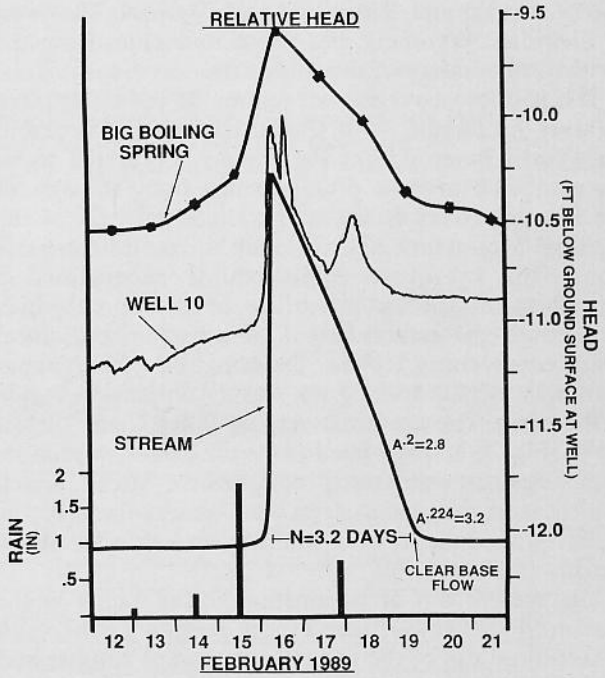

Fig. 4. The relative head values of groundwater and surface water show rapid responses to rain events. The well and spring rise before the stream rises, thus indicating rapid groundwater response.

Structural Analysis of the Walker Mountain-Northern Piney Creek Area, Bighorn Mountains, Wyoming

Richard Brian Furner

Oppositely verging Precambrian basement blocks are typical throughout the Wyoming Foreland. The purpose of this study was to analyze the structural style and tectonic development of the Walker Mountain-northern Piney Creek area and investigate the change in structural style across the Piney Creek tear fault. This change in structural style is most evident when one compares the southwest-vergent Walker Mountain Fault to the northeast-vergent Piney Creek Thrust, both involving Precambrian and Paleozoic rocks. Understanding the style and formation of adjacent, oppositely verging mountain-flank structures that are along the same trend is important when exploring for hydrocarbon accumulations along buried or obscured mountain flanks.

The area of this investigation lies along the northeast flank of the Bighorn Mountains Uplift in north-central Wyoming (Fig. 1). The study comprises an area of approximately 315 square miles within Sheridan and Johnson Counties, Wyoming, between Townships 53 and 56 North, and Ranges 83 and 87 West. The town of Sheridan, Wyoming, lies about four miles from the northeast boundary of the study area.

The southwest-verging structures of the study area (Walker Mountain, Wolf Creek, Red Grade, Beckton, and North Piney Creek; Fig. 2) are interpreted to be the combined product of subsidence along the axis of the Powder River Basin, uplift along the axis of the Bighorn Mountains, and regional horizontal compression. This subsidence-uplift couple necessitated a shortening of the outer surface of the crust, which resulted in the establishment of an additional, local compressive stress regime. Deformation of the upper crust was localized along the steeply dipping west side of the basin. The northeast-verging Piney Creek thrust-block (Fig. 3) is interpreted to be the exclusive product of a regional, horizontal compressive stress, which uplifted and thrust the steep, east-central flank of the Bighorn Mountains over the adjacent Powder River Basin.

The present dip of basement-involved faults in the Walker Mountain-northern Piney Creek area is the result of the initial dip of the fault at the time of rupture and any subsequent rotation associated with the general uplift of the Bighorn Mountains. The southwest-verging faults nearest to the mountain flank demonstrate considerable rotation, indicating that they developed prior to significant uplift of the range. The northeast-verging Piney Creek thrust fault demonstrates no significant rotation, indicating that it developed subsequent to the primary uplift of the range.

As indicated by subsurface data, the Piney Creek thrust fault displays approximately 15,200 feet of horizontal separation and 7,000 feet of vertical separation. The fault dips about 30° southwest near the surface, but shallows to a constant 25° slope at depth, thus proving reverse, left oblique-slip on the near-perpendicular Piney Creek tear fault.

The North Piney Creek structure is interpreted to be the preserved remnant of a southwest-verging, basement-involved structure, now rotated because of drag effects on the Piney Creek thrust fault. Truncation of the controlling fault by the Piney Creek Thrust is shown in Figure 3.

The large discrepancy between crustal shortening values on opposite sides of the Piney Creek tear fault provides the strongest evidence against a compartmental-fault interpretation. A preponderance of the evidence indicates that structures on opposite sides of this transverse fault did not develop simultaneously. The younger, northeast-verging Piney Creek thrust fault was part of a large-scale tectonic event that was superimposed upon the older, southwest-verging structures.

The substantial magnitude of left-lateral offset (three miles) along the Piney Creek tear fault strongly implies that some inherent zone of weakness was present within the Precambrian basement, at least in the vicinity of the tear fault itself.

There is no evidence in support of high-angle movement along northwest-striking faults as predicted by the vertical block-uplift theory of foreland deformation. All northwest-striking faults identified within the study area were either observed or interpreted to be genetic thrust faults with primary dip angles of 25-45°. The uniform orientation of structures within the study area, which developed in sequence from middle Paleocene to Eocene time, tends to support the hypothesis of an essentially constant direction of horizontal maximum compression for this area during the Laramide Orogeny.

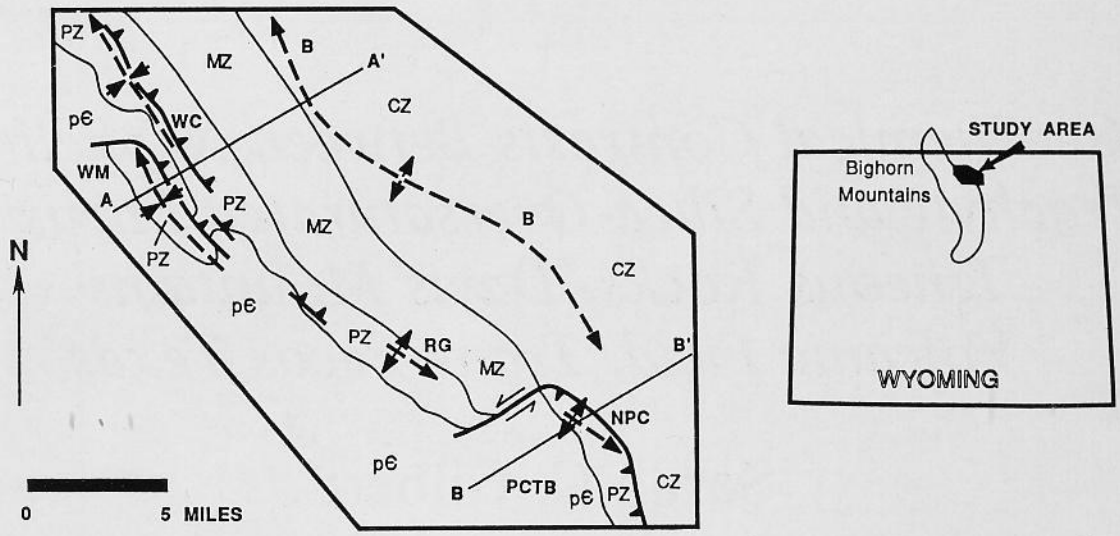

Fig. 1. General tectonic map of the study area showing the distribution of significant tectonic elements. Structural cross sections A-A′ and B-B′ (Figs. 2 and 3) are also shown. Abbreviations: WM = Walker Mountain structure; WC = Wolf Creek structure; B = Beckton structure; RG = Red Grade structure; NPC = North Piney Creek structure; PCTB = Piney Creek thrust block; pЄ = Precambrian basement; Pz = Paleozoic sedimentary rocks; Mz = Mesozoic sedimentary rocks; Cz = Cenozoic sedimentary rocks.

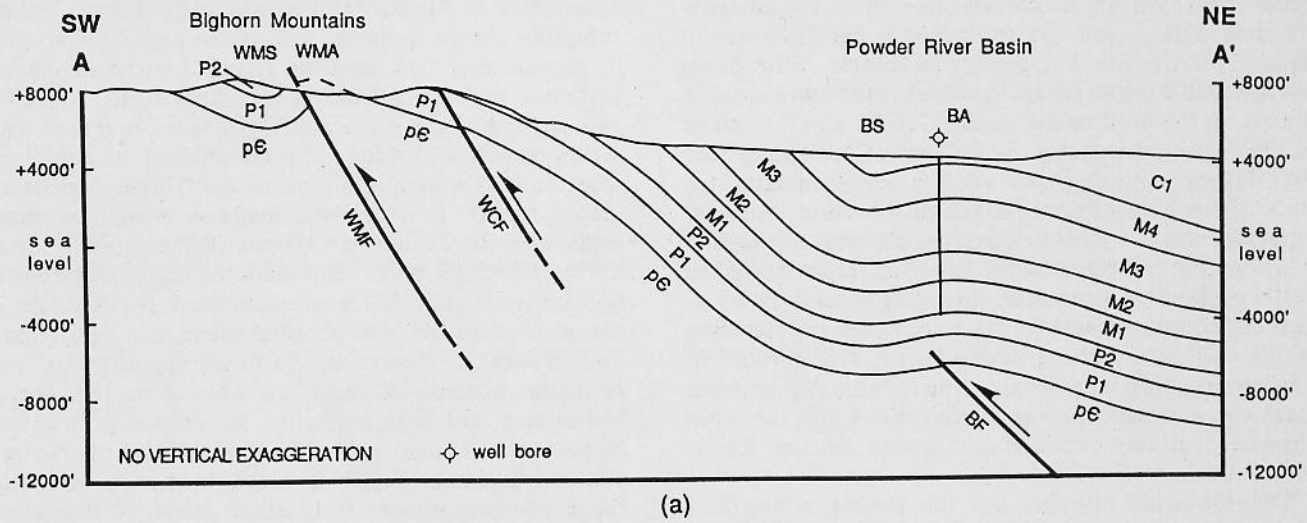

Fig. 2. Structural cross section A-A′ is drawn northwest of the Piney Creek tear fault and displays southwest-verging reverse faults and associated folds indicating tectonic transport out of the Powder River Basin and onto the Bighorn Mountains.

Abbreviations: WMS = Walker Mountain Syncline; WMA = Walker Mountain Anticline; WMF = Walker Mountain Fault; WCF = Wolf Creek Fault; BS = Beckton Syncline; BA = Beckton Anticline; BF = Beckton Fault; PCTF = Piney Creek thrust fault; SAF = Synclinal Axis Fault; NPCS = North Piney Creek structure; pЄ = Precambrian basement; P1 = Cambrian-Ordovician; P2 = Devonian-Pennsylvanian; M1 = Permian-Cretaceous; M2, M3, M4 = Cretaceous; C1, C2 = Tertiary.

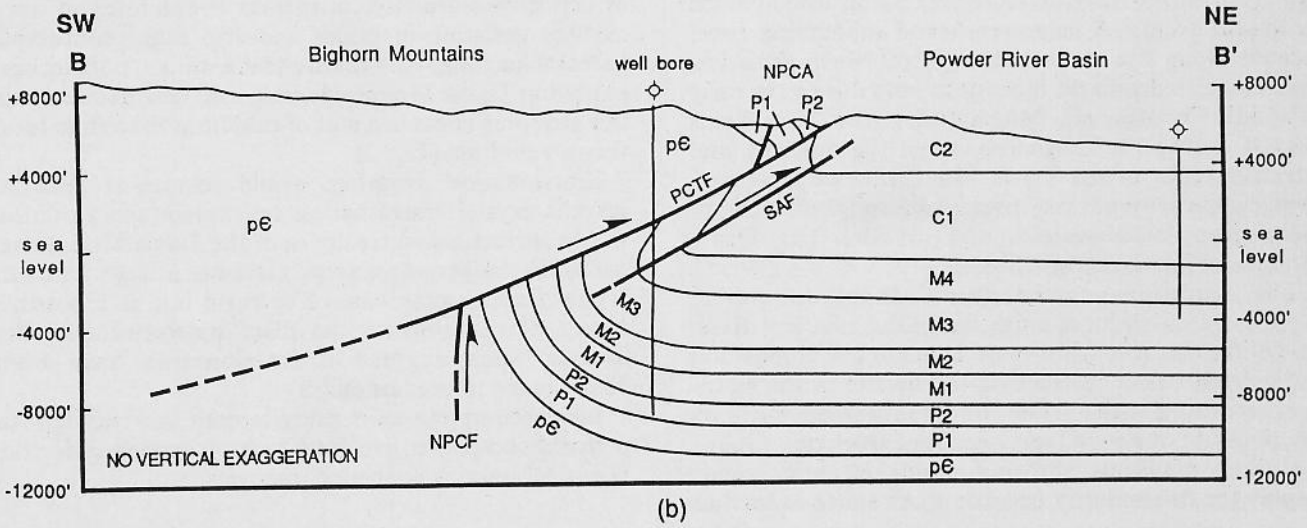

Fig. 3. Structural cross section B-B′ is drawn southeast of the Piney Creek tear fault and displays a northeast-verging reverse fault and associated folds indicating tectonic transport of the Bighorn Mountains over the Powder River Basin. See Figure 2 for explanation of abbreviations.

Geochemical Contrasts Between Nepheline Trachyte and Silica-Oversaturated Intrusive Igneous Rocks, Davis Mountains Volcanic Field, Trans-Pecos Texas

Sarah C. Gilbert

Nepheline trachyte instrusions of the Davis Mountains occur only within a narrow northwest-to-southeast trending belt in Jeff Davis and Brewster Counties in Trans-Pecos Texas. Far greater in volume is the silica-oversaturated basalt to trachyte to rhyolite sequence that makes up the bulk of the volcanic rocks and intrusions in the Davis Mountains. Some studies have suggested that the nepheline trachytes and the silica-oversaturated suite of the Trans-Pecos Magmatic Province represent separate lines of liquid descent dominated by crystal fractionation. Other studies, however, have suggested that open system processes, including crustal assimilation of nepheline trachyte, are responsible for variation within the silica-undersaturated rocks. The purpose of this investigation is to examine the relationship between these unusual nepheline-normative rocks and the more abundant silica-oversaturated rocks of the Davis Mountains.

The Davis Mountains are the largest contiguous outcrop area of volcanic rocks in the Trans-Pecos Magmatic Province. Trans-Pecos Texas is located along the northeastern margin of the Basin and Range Province and lies west of the Pecos River. Igneous activity, such as late-stage compression of the Laramide Orogeny and extension during Basin and Range faulting, accompanied structural events. A paleotrench and subduction zone, located along the western margin of North America, were associated with the igneous activity during the early to middle Cenozoic era. Magmatism in the Trans-Pecos peaked during the Oligocene, when the volcanic and intrusive rocks of the Davis Mountains were formed. Two chemical trends are present in volcanic rocks of the region: alkali-calcic, and alkalic. The Davis Mountains intrusions are alkalic.

The instrusions of the Davis Mountains are all hypabyssal and occur as plugs, laccoliths, sills, and dikes. Laccoliths, however, are most abundant. Composition varies from basalt to trachyte to rhyolite in the silica-oversaturated suite. The undersaturated suite is composed of one rock type: nepheline trachyte.

Harker diagrams showing major element trends display the dissimilarity between these suites at least as far back as the basaltic stage. Trace element variation diagrams also illustrate this dissimilarity. Figure 1 plots rubidium versus niobium and shows this dissimilarity in the form of two separate trends for the nepheline trachytes and the silica-over-saturated suite. Niobium was incompatibile in Davis Mountain magmas and serves as a good index. The enrichment of rubidium suggests its incompatibility in the Davis Mountain magmas also. Two parental magmas must have been feeding the two systems: a silica-oversaturated, quartz-normative basalt, and a silica-undersaturated, nepheline-normative basalt. Silica-oversaturated rocks show a complete evolution from parental basalt through rhyolite and trachyte. However, parental basalts for the nepheline-normative suite are absent in the Davis Mountains, although nepheline basalt occurs in a few Basin and Range age intrusions. Oceanic suites containing similar nepheline trachyte show a complete range of compositions from alkali basalt to nepheline trachyte to phonolite. Parental alkali basalt is nepheline-normative in these oceanic suites.

Major and trace element variation among the Davis Mountains nepheline trachytes suggests the possibility of several parental magma systems. Geographic grouping of nepheline-normative intrusions is exhibited in trace element variation diagrams and also suggests multiple parental magmas. Rubidium and zirconium, both incompatible in Davis Mountains magmas, best demonstrate this grouping effect in a plot of rubidium/zirconium ratio versus rubidium (Fig. 2).

Fractionation modeling would require at least 50 percent crystal fractionation to explain the variation within the nepheline trachytes of the Davis Mountains. Although 50 percent crystallization is a large amount, crystal fractionation cannot be ruled out as a possible source of variation for the silica-undersaturated suite because such degrees of fractionation have been documented in oceanic suites.

More complete mineralogic data are needed to perform comprehensive fractionation modeling for the Davis Mountains nepheline trachytes.

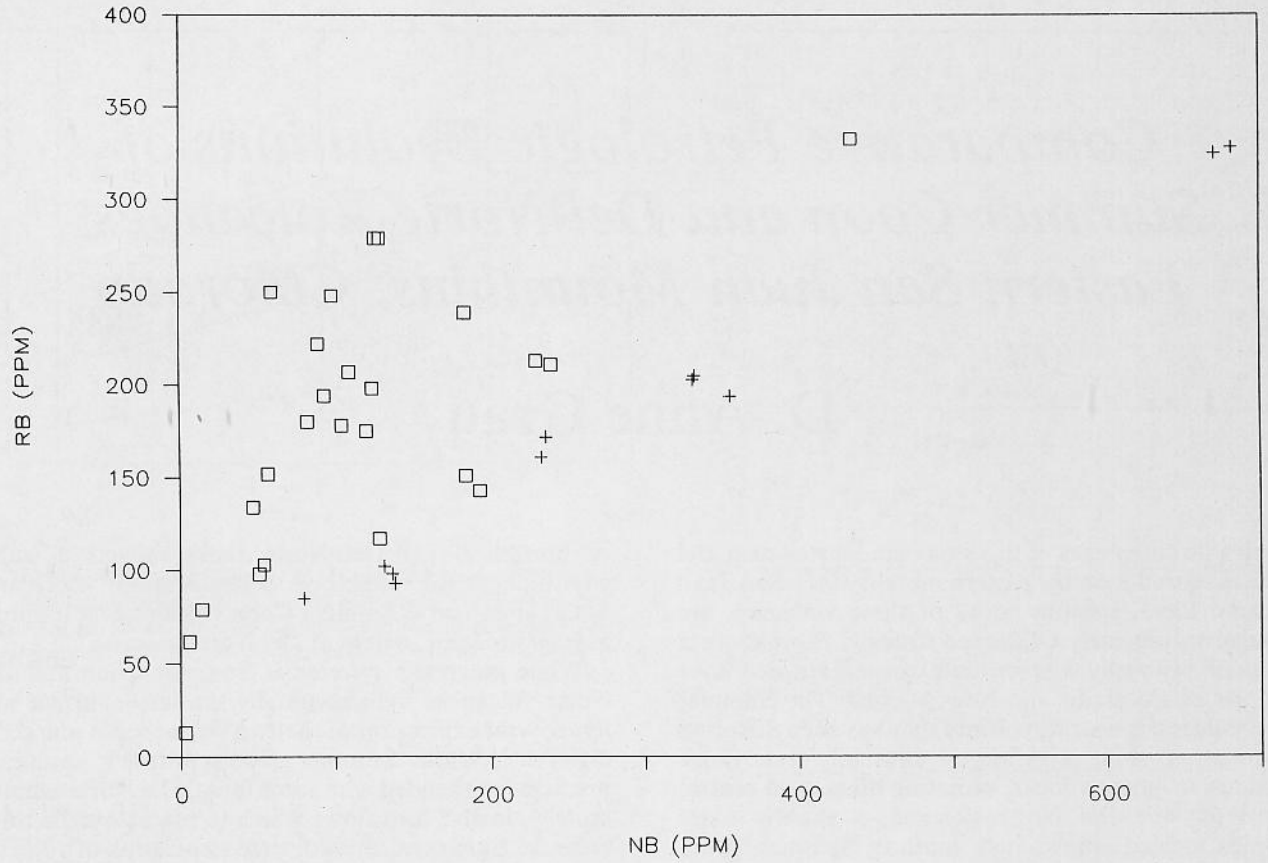

Fig. 1. Rubidium-niobium variation diagram. Silica-oversaturated rocks (□) show two trends with some scatter. Silica-undersaturated rocks (+) show a linear increase in rubidium with increasing niobium concentration, but with a lower slope than the silica-oversaturated suite.

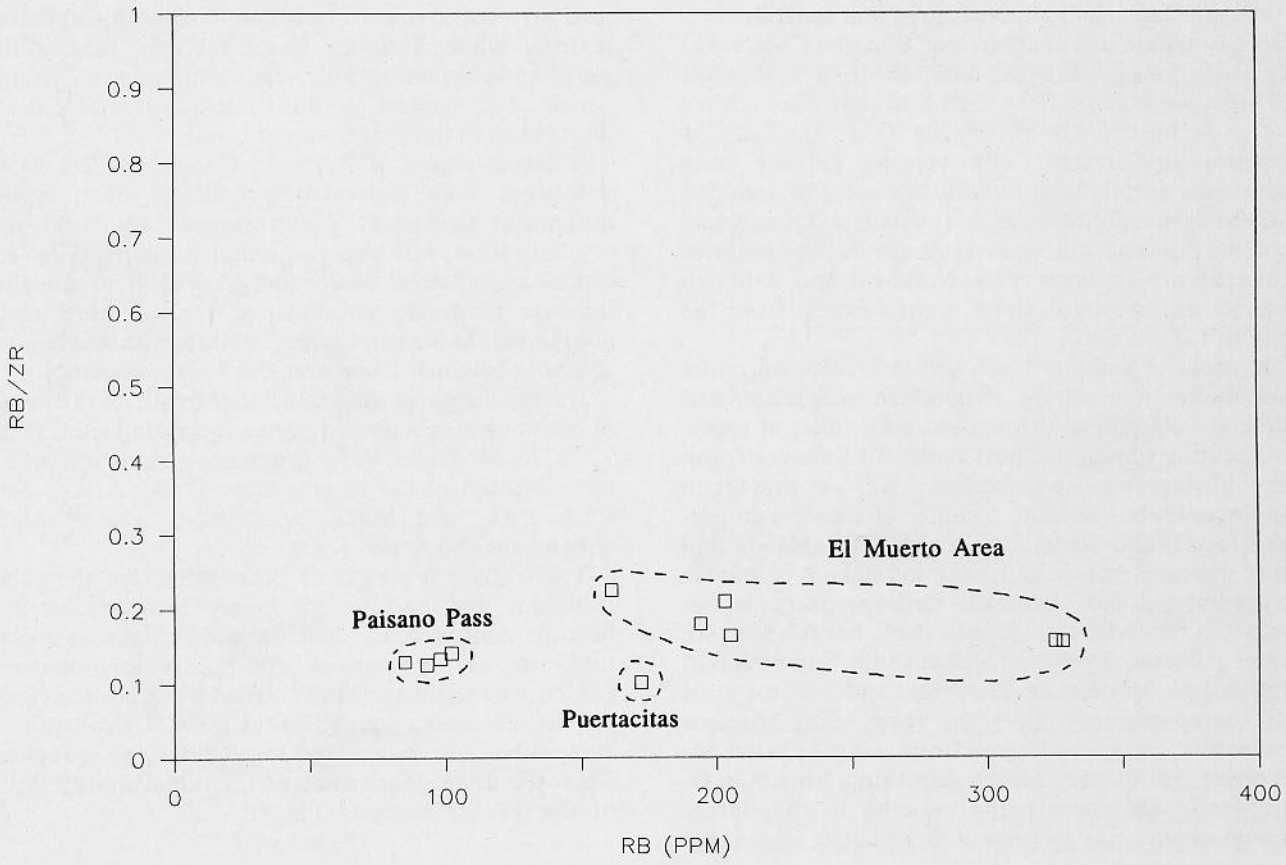

Fig. 2. Rubidium/zirconiun versus rubidium for silica-undersaturated suite. Rubidium and zirconiun maintain the same ratio throughout the suite, suggesting possible relations between rocks by fractional crystallization.

Comparative Petrologic Evolutions of Summer Coon and Del Norte Volcanoes, Eastern San Juan Mountains, Colorado

D. Anne Grau

Volcanic complexes of this study are located near Del Norte, Colorado, on the eastern margin of the San Juan Volcanic Field. Igneous rocks of these volcanoes are included in the early Oligocene Conejos Formation, a group of primarily intermediate rocks extruded over portions of Colorado and New Mexico. The Summer Coon volcano is a stratovolcano that has been dissected by stream erosion, revealing an unusually wide range of extrusive igneous rocks, radiating dikes, and central intrusives. The Del Norte volcano, a slightly older complex located immediately south of Summer Coon, is also well exposed, but lacks the variety of rock facies and compositions present at Summer Coon. The Del Norte volcano is a shield volcano with no known dikes or central intrusives, and consists primarily of massive hornblende dacite and andesite flows and breccias.

Both suites are rich in potassium: Summer Coon rocks are classified as high-K basaltic andesite to rhyolite, while Del Norte rocks range from high-K hornblende andesite to high-K hornblende rhyodacite (Fig. 1). Eruptive sequences at Summer Coon volcano indicate early voluminous eruptions of basaltic andesites to andesite, followed by smaller volumes of rhyolite, and finally late eruptions of silicic andesite and dacite. A clear eruptive sequence is not apparent at Del Norte volcano, although the most differentiated flows occur furthest from the center of the volcano.

The rocks of Summer Coon and Del Norte volcanoes share similar mineralogy. Plagioclase, magnetite, and apatite are ubiquitous throughout both suites of rocks, and zircon is present in most rocks. In Summer Coon rocks, olivine and clinopyroxene (cpx) are present in basaltic andesite. Andesite contains cpx and orthopyroxene (opx), and sometimes olivine. Hornblende and biotite appear in silicic andesites and dacites as olivine disappears and cpx dwindles. Orthopyroxene is not present in rhyodacites. Biotite and hornblende are present in dacite, rhyodacite, and rhyolite. Some evolved rhyolites lack hornblende. Del Norte andesite, the most mafic composition in the Del Norte suite, contains hornblende, cpx, and sometimes opx. Pyroxenes disappear in dacite, which contains hornblende. Hornblende dominates mafic minerals in rhyodacite, although biotite may be present as well. The abundance of hornblende in Del Norte rocks reflects a stable environment for amphibole crystallization, which was not as abundant at Summer Coon volcano, and supports a deeper magma system at Del Norte volcano.

While magmatic systems at Summer Coon and Del Norte volcanoes were essentially the same, surface and hypabyssal expression of the two volcanoes is markedly different. While Summer Coon erupted abundant breccias interbedded with some lavas, Del Norte erupted mostly massive lava flows which in places overlie thick breccias. Summer Coon's diverse association of volcanic facies is associated with a shallow magma chamber; a more limited and consistent eruptive style at Del Norte indicates that this volcano is situated above a more deeply seated magma chamber. Del Norte rock textures tend to evolve toward medium porphyritic-aphanitic texture, while Summer Coon textures remain fine porphyritic-aphanitic. This relationship suggests a longer period of crystallization in the late differentiates at Del Norte than in those at Summer Coon.

Volcanic suites of Summer Coon and Del Norte volcanoes were generated by similar open system magmatic processes predominated by fractional crystallization, but also including magma mixing and crustal assimilation. Major and trace element modeling indicate moderate amounts of fractionation could accommodate the petrogenesis of differentiated compositions at Summer Coon and Del Norte volcanoes.

Harker diagrams illustrate linear trends of the oxides of major elements plotted versus increasing silica (Figs. 2, 3). Most oxides show progressive depletion within the evolution of the magma suite (TiO_2, Al_2O_3, FeO, CaO, P_2O_5, and MnO), while other oxides exhibit enrichment (Na_2O and K_2O).

Trace element trends of both suites are the same: rubidium and barium are highly incompatible and become enriched in differentiated rocks. Yitrium, niobium, and zirconium are mildly incompatible, exhibiting a slight enrichment trend when plotted versus Rb as an index of differentiation. Strontium is compatible and is depleted throughout the sequences. These trends are consistent with fractional crystallization of observed phenocrysts (Fig. 4).

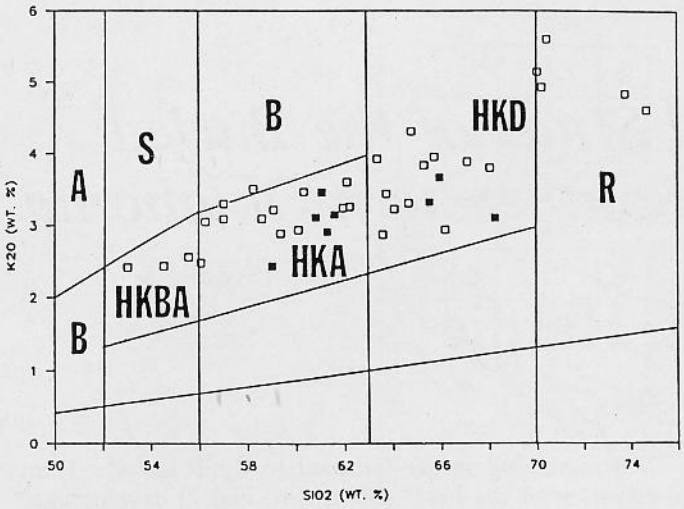

Fig. 1. Classification of Summer Coon and Del Norte rocks using the classification scheme of Peccerillo and Taylor (1976). The rock suites plot as follows: HKBA = high-potassic basaltic andesite; HKA = high-potassic andesite; HKD = high-potassic dacite; R = rhyolite.

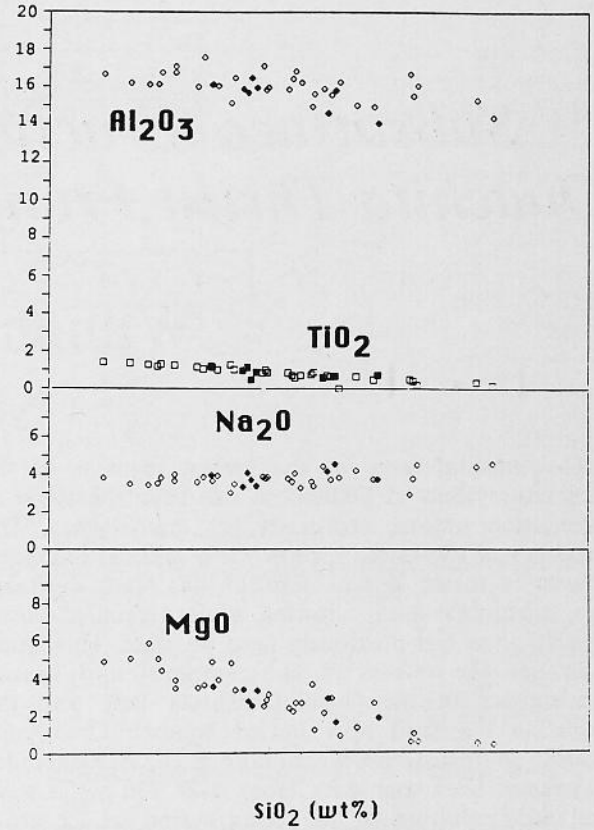

Fig. 2. Harker diagrams for Al_2O_3, TiO_2, Na_2O, and MgO plotted versus increasing silica. Open symbols = Summer Coon volcano; closed symbols = Del Norte volcano.

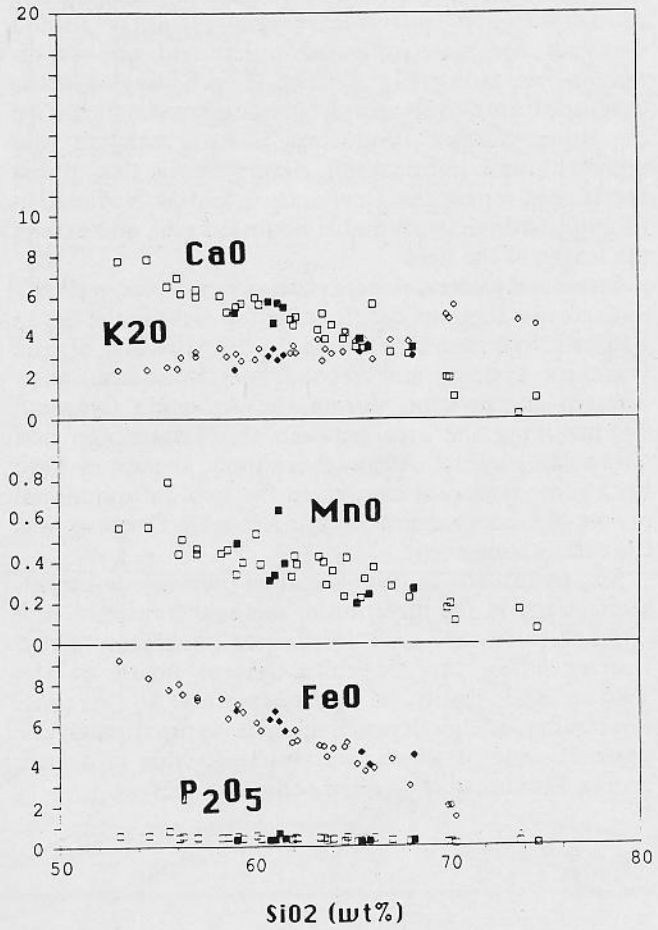

Fig. 3. Harker diagrams for CaO, K_2O, MnO, FeO, and P_2O_5 plotted versus increasing silica. Open symbols = Summer Coon volcano; closed symbols = Del Norte volcano.

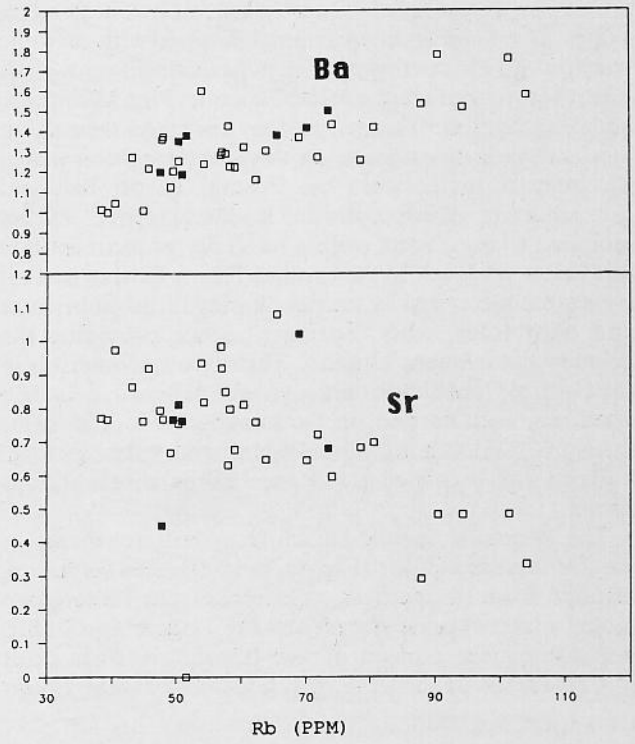

Fig. 4. Barium and strontium versus rubidium. Barium, a strongly incompatible trace element exhibits an enrichment trend, while strontium, the only compatible trace element at Summer Coon and Del Norte volcanoes, is depleted with increasing rubidium. Open symbols = Summer Coon volcano; closed symbols = Del Norte volcano.

Subsurface Structural Study of the Buried Ouachita Thrust Front, Southeastern Oklahoma

William E. Hardie

The unusual trace of the buried segment of the Ouachita system in Oklahoma has been the topic of speculation among geologists for many years. The discovery of the Isom Springs Field and the increased interest in thrust belt exploration has made available new subsurface data, allowing a more detailed investigation than has previously been possible. This study examines the effects of the temporal and spatial convergence of the Ouachita Thrust Belt with the Arbuckle Foreland now buried beneath Cretaceous cover in southeastern Oklahoma (Fig. 1). Over 900 miles of seismic lines and data from over 230 wells were analyzed, resulting in the construction of 22 cross sections, a subcrop map of the pre-Cretaceous surface, and a structural contour map of the basal sole thrust.

A cross section through the southeasternmost exposure of the Ouachita Mountains provides the best indication of structural style of the thrust front before it disappears beneath Cretaceous cover (Fig. 2). Rocks are exposed in a series of northeast-southwest trending ridges that have resulted from thrusting, with tectonic transport to the northwest. The major thrust faults, from northwest to southeast, are the Choctaw, Pine Mountain, and Windingstair Thrusts, and an unnamed thrust that dies out to the northeast. In the Ouachita Mountains, the interactions between the Frontal Thrust Belt and the adjacent Arkoma Basin is characterized by an incipient triangle zone, with a basal detachment at 7000 feet below sea level. In the Frontal Thrust Belt, structural style is characterized by steeply dipping thrust imbricates and tight folds, with "Springer" Shale providing the primary detachment horizon. Thrust belt geometries in the Central Ouachita Province consist of broad, detached synclines, each carried on the hanging wall of a major thrust. Ordovician Womble Shale provides the "gliding" horizon and is carried at the base of the allochthonous sheets.

The reentrant in the Ouachita system southeast of the Tishomingo Uplift (Fig. 1), is interpreted as having resulted from the buttressing effects of the Tishomingo block, a later episode of uplift on the Tishomingo Uplift, and subsequent erosion of the Ouachita thrusts prior to Cretaceous deposition. Effects of the Frontal Thrust Belt impinging on the Tishomingo Uplift include: 1) an elevation of the basal sole thrust; and 2) development of a transfer zone, such that displacement on leading edge imbricates is transferred to older, overlying thrusts by duplex development, as they pass southward around the southeast end of the Tishomingo Uplift.

In the Bryan Salient (Fig. 1), thrust belt geometries are almost identical to those in the Central Ouachita Province, with Womble Shale acting as the primary detachment horizon. The interaction between the frontal thrust of the Bryan Salient and the adjacent Ardmore Basin is likewise characterized by a steep-sided triangle zone, with a basal detachment at 10,000 feet below sea level. In the Bryan Salient, however, this thrust belt style has been overprinted with a foreland style consisting of dominantly southwest-vergent, tightly folded synclines, which are sometimes overturned, and out-of-the-syncline faults (Fig. 3). The Isom Springs Field is developed along the steeply dipping frontal thrust of the Bryan Salient. Production is from hanging wall anticlines and imbrications developed in two thrust sheets that repeat the Devonian Arkansas Novaculite-through-Ordovician Womble Shale interval, and extend the length of the field.

Structural relationships, as shown in this study, clearly indicate two stages of deformation for rocks in the Bryan Salient: first, northwest-directed thrusting of the Ouachita system; and second, northeast-southwest-directed compression during the Arbuckle Orogeny, downwarping the area between the Tishomingo and Criner Hills uplifts. Although, initially, there may have been some temporal overlap in the two deformational events, the compression of the Arbuckle Orogeny was the culminating event.

Major thrusts in the Ouachita system developed sequentially in the direction of tectonic transport, in a "higher-to-lower" or "inside-out" fashion. Total shortening in the Ouachita system north of the Tishomingo Uplift is approximately 46 percent. Shortening in the Bryan Salient is approximately 67 percent, some of which is undoubtedly due to a later northeast-southwest-directed compression.

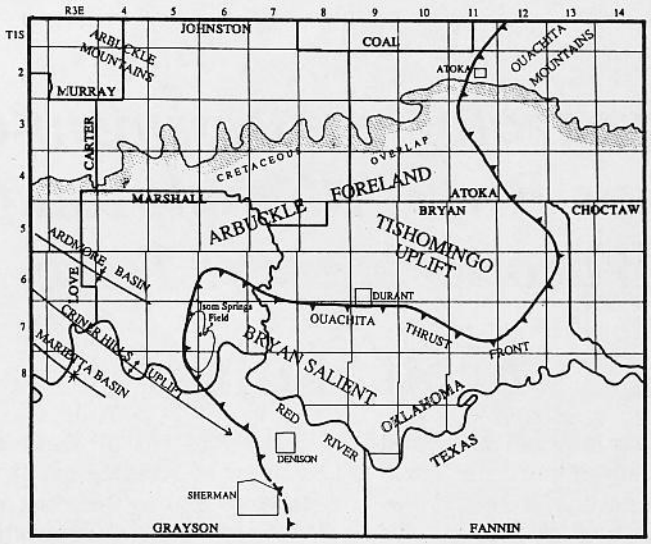

Fig. 1. Index map showing location of Ouachita Thrust Front and its relationship to the adjacent foreland beneath Cretaceous cover.

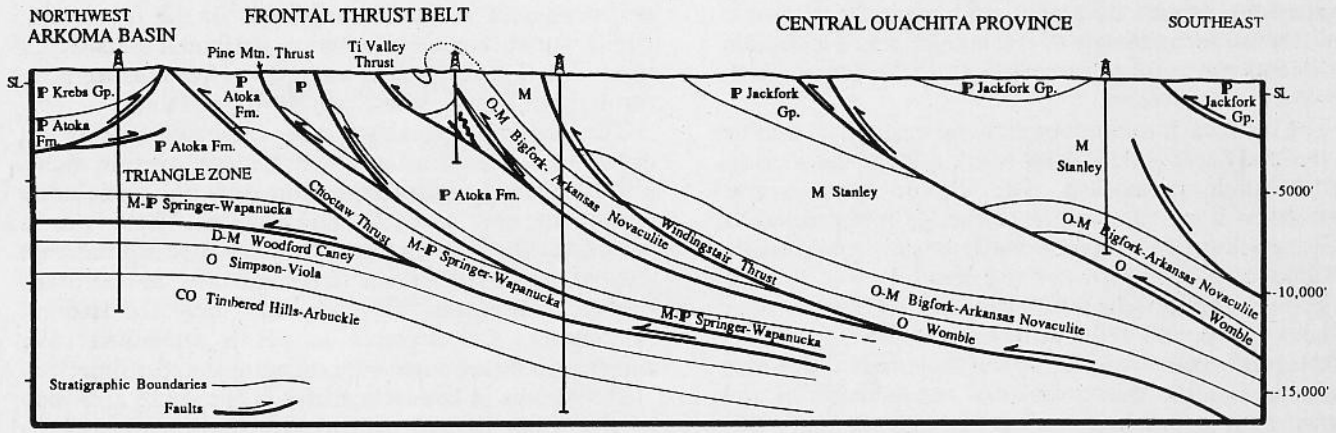

Fig. 2. A northwest-southeast cross section through the southernmost exposure of the Ouachita Mountains and Arkoma Basin.

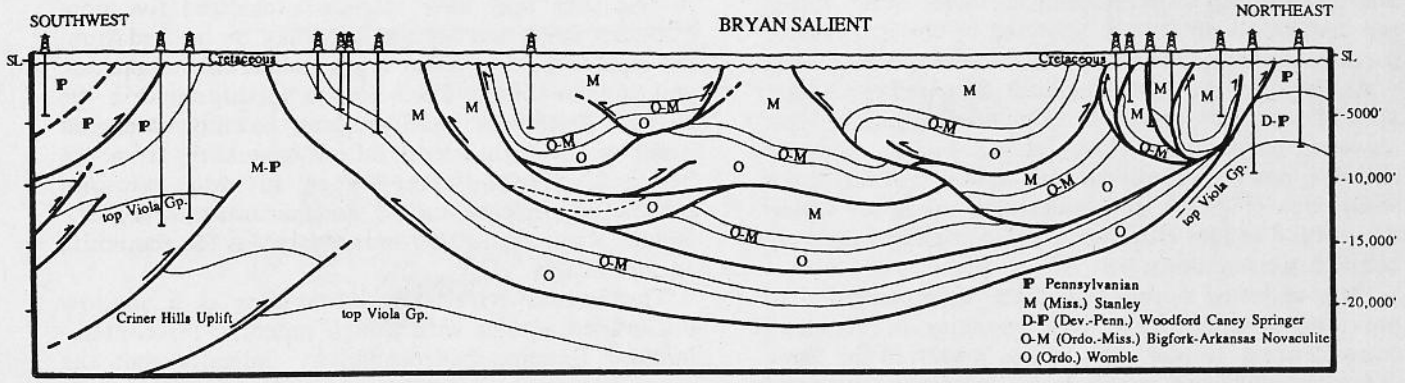

Fig. 3. A northeast-southwest cross section through the Bryan Salient illustrating the complex out-of-the-syncline movement that characterizes the "Arbuckle" style of deformation.

A Hydrogeologic Assessment of the Brazos River Alluvial Aquifer, Waco to Marlin, Texas

Scott Harlan

The Brazos River alluvial aquifer is a sand and gravel aquifer along the Brazos River extending from north of Waco, Texas, to the Gulf Coast. The aquifer has been an easily accessible, high quality water source for over one hundred years. However, the aquifer is easily contaminated due to its shallow nature. Therefore, this study evaluates the hydrogeologic and hydrogeochemical aspects of the aquifer.

The aquifer between Waco and Marlin is composed of floodplain deposits and multiple terraces. The floodplain comprises sandy clay overlying a fairly continuous deposit of gravel, and ranges from just a few feet to approximately 80 feet in thickness. Floodplain sediments are more calcareous than the terraces, which appear more siliceous.

The bedrock formation underlying the alluvial mantle in the study area is the Taylor Marl, a dense, calcareous, brittle shale formation. The Taylor Marl is not considered a regional aquifer, although recent research indicates that the formation may transmit considerable volumes of groundwater in some areas.

Water levels in wells were measured periodically over a three-year period and a groundwater flow budget was developed from low and high rainfall periods. The water budgets indicate that hydraulic conductivity in the Taylor Marl ranges from 1.45×10^{-7} cm/s to 5.52×10^{-7} cm/s. This range is representative of an unweathered clay and indicates that the Taylor Marl does not contribute large volumes of groundwater to the floodplain aquifer.

Groundwater samples were collected throughout the aquifer during three different sampling periods. Samples were collected to: 1) develop a baseline chemical index; and 2) ascertain if hydrochemical facies occur within the aquifer. Samples were analyzed by the investigator for most inorganic species as well as for five heavy metals.

Analysis of the hydrochemical data indicated that groundwater is primarily a calcium-bicarbonate type; however, calcium-chloride, calcium-sulfate, sodium-chloride, and non-dominant type waters exist within the study area (Fig. 1). Iron cqncentrations occur within the normal range; all other metal concentrations were below detection limits.

Data collected during this study were compared to previous investigations. Discrepancies in chemical concentration ranges and means observed in these comparisons can be attributed to sample location and sampling period. In order to determine if the variations in chemical concentrations reflected different chemical populations, a statistical analysis was conducted.

The Analysis of Variance Model (ANOVA) allows analysis of variance by: 1) variance due to location; 2) variance due to sampling period; and 3) variance due to the combination of location and sampling period.

Analysis detected significantly different concentrations with respect to sample location and sampling period. Chemical data indicate that groundwater in floodplain wells contained significantly higher values of calcium, magnesium, and sulfate than terrace well samples. These higher concentrations can be attributed to temporal variation in recharge rates and higher percentages of calcareous materials in the floodplain. Higher sulfate concentrations are attributed to residence time in the Taylor Marl as water flows from the terraces, through the Taylor Marl, into the floodplain.

The statistical analysis also indicated significant differences in parameter concentrations over an eight-month period. Increased concentrations included potassium and specific conductance. There was a decrease in the pH over time. Increases of both potassium and specific conductance are attributed to increased rainfall, subsequent recharge, and increased mineral solutioning. The decrease in pH is attributed to a decrease in bicarbonate concentrations across time.

Differences in hydrochemistry in the study area may be the result of hydrochemical evolution along flow paths. A two-dimensional model is presented (Fig. 2) in which recharge-discharge relationships, residence time, and mineralogic composition dominate groundwater chemistry. Zone A is composed of relatively young groundwater with minimal residence time and a non-dominant type of chemistry. Zone B is a zone of sluggish movement and extended residence time. Groundwater in this zone may have calcium exchanged for more attractive ions, and sulfate ions may be leached from the aquifer matrix. Water types include calcium-sulfate and sodium-sulfate. Zone C is a mixing zone in the shallow floodplain aquifer. Here, recently recharged water mixes with lateral inflow emanating from the bedrock. Groundwater types include calcium-bicarbonate, calcium-sulfate, and calcium-chloride. The Brazos River forms the discharge point for the entire aquifer matrix.

The Brazos River alluvial aquifer is a shallow unconfined aquifer with a high potential for contamination. Baseline hydrochemistry indicates that the groundwater is of high quality. Hydrochemistry is controlled by recharge-discharge mechanics and by mineralogic variation within the aquifer matrix.

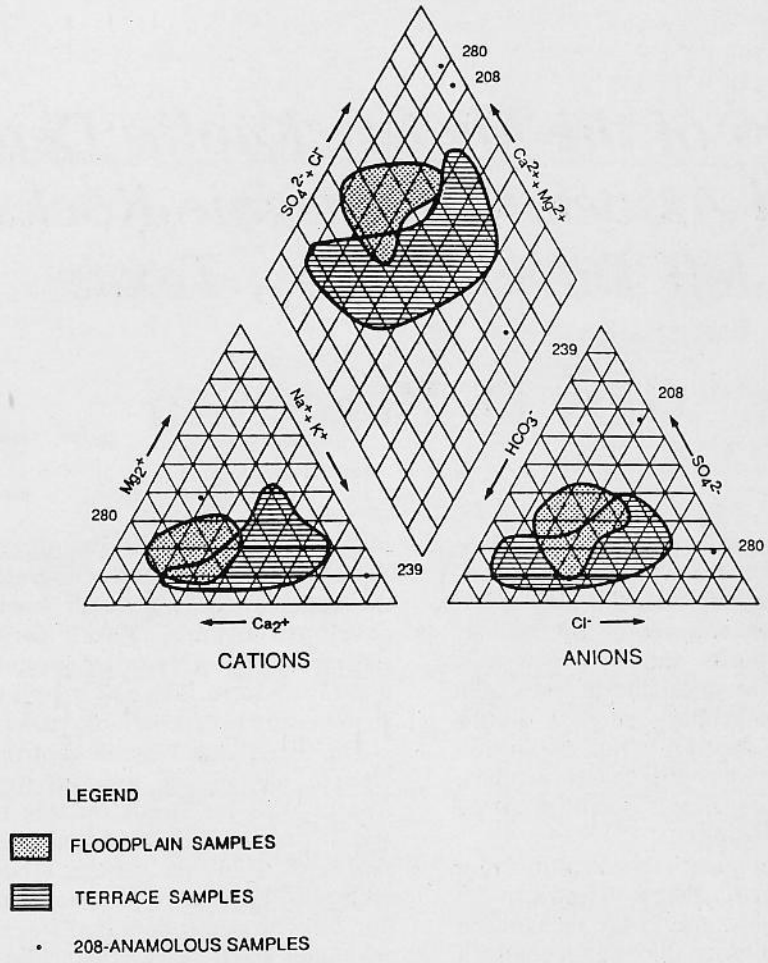

Fig. 1. Trilinear plots for three sample sets collected from the Brazos River alluvial aquifer. The plot shows that floodplain samples have higher concentrations of both calcium and bicarbonate than terrace samples. The higher calcium concentrations in floodplain samples may be due to the higher percentage of calcareous sediments in the floodplain.

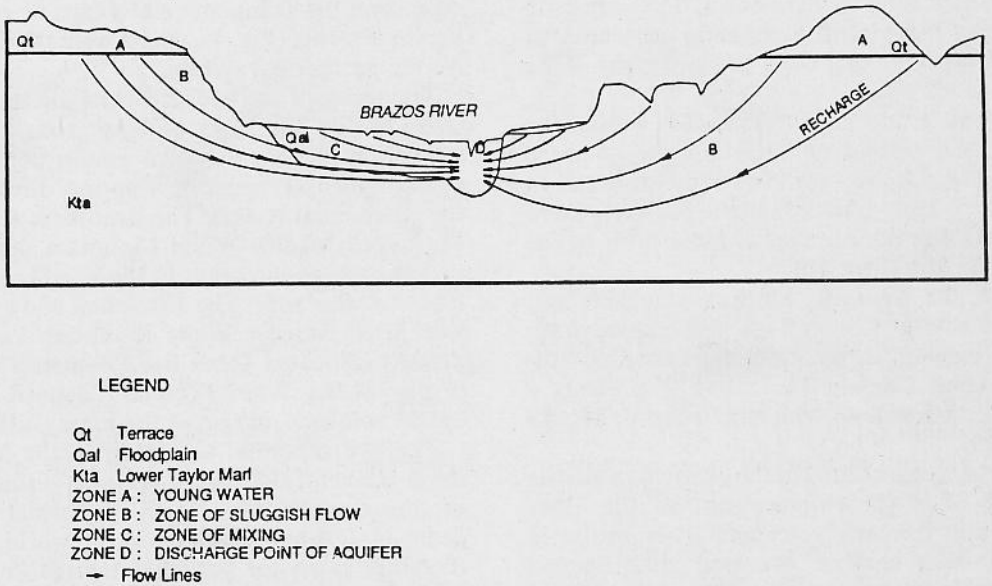

Fig. 2. Groundwater chemistry is dominated by recharge areas, shallow flow-through zones, mixing zones, and aquifer discharge points. Zone A is composed of young water with minimal residence time. This water has a non-dominant type chemistry. Zone B is a zone of sluggish movement and extended residence time. Groundwater in this zone may have calcium exchanged for more attractive ions, and sulphate ions may be leached from the aquifer matrix. Zone C is a mixing zone in the shallow floodplain aquifer. Here recently recharged water mixes with water originating from the bedrock areas.

Geology of the Medley Kaolin Deposits and Associated Volcanic Rocks, Jeff Davis County, Texas

Gary D. Henderson

Two kaolin deposits, one with rutile, in the Davis Mountains of Trans-Pecos Texas have been known and intermittently explored and mined since the early 1900s. Prior studies in this area concentrated on the geology and mineralogy of the deposits and were primarily directed toward evaluating the suitability of the kaolin and rutile for mining. The primary purpose of this research was to evaluate the deposits within the overall volcanic framework of the area as well as to investigate the deposit geology, mineralogy, and potential of the area for epithermal mineral deposits.

The main results of this study are: 1) the identification of the large Paradise Mountain caldera complex in the south-central Davis Mountains, and 2) the recognition of the intimate relationship between the caldera complex and the kaolin deposits.

The Paradise Mountain caldera (36.4 m.y. ago and 27 x 16 km) collapsed in at least two stages in response to the voluminous eruption of quartz trachyte to rhyolitic Barrel Springs ash-flow tuff. A small lake probably developed within the caldera during a period of relative volcanic quiescence after caldera formation. Trachyte porphyry lavas of the Merrill Formation were erupted before caldera collapse along the western margin of the caldera.

The Pine Peak caldera, either nested within the Paradise Mountain caldera or breaching the northern margin of the older caldera, was formed by the eruption of the Wild Cherry Tuff. Quartz trachyte porphyry lavas of the Mt. Locke Formation were erupted prior to the eruption of the Wild Cherry Tuff.

Volcanism in the Paradise Mountain caldera was renewed after the Wild Cherry Tuff was erupted from the Pine Peak caldera. A localized rheomorphic ash-flow tuff, the Goat Canyon Formation, represents a venting episode associated with the nearby Merrill Canyon intrusion.

Magma resurgence and tilting of the overlying volcanic cover occurred after the emplacement of the Goat Canyon Formation. Renewed volcanic activity, probably from the Pine Peak caldera, occurred after magma resurgence, representing venting of the resurgent magma.

A geothermal system with two primary surface discharge points (hot springs) was established within the inner collapse zone of the Paradise Mountain caldera during the waning stages of magmatic activity (Fig. 1).

Meteoric water from rainfall and the caldera lake provided recharge to the developing groundwater system. The meteoric water migrated downward through the volcanic rocks through fractures and faults that developed during caldera formation and magma resurgence. The descending groundwater was heated by underlying intrusions and driven upwards, establishing a circulating hydrothermal system.

The underlying magma contributed heat and sulfur dioxide gas to the groundwater. The groundwater reacted with the sulfur dioxide to form sulfuric acid and hydrogen sulfide. As the heated aqueous phase ascended back to the surface, it boiled due to a pressure decrease. The vapor phase contained a high concentration of hydrogen sulfide that was subsequently oxidized at shallow levels to form an acidic hydrothermal fluid.

The acidic fluid reacted with volcanic glass and feldspar in the Barrel Springs Tuff to form the kaolin deposits. The reaction between the fluid and the host rock involved primarily solubilization of iron, sodium, and potassium, and desilication reactions. Silica that was mobilized during kaolinization reactions was reprecipitated as massive silica caps or gossans near the kaolin deposits (Fig. 1), which were the discharge points for the geothermal system.

The result of the hydrothermal alteration of volcanic rocks within the inner collapse zone of the Paradise Mountain caldera was two kaolin deposits, one with rutile, which represent hot spring discharge points in the geothermal system. The stratiform and incompletely kaolinized Medley White Mountain deposit is located near a shallow intrusion in the northern portion of the inner collapse zone. The discordant and more completely kaolinized Mueller White Mountain kaolin and rutile deposit is located about five kilometers (3 miles) south of the Medley White Mountain deposit and is situated on the southern margin of the inner collapse zone.

The hydrothermal alteration in the Medley area of the south-central Davis Mountains is similar to the type of alteration associated with epithermal precious metal deposits in other locations in the world. The potential therefore exists for buried epithermal mineral deposits in this area of the Davis Mountains.

This research has, for the first time, provided, an overall geologic framework within which to understand the genesis of the Medley area kaolin deposits and the associated Paradise Mountain caldera complex.

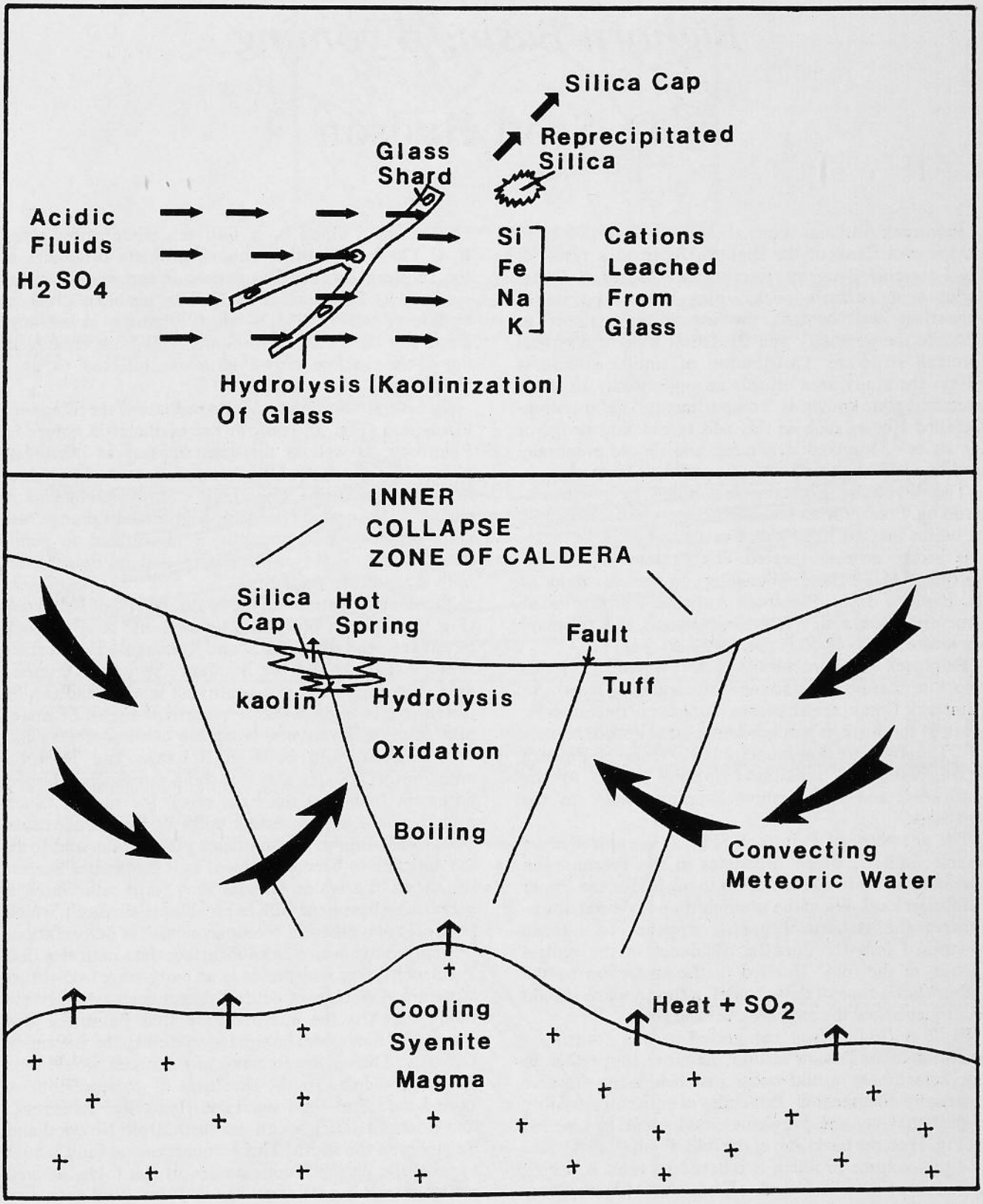

Fig. 1. Model for the formation of the kaolin deposits in the Medley area. The lower part of the diagram shows the hydrothermal system on a large scale. The upper part of the diagram shows the microscopic model for alteration of volcanic glass to kaolin.

Structural Analysis of Paintrock Anticline Bighorn Basin, Wyoming

D. Scott Hudson

Paintrock Anticline is one of several structures formed on the east flank of the Bighorn Basin as a result of the Laramide Orogeny. Excellent exposures of Cretaceous and Jurassic rocks, plus several points of subsurface well control, provide an opportunity to describe the geometry and structural style of a typical foreland structure. Distribution of similar structures within the study area affords an opportunity to study a tectonic style known as "compartmental" deformation. Detailed studies such as this add to our knowledge of the styles of foreland structures, and should eventually lead to a thorough understanding of their formation.

The Wyoming Foreland is typified by northwest-trending, Precambrian basement-cored uplifts, separated by basins that are filled with Eocene and younger rocks. The study area is located approximately 18 miles northeast of Worland, Wyoming, on the east flank of the Bighorn Basin. Paintrock Anticline and four other structures (Bonanza, Hyattville, Nowood, and Zeisman) are located in T. 49-50 N., R. 89-91 W. (Fig. 1).

Paintrock Anticline trends N 32° W, and is eroded into the Jurassic Sundance Formation. North of Paintrock Creek, the structure plunges northwest at 5°; south of the creek, it plunges southeast at approximately 10°. The structure is asymmetric away from the Bighorn Basin, with the backlimb dipping 10-17° to the southwest, and the forelimb dipping 45-60° to the northeast.

The geometry of Paintrock (Fig. 2) is controlled by reverse fault C, which originates in the Precambrian basement and dies out upward into the fold at the Upper Cambrian level. When the geologic map is viewed down-plunge, the structural profile appears to tighten downward into the Jurassic Sundance in the central portion of the fold. This led to the prediction by the author that a zone of detachment in the anticline should occur just below the exposed Jurassic rocks.

Fault A (Fig. 2) was recognized in well control by repetition in the Triassic section; therefore, the prediction that detachment would occur just below the Jurassic is partially documented. Principles of concentric folding suggest that volume problems could occur in syncline S_1 (Fig. 1) on the backlimb of the fold. Figure 2 illustrates how this volume problem is relieved by fault B, which rises out of bedding, and offsets the Mississippian-through-Triassic section along two imbricates ($B_{1, 2}$). Displacement along B_1 is 140 feet, while offset along B_2 is 120 feet. Another volume problem originates in the Tensleep-Amsden Formations in syncline S_2 on the east side of Paintrock (Fig. 1). This problem is solved by reverse fault D (Fig. 2), which originates as bedding-plane slip on the steep forelimb. This fault creates an out-of-the-syncline crowd structure referred to as a "rabbit-ear."

Structural contours drawn on the base of the Sundance Formation (Fig. 3), confirm the asymmetric nature of Paintrock, as well as the constant rate of northwest plunge. The constant plunge rate results from the gradual loss of displacement along fault C and detachments A and B. The repeated change in southeastern plunge rate from gentle-to-steep-to-gentle is interpreted to result from abrupt loss of displacement, first on detachment fault A, and then on fault B.

The contour pattern on the southeast end of Paintrock (Fig. 3) becomes blunt or "squared-off" as Paintrock terminates, and synclines S_1 and S_2 merge. From surface geology (Fig. 1) and the Sundance structural contour map (Fig. 3), a northeast-southwest linear trend can be interpreted to begin at the steep north plunge of Zeisman, pass south of Hyattville, along the blunt southeast end of Paintrock, and between Bonanza and Nowood anticlines. It is likely that this trend represents a buried basement fault that does not reach the surface. Such a fault would accommodate uplift of Paintrock, cause a sharp increase in the southeast plunge rate, and force the anticline to become blunted as it terminates against this trend. Laramide stresses may have reactivated a preexisting basement fault as an oblique-slip fault, which separates two different "compartments" of deformation.

Analysis of surface and subsurface data indicates that Paintrock is best interpreted as an early-stage fold-thrust structure. Presence of several detachment-type reverse faults supports the interpretation that Paintrock was formed by horizontal compression during the Laramide Orogeny. The northwest trend of Paintrock would thus be perpendicular to the direction of compression. A buried basement fault separates Hyattville, Paintrock, and Bonanza anticlines on the north, from Nowood and Zeisman on the south. This compartmental fault would explain the discontinuous nature of the folds, as well as the change in rate of plunge and structural geometry at the south end of Paintrock Anticline.

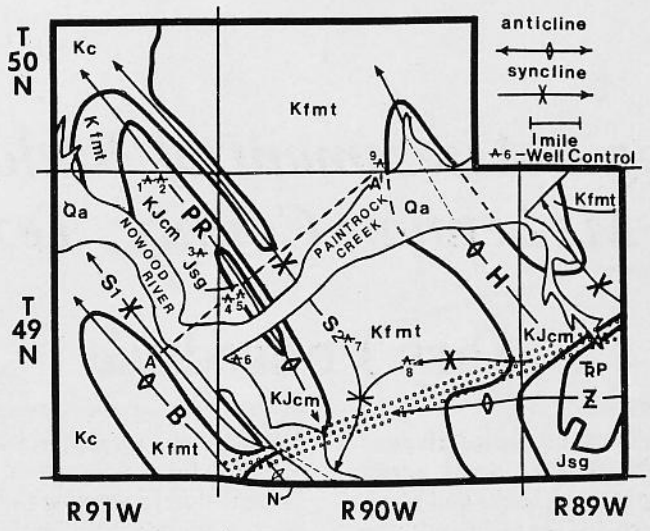

Fig. 1. Geologic map of the Paintrock area. Anticlinal structures are: Bonanza (B), Nowood (N), Paintrock (PR), Hyattville (H), and Zeisman (Z). Synclines referred to in the text are S_1 and S_2. Stratigraphic units, from younger to older, are: Qa = alluvium; Kc = Cody Shale; Kfmt = Frontier, Mowry, and Thermopolis; KJcm = Cloverly and Morrison; Jsg = Sundance and Gypsum Spring; T_RP = Triassic and Permian. Stippled pattern marks location of buried compartmental fault. Small derricks numbered 1-9 represent subsurface well control. Cross section in Figure 2 is located along line A-A'.

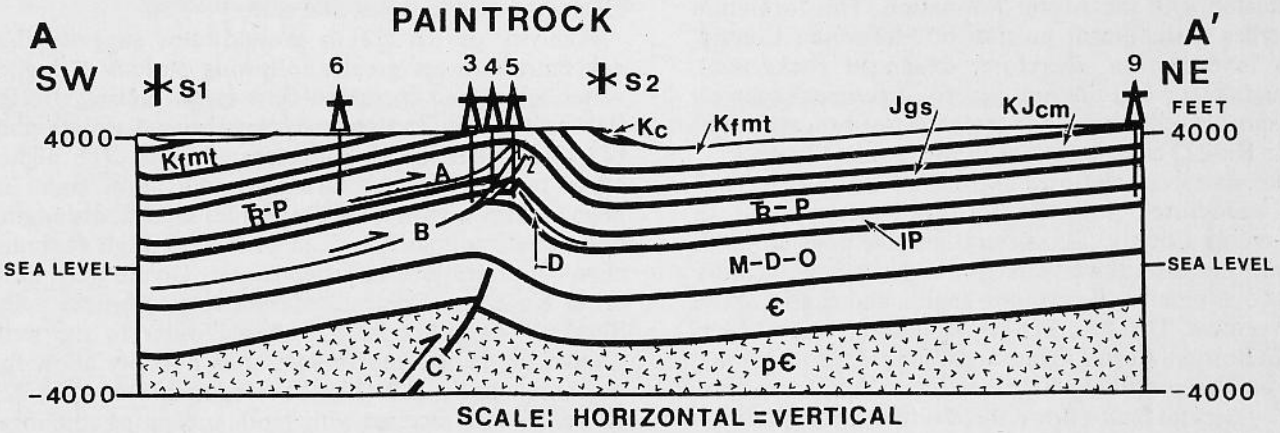

Fig. 2. True-scale southwest-to-northeast structural section A-A' across Paintrock Anticline. Overall geometry of the fold is controlled by fault C, which cuts the top of the Precambrian basement. Older rock-unit symbols are: IP = Pennsylvanian; M-D-O = Mississippian, Devonian, and Ordovician; C = Cambrian; and pC = Precambrian basement. Faults A, B_1, B_2, and D are volumetric adjustments which originated as detachment faults in synclines S_1 and S_2. Numbered derricks as in Figure 1.

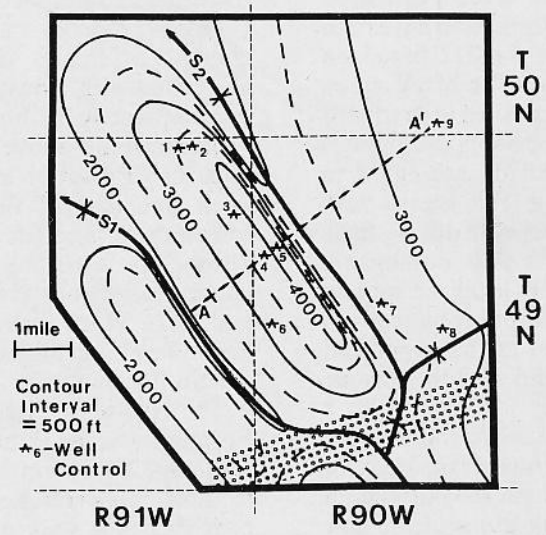

Fig. 3. Structure contour map, drawn on the base of the Jurassic Sundance Formation, depicts the geometry of Paintrock Anticline above detachment faults A, B, and D. The southeastern plunge of Paintrock is bluntly terminated along a postulated east-northeast trending, buried basement compartmental fault, as indicated by the patterned band. All symbols as in Figures 1 and 2.

Geologic Assessment of Radon-222 in McLennan County, Texas

Mary Podsednik

Radon-222 (Rn-222) is a carcinogenic, radioactive gas produced by the Uranium-238 (U-238) decay series primarily associated with acidic igneous rocks and black shales. Areas of known concern in Texas include the south Texas uranium district, east Texas lignite belt, Panhandle shales, Llano intrusives, and Big Bend intrusives. However, a soil gas survey conducted by the United States Geological Survey in 1988 surprisingly indicated anomalously high Rn-222 concentrations associated with the Austin Formation. This formation underlies a significant portion of McLennan County. This investigation, therefore, examined rocks, soil, groundwater, and indoor air to determine sources, transport mechanisms, and geochemical processes that affect Rn-222 concentrations in McLennan County.

The study concentrated on the Cretaceous bedrock and associated soils and groundwater found in McLennan County, Texas. Stratigraphic units crop out in a northeast-southwest direction and in ascending order include alternating limestones, shales, and chalks of the Georgetown, Del Rio, Pepper/Woodbine, Lake Waco, South Bosque, Austin, Ozan, and Wolfe City formations. The northeast-striking Balcones Fault Zone characterized by normal faults, down thrown to the east, parallels the outcrop trend and transects the county. Shallow groundwater flows through fractures in the weathered bedrock and is controlled primarily by topography. Soils are typically residual clays and silty clays maintaining high shrink-swell potential and low rates of infiltration.

Shales and bentonites of the Lake Waco Formation and phosphatic zones in the Austin Formation have been identified as the primary source of Rn-222 based on Radium-226 (Ra-226) concentrations. The black shales of the Lake Waco Formation were deposited in a reduced marine environment where U-238 commonly precipitates in sea water. The addition of volcanic ash, high in radionuclide concentration, provided ionic species with which U-238 could combine and precipitate during shale deposition. Uranium-238 and Ra-226 commonly precipitate with phosphate, resulting in localized sources for Rn-222 generation. Discontinuous phosphatic zones in the Austin Formation are located at the upper and lower contacts with the Ozan and South Bosque formations, respectively.

Houston and Houston Black clay soils produced the greatest Rn-222 flux concentrations regardless of underlying geology. Radon-222 in these soils originates from bedrock and along the outer portions of the clay matrix near desiccation cracks where it is transported efficiently by the increased permeability of the cracks (Fig. 1). The moisture-holding capacity of the clay matrix allows for increased Rn-222 production and increased Rn-222 flux. Emanation in this case originates within a small outer zone near the desiccation cracks and surface soil. Radon-222 flux concentrations may increase after rainfall events, with increased production caused by moisture. Radium-226 concentrations in clay matrices were anomalously low, indicating that bedrock and groundwater are the probable sources of Rn-222 emanation and that transport is efficient through fractures in the bedrock and soil.

Analysis of Rn-222 in groundwater suggests that concentrations are greater following periods of higher water tables and increased flow rates. During precipitation events, infiltrating water may cause dissolutioning of radionuclides in the unsaturated zone. The higher water table and faster flow rates will allow water to be in contact with more of the aquifer matrix, dislodging additional radionuclides and producing high radionuclide concentrations in groundwater. Divide wells have lower Rn-222 concentrations than down-gradient wells. Shorter flow paths from recharge water to the well, smaller gradients, and thinner soils possibly allow for degassing of Rn-222 (Fig. 2). Radon-222 and Ra-226 concentrations increase with depth, indicating equilibration at the air-water interface. In the study area, the greatest Rn-222 concentrations in groundwater are found in the Austin Formation, relating to a highly fractured flow system where groundwater is in contact with localized zones of radionuclide concentration along fracture and fault faces.

Indoor Rn-222 concentrations were found to be greatest in homes overlying the Austin Formation associated with Houston and Houston Black clay soils. Approximately 13 homes over the Austin had indoor concentrations above 10.0 pCi/L, significantly higher than the EPA action level of 4.0 pCi/L. The high shrink-swell potential of the soil contributes to cracks in foundations, and the fractured nature of the bedrock allows for efficient transport of Rn-222. Indoor concentrations of homes overlying the Woodbine/Pepper and Lake Waco formations were also above the EPA action level, but slightly lower than those overlying the Austin Formation.

The results of this investigation identify the Austin Formation as the greatest potential threat for producing high Rn-222 concentrations. Five factors that contribute to threatening situations are highly faulted or fractured bedrock, thin soils over bedrock, residual soils with desiccation cracks, topographic locations where thin soils exist and groundwater flow is increased, and increased moisture content in soils and bedrock.

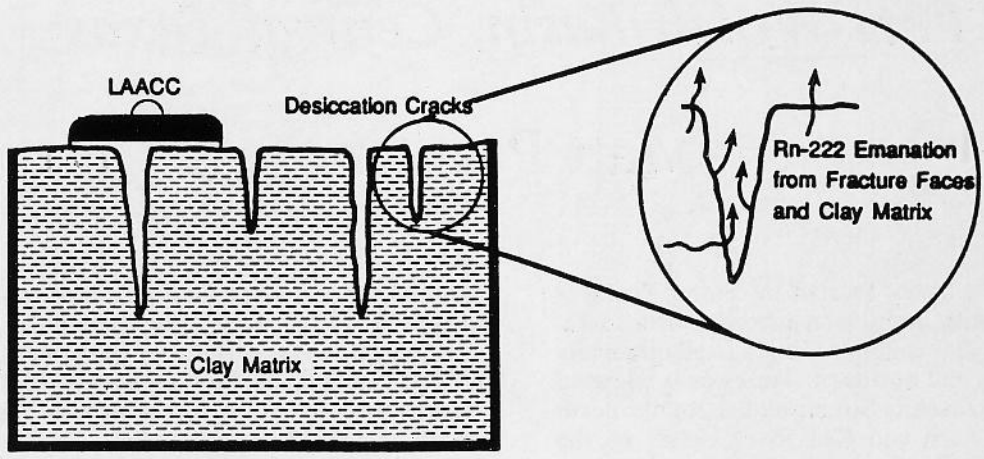

Fig. 1. Radon-222 emanation from desiccation cracks in a clay soil. The desiccation cracks provide increased surface area from which Rn-222 may be produced, efficiently transported, and absorbed by charcoal in the Large Area Activated Charcoal Canister (LAACC).

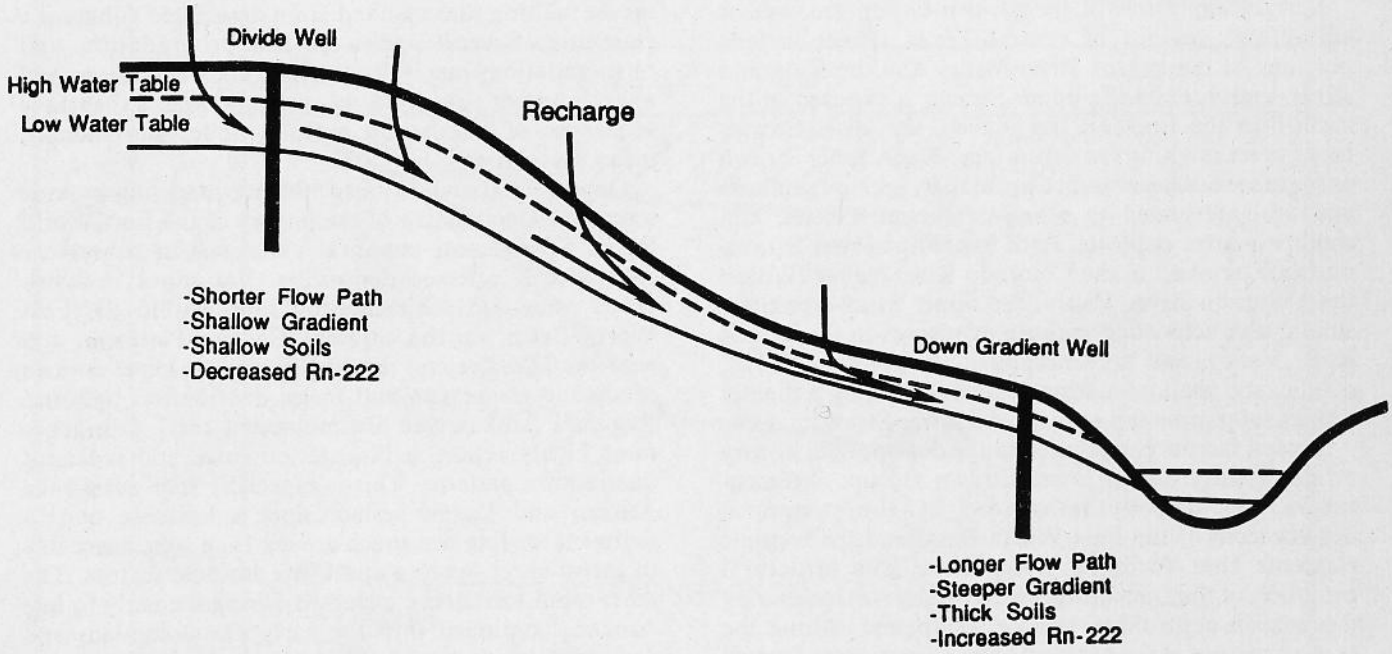

Fig. 2. The effect of topographic location on Rn-222 concentrations in groundwater. The down-gradient well has higher Rn-222 concentrations produced from dissolutioning and dislodging radionuclides by infiltrating water, faster flow rates, and water transported through more of the aquifer than a divide well.

Facies Analysis of the Strawn Submarine Fan Complex, Fort Worth Basin, Central Texas

Matt Pranter

The Fort Worth Basin, located in central Texas, is a Paleozoic Foreland Basin, which trends north-south, is approximately 200 miles in length, and gradually deepens to the east and northeast. The basin is bounded on the east by the Ouachita Structural Belt, on the north by the Muenster Arch and Red River Uplift, on the west by the Concho Platform and on the southwest by the Llano Uplift (Fig. 1). The principal depositional systems that were active within the Fort Worth Basin during the late Atokan and early Desmoinesian stages included fan delta, submarine fan, and related slope systems associated with the Pennsylvanian lower Strawn Group (Fig. 2). These sediment dispersal systems provided the majority of the clastic sediment that eventually filled the Fort Worth Basin, while shelf-edge and platform carbonates formed the adjacent Concho Platform to the west. Stratigraphic relationships and sediment geometries reflect the changes in the evolving Fort Worth Basin and its associated tectonic elements.

Surface exposures of the Strawn Group are present within two regions of central Texas. These include portions of the Brazos River Valley and the Colorado River Valley. Only the upper Strawn is exposed at the surface in the Brazos River Valley, the lower Strawn being present within the subsurface. These upper Strawn exposures have been studied in detail by previous authors and are interpreted to represent fluvial, deltaic, and shallow-marine deposits. Both upper and lower Strawn units are exposed in the Colorado River Valley. Within the Colorado River Valley, the upper Strawn exhibits similar characteristics as those exposures in the Brazos River Valley, and are interpreted to represent fluvial, deltaic, and shallow-marine deposits overlying a slightly deeper submarine fan sequence of lower Strawn.

Several factors contributed to the depositional history of the Pennsylvanian lower Strawn Group. Sedimentation was directly influenced by the structural development of the Fort Worth Basin and the tectonic elements that form its boundaries. The structural evolution of the Ouachita Structural Belt was the driving mechanism controlling basin development. Along the eastern margin of the basin, uplifted thrust sheets formed a prominent mountain range that served as the primary source for the majority of the clastic sediment filling the basin. Several lines of evidence, including paleocurrent information, net sandstone distribution patterns, dip meter values, petrographic data, and subsidence patterns, support a northeastern and eastern sediment source. The nature and distribution of depositional environments was controlled by active subsidence within the Fort Worth Basin. Both sediment loading and crustal downwarping following thrust sheet propagation were the major contributors to basin subsidence. Increased subsidence, flexure of the lithosphere, and lateral sediment infilling caused the basin axis and depocenters to shift progressively westward. As a result, Marble Falls, Big Saline, and Caddo carbonate platform facies were shifted westward. Large quantities of sediment derived from the Ouachita Structural Belt formed fan delta and submarine fan depositional systems, which prograded southwestward across the Fort Worth Basin. Localized block faulting within the Llano region produced a series of horsts and grabens that served as conduits for sediment dispersal and accumulation. Several obvious structural features associated with the localized block faulting include asymmetric folding and small-scale thrust faulting that resulted from associated submarine slumping. Several cycles of fan progradation and retrogradation, as well as fan lobe migration and abandonment, resulted in surface and subsurface sequences of alternating channel, lobe, and interfan facies associations.

Depositional and basin subsidence modeling provide a better understanding of the history of the Fort Worth Basin. Spatial and temporal variations in subsidence rates greatly affected deposition. Variations in subsidence rates and sedimentation rates within the Fort Worth Basin, on the adjacent Concho Platform, and near the Llano region resulted in distinct lower Strawn sandstone geometries and facies distribution patterns. Regional Atokan and Desmoinesian total subsidence rates highly reflect sedimentation rates and sediment distribution patterns. This is especially true during the Atokan and Desmoinesian, since subsidence due to sediment loading was much greater than subsidence due to thrust sheet loading and other tectonic factors. The most rapid subsidence occurred during the early to late Atokan, continued into the early Desmoinesian, and decreased during the late Desmoinesian and Missourian stages (Fig. 3). Decreasing rates of subsidence and sedimentation during the late Desmoinesian and Missourian established suitable conditions for upper Strawn carbonate and fluvio-deltaic development.

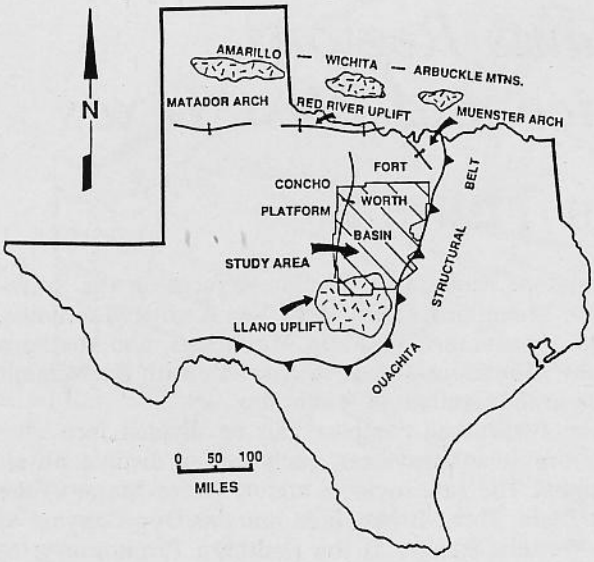

Fig. 1. Tectonic setting for central Texas during the Atokan and Desmoinesian stages (modified from Wermund, E. G., and Jenkins, W. A., 1969, Late Pennysylvanian Series in North-Central Texas, *in* A guidebook to the late Pennsylvanian shelf sediments, North-Central Texas: Dallas Geological Society, Dallas, Texas).

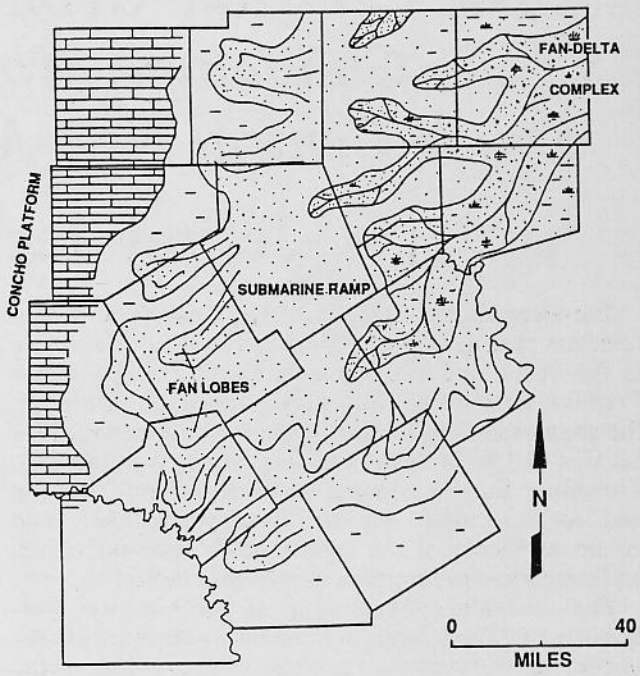

Fig. 2. Late Atokan and early Desmoinesian depositional systems active within central Texas. Sediment dispersal systems included fan-delta, submarine fan, and platform carbonate depositional systems.

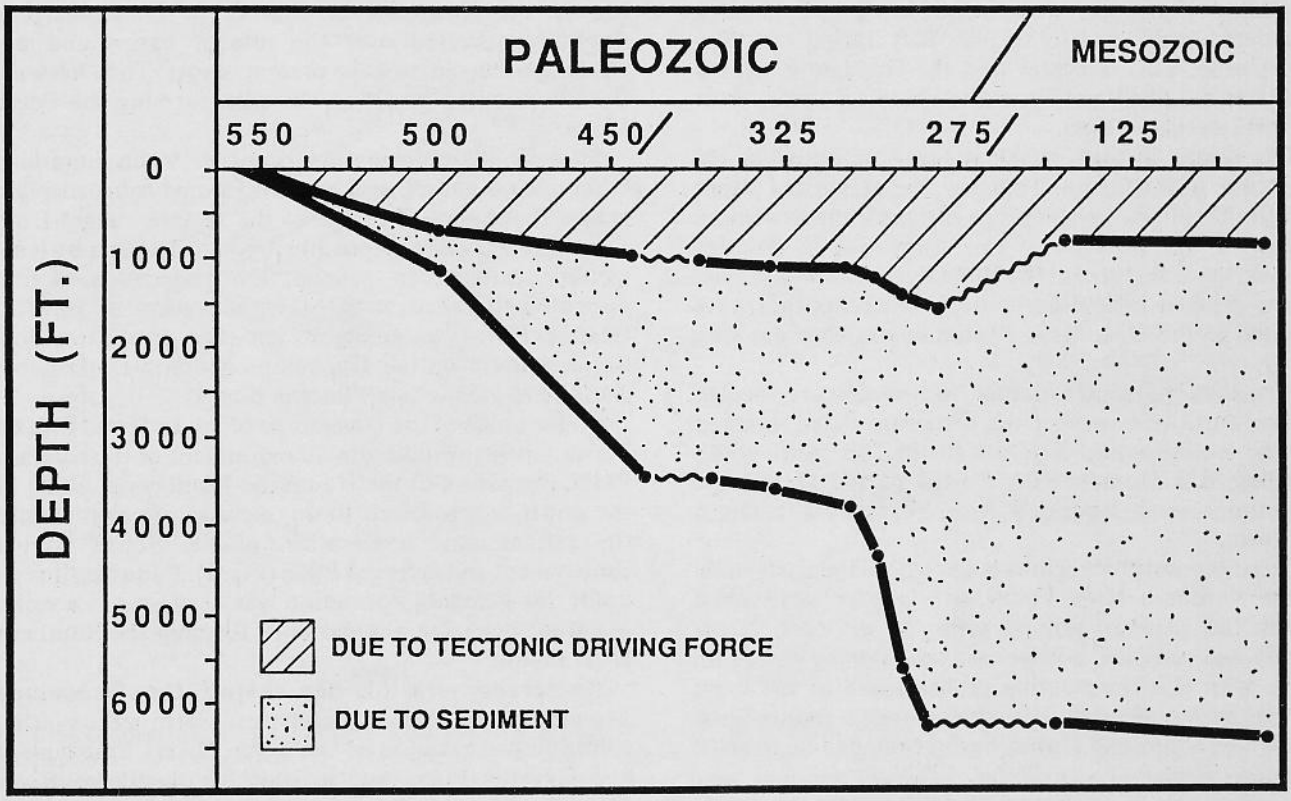

Fig. 3. Fort Worth Basin subsidence curves including total (lower curve) and tectonic (upper curve) subsidence curves. Lower Strawn deposition occurred during the late Atokan and early Desmoinesian, approximately 300 to 295 million years ago. This period is noted by a change to rapid subsidence (steeply dipping curve).

The Cenozoic Geomorphic History of the Guadalupe Mountains Regions, South-Central New Mexico and West Texas

Jeffrey Jackson Thuma

The Permian stratigraphy of the Guadalupe Mountains has been as extensively studied as any other section in the world, and has become a classic example of the Permian Reef system in geologic education. However, the geomorphology of this region in south-central New Mexico and West Texas has been relatively untouched. Therefore, to give a more complete geologic picture, and to incorporate the stratigraphy, structure, and erosional history of the region into a coherent whole, an interpretive geomorphic approach is desirable.

The Guadalupe Mountains of south-central New Mexico and West Texas are uniquely positioned on the border of two major geomorphic provinces, the extensional block-faulted Basin and Range to the west, and the relatively stable Great Plains to the east. The Salt Basin Graben and the adjacent Western Range of the Guadalupe Mountains mark the easternmost Basin-and-Range features. From the crest of the Western Range the land slopes gently eastward to the relatively stable Great Plains. Geologists have suggested that the Guadalupe Mountains were uplifted in a large fault block associated with the Rio Grande Rift during the Plio-Pleistocene. This indicates that the Guadalupe Mountains are relatively young with a complex history over a short interval of time.

The recent history of the range is reflected in the landscape of the region. Together, the major and minor landforms reflect a chronology of landscape evolution. Therefore, the purpose of this study was to describe the landscape features of the Guadalupe Mountains, and to construct a logical chronology of events that have resulted in the Guadalupe Mountains as they are seen today.

Structurally, the Guadalupe Mountains are located on the northwest shelf of the Delaware Basin, marked by the outcropping Capitan Reef. The north-south trending Rio Grande Rift is west of the Guadalupe Mountains, and separated from them by the Otero Platform.

Three geomorphic regions occur within the study area: 1) the Southern High Plains, a relatively undissected broad, flat plateau, sloping gently to the east; 2) the Guadalupe complex, a large eastward-sloping mountain block with a corresponding graben-basin to the west; and 3) the Rio Grande Rift, north-south trending horst block mountains and graben basins bounded on the east by Otero Mesa.

The Summit Plain, found throughout the region, is an erosional surface made conspicuous by flat-topped, concordant summits and broad plateaus truncating progressively older rocks from east to west across the Guadalupe Mountains. Similar surfaces on the Sacramento Mountains, Otero Mesa, San Andres Mountains, Organ Mountains, Franklin Mountains, and southern Rocky Mountains appear to correlate with the Summit Plain in the Guadalupe Mountains.

The Guadalupe complex can be divided into nine geomorphic subprovinces, each with a distinct physiography. The subprovinces are: 1) Otero Mesa; 2) the Salt Basin; 3) the Brokeoff Mountains/Dog Canyon; 4) the Western Range; 5) the Southern Promontory; 6) the Eastern Range; 7) the Seven Rivers Embayment; 8) the Gypsum Plain; and 9) the Pecos Valley.

The Cenozoic geomorphic evolution of the Guadalupe Mountains region consists of four stages that have shaped the landscape into its present form. They are: 1) Laramide deformation; 2) Summit Plain formation; 3) Guadalupe uplift and Ogallala deposition (Fig. 1); and 4) Quaternary erosion (Fig. 2).

Laramide deformation caused broad warping of the Guadalupe Mountains region, resulting in the overturning of the Haupache normal fault. Down-warping generally occurred over the present basins and up-warping occurred over the present ranges. The Delaware Basin was tilted gently to the east, forming the Pecos Slope.

Summit Plain formation occurred when Laramide compression ended, and erosion formed a broad plain across the region. The age of the surface ranges from Eocene to Pliocene, depending upon disruption by local tectonic activity. In general, the surfaces were first disrupted to the west with the activation of the Rio Grande Rift. The youngest remnant of the regional Summit Plain on the Guadalupe Mountains probably was abandoned in late Pliocene time.

Major uplift of the Guadalupe block occurred in Late Tertiary time, resulting in abandonment of the Summit Plain, formation of the Haupache Monocline, filling of the down-dropped Salt Basin, incision of canyons into the ranges, and excavation of the Seven Rivers Embayment and Gypsum Plain (Fig. 1). Following initial uplift, the Ogallala Formation was deposited in a series of three coalescing alluvial fans, forming the Southern High Plains.

Quaternary erosion has shaped the Guadalupe Mountains by cutting canyons, forming caverns, continuing excavation of the Seven Rivers Embayment and Gypsum Plain, and establishing the Pecos River (Fig. 2). Climatic variation during Pleistocene time played a major role in the timing, rates, and character of erosion during Quaternary time.

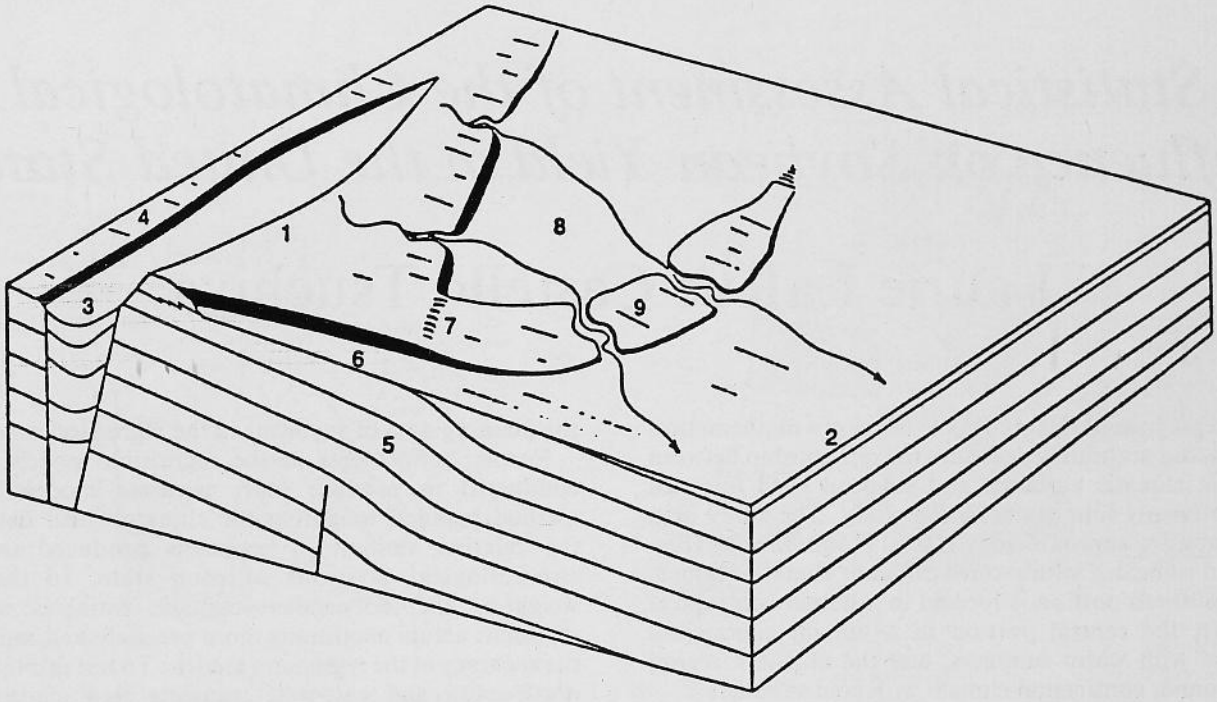

Fig. 1. Block diagram indicating features formed during Stage 3 of geomorphic evolution. Stage 3, Guadalupe uplift and Ogallala deposition, resulted in uplift of the Guadalupe block (1) and down dropping of the Salt Basin (3) due to normal faulting related to Rio Grande Rifting. Otero Mesa (4) did not have significant tectonic movement. The buried Haupache fault was reactivated and folded overlying Permian strata into the Haupache Monocline (5), deforming the Summit Plain (7). Shortly after initial uplift of the Guadalupe Mountains, the Ogallala Formation (2) was deposited. Alluvial streams on this surface were the base level for streams draining the Guadalupe Mountains. In response to uplift and a new base level, streams downcut, abandoning the Summit Plain. Erosion of the Gypsum Plain resulted in the exposure of the Capitan Reef escarpment (6). Streams flowing through the Seven Rivers Embayment downcut to the Bogle Flat level (8) and excavated the embayment. The major streams also downcut through the Eastern Range, isolating Azotea Mesa (9).

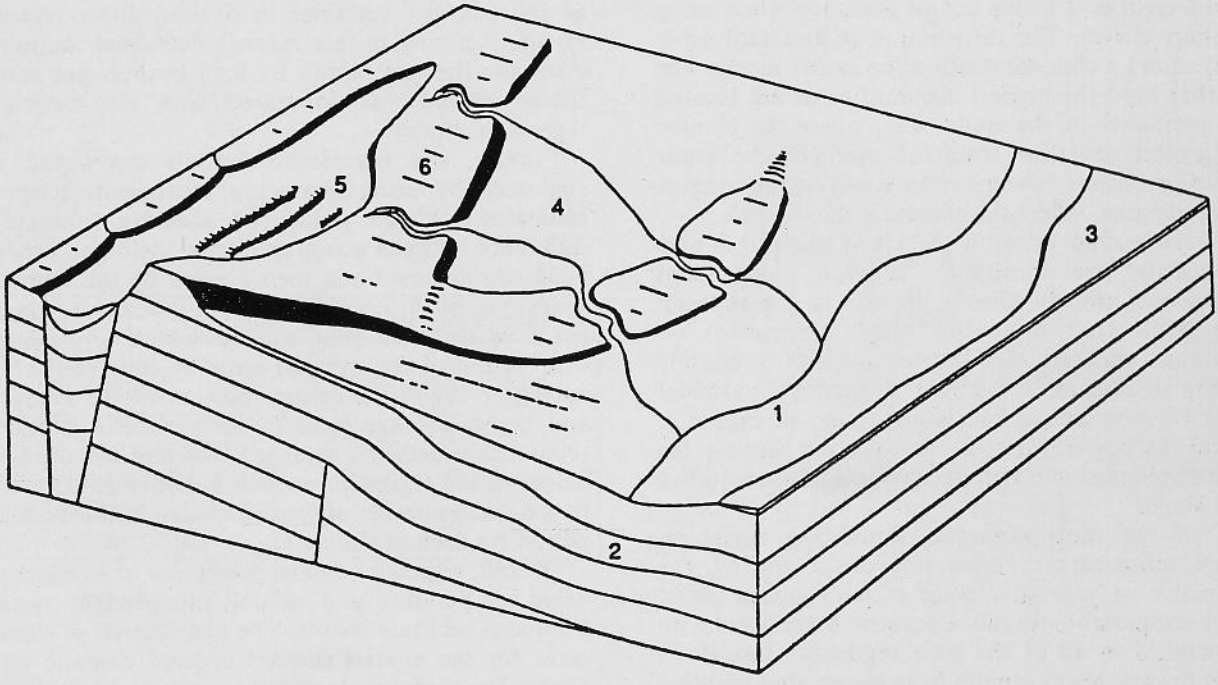

Fig. 2. Block diagram indicating features formed during Stage 4 of geomorphic evolution. Stage 4, Quaternary erosion, was dominated by development of the Pecos River (1). This was caused by deep solutioning of Permian salts resulting in the north-south subsidence trough of the Pecos Valley. Development of the valley caused eastward retreat of the Mescalero Escarpment and isolation of the Southern High Plains (3). Adjustment of streams to the new base level caused streams to cut deeper canyons in the Eastern and Western Ranges (6) and to isolate the Bogle Flat level in the Seven Rivers Embayment (4). Large scale slumping along the western margin of the Guadalupe Mountains, possibly in response to Pleistocene pluvial periods, occurred, forming the Brokeoff Mountains and Dog Canyon (5).

Statistical Assessment of the Climatological Influence on Soybean Yield in the United States

Laurie LaRue Castello Tsuchiya

The purpose of this study is to develop a mathematical model that accurately describes the relationship between specific climatic variables and soybean yield for each of the twenty-four states in the study. The study area encompasses approximately 1,312,192 square miles (Fig. 1), and is located within three different climatic regions. The southern portion is located in a humid subtropical climate, the central portion in a humid, continental climate with warm summers, and the northern region in a humid, continental climate with cold summers.

Crop testing generally has been conducted by 1) using curvilinear regression modeling, or 2) creating a curve that simulates the increase in soybean yield due to technological influences, thereby allowing linear multiple regression modeling. This study uses the second method in order to isolate climatological effects on soybean yield.

The regression models produced in this study show a high correlation between soybean yield and climate. Initially r^2 values of the regression models were used to evaluate the accuracy of the models. However, standard error is a better test of accuracy when using technology curves. The distribution of standard error (Fig. 2) shows a climatic relationship rather nicely. The states that have the highest standard error are located in the perimeter of the study area, where the climate has a greater deviation from the average. The lower standard errors are found in the states in the interior of the study area, where the climate is more stable.

The relationship between yield and climate is also supported by the correlation between independent variables and already known periods in the soybean growth cycle that are more highly dependent on temperature and rainfall. The seven most commonly occurring significant (α = 0.005) independent variables in the state regression models are found in Figure 3. Four of the seven variables listed occur during the reproductive stage and two occur during the vegetative growth stage.

One of the most common significant variables, January temperature, does not occur during the reproductive or vegetative stage of the soybean plant. January temperature reveals a negative correlation with soybean yield in all of the state regression models in which it occurs. Many studies have shown that planting date is a significant factor in soybean yield. All of these studies confirm that the later soybeans are planted, the lower the soybean yield. The author believes that the negative correlation of January temperature represents the planting date of soybeans in the regression models.

Further refinements of the regression models were conducted to produce more accurate models. One method entailed weighting the climatological data by the relative amount of soybeans produced in the climatological divisions of each state. In theory, weighting the independent climatic variables would represent actual conditions more precisely and increase the accuracy of the regression models. To test this theory, north-south and east-west transects were chosen to represent the wide range of climates across the study area. In general, weighting did not improve the unweighted models. The only exception was Louisiana, which showed a twenty percent increase in the r^2 value with weighting, which may be a result of incorporating the localized influences of Louisiana's subtropical latitude and its proximity to the Gulf of Mexico.

The second refinement involved the single state of Iowa. The square root of the deviations above and below average rainfall, along with temperature data, were used as independent variables in a third Iowa regression model. Refining in this manner decreased the average error for the test period by 0.85 bushels per acre, or fifteen percent, as compared with the unweighted regression model.

Finally, the regression models developed were evaluated by using regression coefficients to predict estimated soybean yield. The absolute value of the difference between actual estimated yield and predicted yield was summed and then divided by the number of years evaluated to give the average total error in bushels per acre for each year and each state (Fig. 4). The distribution of the average error by state shows lower average error in the central portion of the study area and higher average error in the perimeter states. The relationship between average error and standard error values of the regression models is not clear. This is due to the small number of years included in the evaluation period for each of the states.

Overall, regression model prediction of soybean yield using temperature and rainfall independent variables produced accurate results. The distribution of standard error for the models showed ordered climatic significance. The model evaluations using average error lacked an ordered distribution. Further refinements, however, did not clearly improve the results of the initial regression analysis.

Fig. 1. General location map of the study area. The map includes twenty-four states that significantly contribute to total soybean production in the United States. The climatic regions included in the study are designated as follows: 1 - marginal steppe climate, 2 - humid continental climate, 3 - humid subtropical climate.

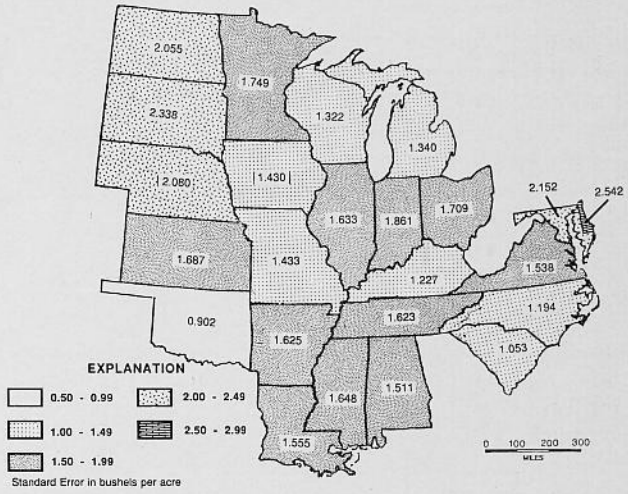

Fig. 2. Map of the study area showing the distribution of the standard error in bushels per acre of the individual state regression models. The numbers presented are the lowest errors generated, whether they were derived from the weighted or primary regression models.

Variable	No. of States Occurred
July Rainfall	12
August Rainfall	10
January Temperature	10
August Temperature	10
June Temperature	8
June Rainfall	7
July Temperature	6

Fig. 3. The seven most commonly occurring significant variables and the number of times occurring in state regression models. If the variable occurred in both the primary and weighted regression model, it was included only once.

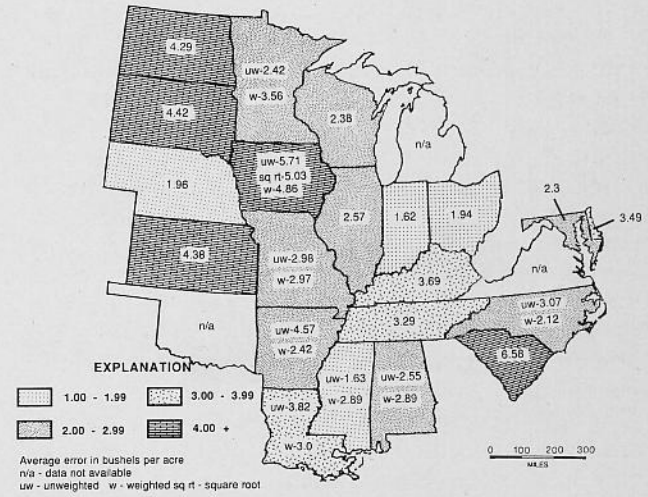

Fig. 4. Location map showing the distribution of the average error of the individual state regression models for the evaluation years. In general, the largest error occurred in states on the western margin of the study area.

BAYLOR GEOLOGICAL PUBLICATIONS*

Baylor Geological Studies

1-8, 12, 16-25, 30: Out of print. For titles see earlier Baylor Geological Studies Bulletins.

†9. Part II: Soils, 1965, Soils and urban development of Waco by W. R. Elder: Baylor Geological Studies Bull. No. 9 (Fall). $5.00.

†10. Part III: Water, 1966, Surface waters of Waco by Jean M. Spencer: Baylor Geological Studies Bull. No. 10 (Spring). $5.00.

†11. Part III: Water, 1976, Subsurface waters of Waco by Siegfried Rupp: Baylor Geological Studies Bull. No. 11 (Fall). $5.00.

15. Boone, Peter A., 1968, Stratigraphy of the basal Trinity (Lower Cretaceous) sands, central Texas: Baylor Geological Studies Bull. No. 15 (Fall). $5.00.

26. Davis, Keith W., 1974, Stratigraphy and depositional environments of the Glen Rose Formation, north-central Texas: Baylor Geological Studies Bull. No. 26 (Spring). $5.00.

27. Baldwin, Ellwood E., 1974, Urban geology of the Interstate Highway 35 growth corridor between Belton and Hillsboro, Texas: Baylor Geological Studies Bull. No. 27 (Fall). $5.00.

28. Allen, Peter M., 1975, Urban geology of the Interstate Highway 35 growth corridor from Hillsboro to Dallas County, Texas: Baylor Geological Studies Bull. No. 28 (Spring). $5.00.

29. Belcher, Robert C., 1975, The geomorphic evolution of the Rio Grande: Baylor Geological Studies Bull. No. 29 (Fall). $5.00.

31. Dolliver, Paul Noble, 1976, The significance of Robert Thomas Hill's contribution to the knowledge of central Texas geology: Baylor Geological Studies Bull. No. 31 (Fall). $5.00.

32. Pool, James Roy, 1977, Morphology and recharge potential of certain playa lakes of the Edwards Plateau of Texas: Baylor Geological Studies Bull. No. 32 (Spring). $5.00.

33. Bishop, Arthur L., 1977, Flood potential of the Bosque basin: Baylor Geological Studies Bull. No. 33 (Fall). $5.00.

34. Hayward, Chris, 1978, Structural evolution of the Waco region: Baylor Geological Studies Bull. No. 34 (Spring). $5.00.

35. Walker, Jimmy R., 1978, Geomorphic evolution of the Southern High Plains: Baylor Geological Studies Bull. No. 35 (Fall). $5.00.

36. Owen, Mark Thomas, 1979, The Paluxy Sand in north-central Texas: Baylor Geological Studies Bull. No. 36 (Spring). $5.00.

37. Bammel, Bobby H., 1979, Stratigraphy of the Simsboro Formation, east-central Texas: Baylor Geological Studies Bull. No. 37 (Fall). $5.00.

38. Leach, Edward Dale, 1980, Probable maximum flood on the Brazos River in the city of Waco: Baylor Geological Studies Bull. No. 38 (Spring). $5.00.

39. Ray, Bradley S., Oklahoma: Baylor Geological Studies Bull. No. 39 (Fall). $5.00.

40. Corwin, Linda Whigham, 1982, Stratigraphy of the Fredericksburg Group north of the Colorado River, Texas: Baylor Geological Studies Bull. No. 40 (Spring). $5.00.

41. Gawloski, Ted, 1983, Stratigraphy and environmental significance of the continental Triassic rocks of Texas: Baylor Geological Studies Bull. No. 41 (Spring). $5.00.

42. Dolliver, Paul N., 1984, Cenozoic evolution of the Canadian River basin: Baylor Geological Studies Bull. No. 42 (Spring). $5.00.

43. McKnight, Cleavy L., 1986, Descriptive geomorphology of the Guadalupe Mountains, South-Central New Mexico and West Texas: Baylor Geological Studies Bull. No. 43 (Spring). $5.00.

44. Matthews, Truitt F., 1986, The petroleum potential of "serpentine plugs" and associated rocks, central and south Texas: Baylor Geological Studies Bull. No. 44 (Fall). $5.00.

45. Surles, Milton A. Jr., 1987, Stratigraphy of the Eagle Ford Group (Upper Cretaceous) and its source-rock potential in the East Texas basin: Baylor Geological Studies Bull. No. 45 (Fall). $5.00.

46. Rapp, Keith Burleigh, 1988, Groundwater recharge in the Trinity Aquifer, central Texas: Baylor Geological Studies Bull. No. 46 (Spring). $5.00.

47. Anderson, L. Marlow, 1989, Stratigraphy of the Fredericksburg Group, East Texas Basin: Baylor Geological Studies Bull. No. 47 (Spring) $5.00.

48. Fall, 1989, Thesis Abstracts: Baylor Geological Studies Bull. No. 48. $5.00

49. Hawthorne, J. Michael, 1990, Dinosaur Track-bearing Strata of the Lampasas Cut Plain and Edwards Plateau, Texas: Baylor Geological Studies Bull. No. 49 (Spring). $5.00.

50. Fall, 1990, Thesis Abstracts: Baylor Geological Studies Bull. No. 50. $5.00.

Baylor Geological Society

101-134, 137, 138, 149: Out of print. For titles see earlier Baylor Geological Studies Bulletins.

139. Urban development along the White Rock Escarpment, Dallas, Texas, 1978. $1.50.

140. Paluxy Watershed. Geology of a river basin in north central Texas, 1979. $1.50.

141. Geomorphic evolution of the Grand Prairie, central Texas, 1979. $1.50.

142. The nature of the Cretaceous-precretaceous contact, Central Texas, 1979. $4.00, a professional level guidebook.

143. The Geology of Urban Growth, 1979. $1.50.

144. A day in the Cretaceous, 1980. $1.50.

145. Landscape and Landuse, 1980. $1.50.

146. Southeastern Llano Country, 1983. $1.50.

147. Early and Late Paleozoic Conodont Faunas of the Llano Uplift Region, Central Texas—Biostratigraphy, Systemic Boundary Relationships, and Stratigraphic Importance, 1987. $12.00.

148. Lower Cretaceous Dinosaur Footprints of the Paluxy River Valley, Somervell County, Texas, 1987..$15.00.

150. Pre-Pennsylvanian Geology of the Arbuckle Mountain Region. Southern Oklahoma, 1987. $10.00.

151. Edwards-dominated Landscapes in the Lampasas Cut Plain: Form, Processes, and Evolution, 1987. $13.00.

*Publications available from Baylor Geological Studies or Baylor Geological Society, Baylor University, Waco, Texas 76798. Prices do not include shipping and handling costs; Texas residents add 8¼ percent sales tax.

†Part of **Urban Geology of Greater Waco**, a series on urban geology in cooperation with Cooper Foundation of Waco.


BAYLOR UNIVERSITY
GEOLOGY